

Master Thesis

The Cooling Effect of Urban Green Spaces in Paramaribo



Tom Remijn

Student ID: 12418684

Master Program: Earth Science (University of Amsterdam)

Date: 20th March 2020

Examiner: Dr. J. Z. Shamoun-Baranes (University of Amsterdam)

Assessor: Dr. E. H. van der Zanden (University of Amsterdam)

Daily supervisor: Dr. N. Schwarz (University of Twente)



Abstract

Currently, from the estimated 7.7 billion people worldwide approximately 55% live in urban environments and this percentage is projected to grow to 68% by 2050. High coverage of impervious surface in urban environments, causes temperatures to be several degrees higher in urban areas compared to their surrounding rural areas, a phenomenon known as the urban heat island effect. The implementation of urban green spaces can mitigate this excess warming and by doing so increase the resilience of urban environments to heat stress. Although a large part of global urbanization is projected in the tropics, the urban heat island and the potential cooling effect of urban green space are not well studied in that region.

Therefore, the main aim of this study was to provide an analysis of the Urban Heat Island effect and of the cooling effect of urban green space in the whole rural-urban region of the tropical city of Paramaribo (Suriname) in both the wet and dry season. The study was based upon a land cover map of the Greater Paramaribo Region and on land surface temperature, derived from Landsat 8 satellite data from both the wet and dry season. In order to study the effects of the composition (trees, mangroves, mixed low vegetation and grass) and configuration of urban green space on land surface temperatures, class metrics including percentage of landscape, aggregation index, landscape shape index, edge density and patch density were used. In addition, the influence of socioeconomic status on land surface temperature was tested. To complete the urban heat island study, air measurements were undertaken to allow for comparison between LST and air temperatures across different land cover types.

The results show that a surface urban heat island effect exists between the urban core and the rural hinterland in Paramaribo. The magnitude was similar in both seasons (ca. 5.2 K). Urban green spaces were found to significantly mitigate this urban temperature increase. This cooling relationship was dependent on the urban green space type present. Trees and mangrove showed the strongest cooling effect on land surface temperature, while mixed low vegetation provided less, but still a significant, cooling effect. On the other hand, grass did not show a clear cooling relationship. Regardless of the type of urban green space, this study shows that increasing the size of urban green space increases the cooling effect. Our results also show that a large aggregated urban green space is favoured over a number of smaller disaggregated ones. The cooling effect of urban green space was slightly stronger in the dry season compared to the wet season. No relationship was found between the shape of urban green spaces and the land surface temperature in Paramaribo. The amount of urban green space was found to differ between neighbourhoods with different socioeconomic status. This resulted in an indirect negative relationship between socioeconomic status and land surface temperature. This relationship did not apply to the neighbourhoods of the lowest SES, since due to the sandy characteristic of the streets in these neighbourhoods, their LST was also low.

Based on these results, it is concluded that there is a substantial urban heat island present in Paramaribo in both the wet and the dry season. In addition, this study also shows that urban green space could provide a nature-based solution to mitigate this UHI in Paramaribo. Due to the lack of studies on urban ecosystem services in the global South, this study in Paramaribo can potentially add to the valuation of urban green spaces in policy across cities in the global South.

Table of Content

1. Introduction	10
1.1. Background and relevance.....	10
1.2. Research aim.....	13
1.3. Research questions	14
2. Materials and methods	14
2.1. Case study description	14
2.1.1. Study Area.....	14
2.1.2 Project: Towards a Green and more Liveable Paramaribo	16
2.2. Data	16
2.2.1. Satellite imagery	17
2.2.2. Land cover map.....	18
2.2.3. Neighbourhood SES classification.....	19
2.3. Temperature extraction.....	20
2.3.1. Cloud correction.....	20
2.3.2. Atmospheric corrections and radiometric calibrations	20
2.3.3. LST extraction.....	21
2.3.4 LST standardization and seasonal composition procedure	22
2.4. Analysis	23
2.4.1. Analysis of the SUHI effect.....	23
2.4.2. Analysis of the cooling effect of UGS.....	24
2.4.3. Analysis of the relationship between LST and air temperature	28
2.5. Workflow.....	30
3. Results.....	31
3.1. Analysis of the SUHI	31
3.1.1. Spatial characteristics of the SUHI in the Greater Paramaribo Region.....	31
3.1.2. Spatial characteristics of the intra-SUHI in the administrative boundary	32
3.2. Analysis of the cooling effect of UGS.....	36
3.2.1. Relationship between the LST and NDVI within the administrative boundary.	36
3.2.2. Relationship between the LST and the land cover composition in the surrounding area within the administrative boundary.....	37
3.2.3. Relationship between the LST and configuration of UGS.....	43
3.2.4. Analysis of thermal centres and the effect on LST of all land cover features combined. ..	45
3.2.5. Detailed cooling effects of green features specific for Paramaribo	49
3.3. Analysis of the relationship between the LST and air temperature	55
3.3.1. SUHI vs CLHI	55

3.3.2. Relationship between LST and air temperature found within the administrative boundary of Paramaribo	56
4. Discussion.....	58
4.1. Reflection on results	58
4.2. Methodological strengths and limitations.....	61
4.3. Ways forward.....	63
5. Conclusion.....	64
References	65
Appendix	72

List of tables

Table 1. Secondary data used in this study.	17
Table 2. Details of Landsat 8 OLI/TIRS imagery used.	18
Table 3. Area covered per land cover type in the Greater Paramaribo Region and the administrative boundary	19
Table 4. Distinction between residential groups, based on spatial criteria (Fung-Loy et al., 2019).	20
Table 5. SUHI indicators used in this study.	24
Table 6. Class metrics used in this study.	26
Table 7. LST of the Greater Paramaribo Region extracted from Landsat images, including minimum, maximum, range, mean and standard deviation.	31
Table 8. LST extracted from Landsat images within the administrative boundary.	33
Table 9. SUHI indicators at 14:00 hrs, local time, for both seasons, once taking only the urban land cover type as "urban" and once using a combination of urban and infrastructure in the form of a reclassified built- up land cover class as "urban"	36
Table 10. Pearson's correlation (r) of seasonal $LST_{s, max}$ values and NDVI once using a sample of the whole administrative boundary and once using a sample after water was excluded from the administrative boundary. N = number of pixels in sample.	36
Table 11. Pearson's correlation (r) of seasonal $LST_{s, max}$ values and PLAND for different radii used in the focal analysis.	38
Table 12. Pearson's correlation (r) of seasonal $LST_{s, max}$ values and PLAND values of the combined land cover class UGS and of all individual land cover types, after 0% values were filtered out. N = number of pixels in sample.	39
Table 13. Linear regression results of $LST_{s, max}$ and PLAND values of the combined land cover class UGS and of all the individual land cover types.	41
Table 14. Multiple linear regressions to predict $LST_{s, max}$ in the dry (upper) and wet season (lower) based on PLAND for all land cover types except bare soil.	42
Table 15. Pearson's correlation of seasonal $LST_{s, max}$ values and the used configurational class metrics, after 0% UGS values were filtered out.	43
Table 16. Pearson's correlation of seasonal $LST_{s, max}$ values and distances between interesting thermal centres.	46
Table 17. Multiple linear regression model 1, used to test the hypothesis: Impervious urban surface heats the surface in the dry season.	47
Table 18. Multiple linear regression model 2, used to test the hypothesis: UGS cools the surface in the dry season.	47
Table 19. Multiple linear regression model 3, used to test the hypothesis: Trees are the UGS type that cools the surface most effective in the dry season.	48
Table 20. Mean $LST_{s, max}$ values and the standard deviation per land cover class in the Greater Paramaribo Region in the dry and wet season.	77
Table 21. Full descriptive analysis of $LST_{s, max}$ within the Greater Paramaribo Region of the different land cover types in the dry season.	78
Table 22. Full descriptive analysis of $LST_{s, max}$ within the Greater Paramaribo Region of the different land cover types in the wet season.	78
Table 23. Full descriptive analysis of $LST_{s, max}$ within the administrative boundary of the different land cover types in the dry season.	79
Table 24. Full descriptive analysis of $LST_{s, max}$ within the administrative boundary of the different land cover types in the wet season.	79
Table 25. Kruskal-Wallis test on the distribution of $LST_{s, max}$ across the different land cover types, including pairwise comparisons adjusted by the Bonferroni correction for multiple tests.	80
Table 26. Results of a non-parametric Wilcoxon signed-rank test of between $LST_{s, max}$ values of different seasons per land cover group. N = number of pixels in sample.	81

Table 27. Results of a non-parametric Wilcoxon signed-rank test of between $LST_{s,max}$ values of different seasons per green feature group. N = number of pixels in sample.....	81
Table 28. Results of a non-parametric Wilcoxon signed-rank test of between $LST_{s,max}$ values of different seasons per cold spot group. N = number of pixels in sample.	81
Table 29. Multiple linear regression model 1, used to test the hypothesis: Impervious urban surface heats the surface in the wet season.	86
Table 30. Multiple linear regression model 2, used to test the hypothesis: UGS cools the surface in the wet season.	86
Table 31. Multiple linear regression model 3, used to test the hypothesis: Trees are the UGS type that cools the surface most effective in the wet season.	86
Table 32. Kruskal-Wallis test on the distribution of $LST_{s,max}$ across the different groups of green features, including pairwise comparisons adjusted by the Bonferroni correction for multiple tests.	88
Table 33. Kruskal-Wallis test on the distribution of $LST_{s,max}$ across the different cold spot groups, including pairwise comparisons adjusted by the Bonferroni correction for multiple tests.	92
Table 34. Kruskal-Wallis test on the distribution of $LST_{s,max}$ across the different neighbourhoods varying in socioeconomic status based on residential class, including pairwise comparisons adjusted by the Bonferroni correction for multiple tests.	93
Table 35. LST and air temperatures measured on 14:00 hrs, local time, at the locations of the measuring stations, Cultuurtuin and Zorg en Hoop, of the meteorological service Suriname.	94
Table 36. Location description, LST and air temperatures on 14:00 hrs, local time, on August 8 th , 2019 at the locations of outdoor temperature loggers.	94

List of figures

Figure 1. Typical diurnal variations of surface and air temperatures over the urban-rural transect, resulting in the difference between the SUHI and CLHI (U.S. Environmental Protection Agency, 2008). 11

Figure 2. Lower left: The location of Suriname in South America. Upper left: The location of Paramaribo in Suriname. Right: The Study area: The administrative boundary of Paramaribo (yellow) and its surrounding Greater Paramaribo Region (red) including all its districts (white). 15

Figure 3. Monthly precipitation values in mm in Suriname from 2011 to 2015 (left), monthly average air temperatures in °C in Suriname from 2011 to 2015 (right) (GBS, 2016). 16

Figure 4. Land cover maps of the Greater Paramaribo Region (left) and the administrative boundary (right) on 12 September 2019. 18

Figure 5. Neighbourhoods in Paramaribo sorted by SES based on residential class (Fung-Loy et al., 2019). 19

Figure 6. Locations of placed outdoor temperature loggers and of the two air measuring stations of the meteorological service. 29

Figure 7. Workflow of methods used in this study. Each box provides the input data and methodology used for a given task. The flow paths (lines) start at boxes on the top (right) that contain the input data, then they proceed to a processing box in the middle to end in an analysis box at the bottom (left). The line colours separate main subjects of the research: LST (blue), local detailed Paramaribo specifics (black), land cover-based analysis (green), and air temperature (red). 30

Figure 8. Spatial pattern of LST_{max} in the dry (a) and wet (b) season and $LST_{s,max}$ in the dry (c) and wet (d) season in the Greater Paramaribo Region. Note: White spots are areas where clouds were present in all the images used to create the seasonal composites, these clouds were removed. Therefore, the white spots in the seasonal images indicate no data. 32

Figure 9. Spatial pattern of LST_{max} in the dry (a) and wet (b) season and $LST_{s,max}$ in the dry (c) and wet (d) season in the administrative boundary. Note: White spots are areas where clouds were present in all the images used to create the seasonal composites, these clouds were removed. Therefore, the white spots in the seasonal images indicate no data. 33

Figure 10. Mean $LST_{s,max}$ values per land cover class, including error bars displaying the standard deviation, in the administrative boundary in the dry and wet season. 34

Figure 11. Scatterplots, including regression line, of $LST_{s,max}$ vs NDVI with water in the dry (a) and wet (b) season, and of $LST_{s,max}$ vs NDVI without water in the dry (c) and wet (d) season. 37

Figure 12. Percentage of UGS in a 90-meter radius around focal cell in the Administrative boundary in the dry (a) and wet (b) season. Note: White spots are areas where clouds were present in all the images used to create the seasonal composites, these clouds were removed. Therefore, the white spots in the seasonal images indicate no data. 39

Figure 13. Scatterplots, including regression line, of $LST_{s,max}$ vs PLAND (90m) values of the combined land cover class UGS and of all individual land cover types in the dry season after the 0% PLAND values were filtered out. 40

Figure 14. Scatterplots, including regression line and equation, of $LST_{s,max}$ by the several configurational class metrics for the dry (left) and wet (right) season after the 0% PLAND UGS values were filtered out. 44

Figure 15. Location of selected green features and cold spots, including their group number (explained in **Figure 16**, **Figure 18** and Appendix 15) in the city of Paramaribo. 49

Figure 16. Typical land cover for six of the thirteen selected green feature groups. 50

Figure 17. Average $LST_{s,max}$ on the selected green feature groups, including error bars displaying the standard deviation, in the city of Paramaribo. 51

Figure 18. Representative land cover for each of the cold spot groups. 52

Figure 19. Average $LST_{s,max}$ on the selected cold spot groups, including error bars displaying the standard deviation, in the city of Paramaribo. 53

Figure 20. Characteristic street image, including vegetation pattern, in neighbourhoods of different SES based on residential class. 54

Figure 21. Mean $LST_{s,max}$ in neighbourhoods, including error bars displaying the standard deviation, in Paramaribo differing in SES once based on residential class. 55

Figure 22. The average daily CLHI during the short rainy season (07-12-2019 – 31-01-2020) between the urban core (outdoor temperature logger 1 & 2) and rural (outdoor temperature logger 13). 56

Figure 23. LST and air temperatures measured on 14:00 hrs, local time, at the locations of the measuring stations, Cultuurtuin and Zorg en Hoop, of the meteorological service Suriname. In the figure, air temperatures measured at Cultuurtuin are depicted in blue and temperatures measured at Zorg en Hoop are depicted in blue. Temperatures measured in the dry season are depicted with squares, while temperatures measured in the wet season are depicted in circles. 57

Figure 24. LST and air temperatures on 14:00 hrs, local time, on August 8th, 2019 at the locations of the outdoor temperature loggers. 58

Figure 25: Outdoor temperature logger 2 op het M.C. Ooftplein. 76

Figure 26. Mean $LST_{s, max}$ values per land cover class in the Greater Paramaribo Region in the dry and wet season. 77

Figure 27. The pixels that were selected as cold spots in the dry season based on their low $LST_{s, max}$ values and small distance to the city centre. 91

Figure 28. The pixels that were selected as cold spots in the wet season based on their low $LST_{s, max}$ values and small distance to the city centre. 91

List of abbreviations

AI	Aggregation Index
CLHI	Canopy Layer Heat Island
DN	Digital Number
ED	Edge Density
LSI	Landscape Shape Index
LST	Land Surface Temperature
LST _{max}	Maximum Land Surface Temperature
LST _{s, max}	Maximum Standardized Land Surface Temperature
NDVI	Normalized Difference Vegetation Index
NIR	Near InfraRed
OLI	Operational Land Imager
PD	Patch Density
PLAND	Percentage of LANDscape
QA	Quality Assessment
SES	SocioEconomic Status
SUHI	Surface Urban Heat Island
TIRS	Thermal InfraRed Sensor
TOA	Top Of Atmosphere
UHI	Urban Heat Island
UGS	Urban Green Space
USGS	United States Geological Survey
UTM	Universal Transverse Mercator

1. Introduction

1.1. Background and relevance

Currently, from the estimated 7.7 billion people worldwide approximately 55% live in urban environments and this percentage is projected to grow to 68% by 2050 (United Nations, 2019a). This implies that the world population is projected to grow to 9.7 billion by 2050, and urban areas are expected to absorb nearly all of the projected population growth (United Nations, 2019b).

Consequentially, an extra 2.4 billion people are expected to reside in urban areas by 2050 (The Nature Conservancy, 2018). Although climate change is a global process with implications for the entire planet, from a human perspective its impacts are to a large extent experienced in urban environments (Jiménez Cisneros et al., 2014). Insight into these impacts is therefore vital to show to what extent urban population is exposed to future climate risks. Although the expected increase in urban population will enhance human vulnerability in urban environments, it also provides an opportunity to formulate a suitable mitigation plan (Argüeso, Evans, Pitman, & Di Luca, 2015). The role cities play in sustainable development is also acknowledged by international policy through Sustainable Development Goal 11 which targets urban areas and aims to “Make cities and human settlements inclusive, safe, resilient and sustainable” (United Nations, 2015).

The process of urbanisation is inevitably related to the transformation of land from rural to urban land (Yao, Chen, Wei, & Sun, 2015). As a result, a total area of 1.2 million km² is predicted to be urbanised in the coming two decades (The Nature Conservancy, 2018). The transformation of rural to urban use generally reduces green area and increases impervious surfaces. This leads, among other impacts, to a decrease in surface albedo and an altered geometry compared to rural surfaces (Chapman, Watson, Salazar, Thatcher, & McAlpine, 2017). These changes in surface characteristics result in higher temperatures in urban areas than in the surrounding rural areas, a phenomenon that is better known as the Urban Heat Island (UHI) (Luber & McGeehin, 2008; Oke, 1982). Ongoing global warming means temperatures are likely to increase by 1.5°C between 2030 and 2052 (IPCC, 2018). This temperature increase is superimposed on this UHI and has substantial implications on the temperature increase, energy usage, human health, air pollution and greenhouse gas emission in urban environments (Giridharan & Emmanuel, 2018). Ever since the first UHI study of Oke (1982), most studies show that the UHI causes an increase of several degrees of the air temperature in urban-rural transects. As a result, more hot days and heat waves occur in urban areas compared to their rural surroundings (Tan et al., 2010). This increased heat exposure through the UHI is already epidemiologically linked with increased mortality rates in cities, a process that will be exacerbated by the expected global warming (Luber & McGeehin, 2008).

Most of the 21st century global urbanisation is concentrated in the developing world, of which a large part is located in the tropical (23.5 °N and 23.5° S) and sub-tropical zones (up to 30° N and 30°S) (Giridharan & Emmanuel, 2018; United Nations, 2019b). Despite this rapidly growing urban population, processes of local climate change altered by urban growth, such as the UHI, are not well studied in the tropics (Giridharan & Emmanuel, 2018; Perera & Emmanuel, 2018). However, the need for research focusing on the UHI in the tropics is urgent, since a ‘developmental’ transition is visible from excess deaths associated with rainfall to excess deaths related with thermal conditions (Giridharan & Emmanuel, 2018). The contribution of the UHI in combination with the large growth potential of the urban population in the tropics, shows the need to study the nature of the UHI in the tropics.

Studies focussing on the UHI have increased over the past 40 years. During this period, several methods were used to study the associated processes and effects of the UHI. Currently, the most

common technique used is remote sensing (e.g. Du et al., 2019; Marando et al., 2019; Schwarz, Lautenbach, & Seppelt, 2011; Simwanda et al., 2019; Voogt & Oke, 2003). This technique is often used because it enables temperature extraction covering whole rural-urban regions (Anniballe, Bonafoni, & Pichierri, 2014). However, the use of remote sensing for temperature extraction has some limitations. Firstly, by means of remote sensing, it is only possible to extract the land surface temperature (LST) instead of the air temperature, which is the temperature that is experienced by humans. Secondly, LST can only be correctly extracted from satellite images on clear sky days, because clouds interfere with the signals sent and received by the satellite. Air temperature measurements are only obtainable at the location of the measuring device, which means that information about the air temperature is only available in limited places. Therefore, the continuous LST information that remote sensing provides is better suited to study the spatial characteristics of the UHI across an urban environment (**Figure 1**). Since the LST is extracted through remote sensing, the Surface Urban Heat Island (SUHI) is measured, describing the increase in LST across an urban-rural transect, as opposed to the UHI, sometimes also referred to as the Canopy Layer Heat Island (CLHI), which describes the increase in air temperature in the canopy layer across an urban-rural transect (**Figure 1**). Although LST and air temperature strongly correlate, their relation tends to vary across atmospheric conditions, time of day, and land cover types as is also illustrated by **Figure 1** (Balogun & Balogun, 2014; Mutibwa, Strachan, & Albright, 2015; U.S. Environmental Protection Agency, 2008; Voogt, 2007). In previous studies, different indices were used to measure the SUHI in different urban environments. Frequently used SUHI indices are, for example, the difference between the average LST and the maximum LST in a city and the difference in average LST between the urban core and the rural hinterland. These indices should provide similar, however the study of Schwarz et al. (2011) showed that SUHI magnitudes differed due to the use of different indices. For comparability reasons it is therefore recommended to use more than one index (Schwarz et al., 2011).

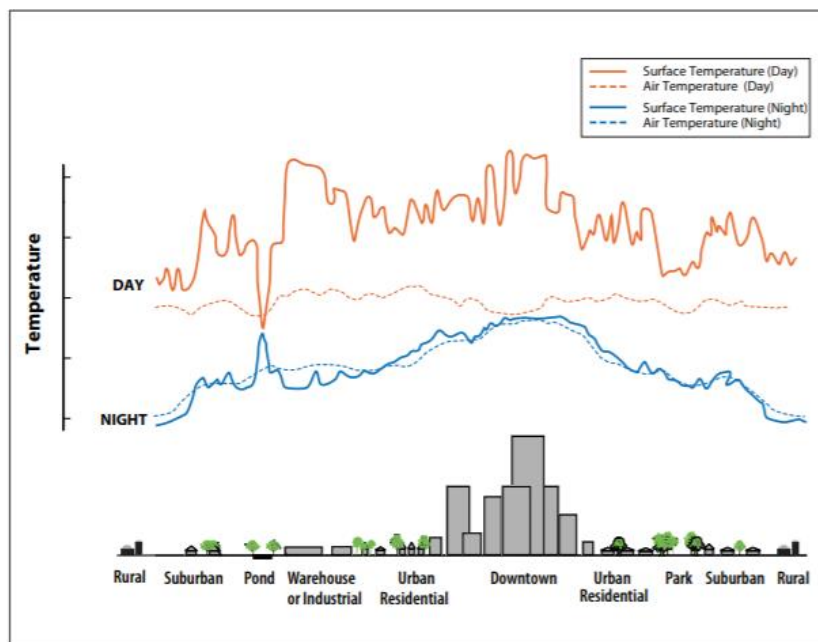


Figure 1. Typical diurnal variations of surface and air temperatures over the urban-rural transect, resulting in the difference between the SUHI and CLHI (U.S. Environmental Protection Agency, 2008).

Previous studies have shown that the UHI intensity varies across an urban area and throughout the day due to the different impact of various surface features on the local temperature (**Figure 1**). An adaptation strategy proposed in previous research to mitigate the increased UHI-related

temperature in urban areas is urban greening (e.g. Bowler, Buyung-Ali, Knight, & Pullin, 2010; Demuzere et al., 2014; Estoque, Murayama, & Myint, 2017; Marando et al., 2019; Wardana, 2015). Increasing Urban Green Space (UGS), which typically includes urban forests, parks, shrubs, lawns, gardens, and street trees, could provide urban cooling mainly through evapotranspiration and shading (Demuzere et al., 2014). This makes urban greening a natural adaptation measure that increases the resilience of urban areas to the environmental threats imposed by global climate change (Du et al., 2019; Jenerette et al., 2007; Marando et al., 2019; Tang, Di, Xiao, Lu, & Zhou, 2017; Wardana, 2015). However, in urban planning there is a trade-off between the costs and benefits of different urban designs and the benefits of UGS in urban centres often are considered less valuable than the economic gain resulting from built-up surfaces (Yu et al., 2017).

Due to the limited space in the hot city centres, it is vital to design UGSs in such a way that they reduce heat most efficiently. Previous research suggests that the type of UGS has the strongest influence on the LST, but acknowledges that the shape and distribution of UGS also contributes to its cooling effect (Du et al., 2019; Estoque et al., 2017; Maimaitiyiming et al., 2014; Marando et al., 2019; Simwanda et al., 2019; Wardana, 2015). Most studies argue that trees are the type of UGS that most effectively cool the surface, mainly because of the high amount of shading (Brown, Vanos, Kenny, & Lenzholzer, 2015; Jaganmohan, Knapp, Buchmann, & Schwarz, 2016; Kong, Yin, James, Hutyra, & He, 2014; Vanos et al., 2012). However, the magnitude of this cooling effect is found to be dependent on local atmospheric conditions such as the overcast ratio. Regarding the effect of size, distribution and shape of UGSs on their cooling effect, most previous studies point out that large, aggregated UGSs provide the strongest cooling effect (Cao, Onishi, Chen, & Imura, 2010; Huang, Cui, & He, 2018b; Jaganmohan et al., 2016). However, the study of Kong et al. (2014) shows that multiple disaggregated UGSs are more beneficial for cooling. Studies are also contradicting regarding the influence of the shape of UGSs on the cooling effect. Therefore, it is important to further investigate the influence of both composition and configuration on the cooling effect of UGS. Spatial class metrics are most commonly used to study the influence of different configurations and distribution patterns within the urban green city structure.

Most research focuses on the effect of land use characteristics on the UHI. In addition, research of Tang et al. (2017) and Jenerette et al. (2006) point out that the UHI is a complex phenomenon that is also influenced by socioeconomic factors such as income. This influence is mainly indirect due to the correlation income has with impervious surface and vegetation. As income increases in neighbourhoods, vegetation tends to increase and impervious surface tends to decrease (Jenerette et al., 2007; Tang et al., 2017). This indirect relationship between socioeconomic factors and the UHI could provide useful information for urban planners. However, this relationship has not yet been well studied in cities in the Global South.

Previous research points out that one of the main reasons for the low level of knowledge about UHI distribution across urban environments in the tropics is the lack of available data, both in terms of the spatial distribution of land cover types and of the influence of land cover types on the local temperature (Amorim, 2018; Balogun & Balogun, 2014; Ojeh, Balogun, & Okhimamhe, 2016; Perera & Emmanuel, 2018). Since the influence of land cover on the local temperature is not well studied in the tropics, there also exists a knowledge gap on the cooling potential of different UGS types during the wet and dry season in tropical cities (Giridharan & Emmanuel, 2018; Perera & Emmanuel, 2018). This unique seasonal characteristic of the tropical climate has serious impacts on the leaf and flowering characteristics of plants which in turn determines their cooling potential. On top of this, a plant's cooling potential is also modulated by humidity and therefore may vary greatly between wet and dry season (Balogun & Balogun, 2014; Barradas, 1991; North Carolina Climate Office, n.d.; Ojeh

et al., 2016; Tan et al., 2010; Tropenbos Suriname, 2019; Zhang, Lv, & Pan, 2013). As a result, in the tropics the wet and dry seasons may not show a constant relationship between air and surface temperature. So, it is known that there is a "cooling effect" due to UGS, but the magnitude of this, as well as its influencing factors, are not yet understood in the tropics (Tropenbos Suriname, 2019).

Therefore, this study focuses on the influence of both the composition and configuration of UGS on the LST in a tropical city using remote sensing images. This is based on a case study of Paramaribo in Suriname since this city experiences a typical tropical climate including a wet and dry season. Furthermore, this study will facilitate valuation of the important urban ecosystem services provided by UGS, since these are usually undervalued in urban planning efforts within most cities in the global South (Tropenbos Suriname, 2019).

1.2. Research aim

The aim of this research is to provide an analysis of the UHI effect in the whole rural-urban region of Paramaribo and of the cooling effect of UGS in both the wet and dry seasons based upon LST.

This study investigates the SUHI by comparing the temperature differences between the urban centre (the administrative boundary) of Paramaribo and its rural hinterland (the Greater Paramaribo Region) (**Figure 2**). Furthermore, this study analyses the relationship between LST and land cover type. In this land cover-based analysis the main focus is on the influence of different types of UGS within the administrative boundary during the wet and dry season to study the difference in cooling effect between the two seasons. This analysis includes the influence of UGS composition as well as the influence of UGS configuration on the cooling effect. Distances from thermal centres such as the city centre, the river and the ocean are also considered in this study. Due to the different atmospheric conditions and vegetation types present in the tropics, compared to those in cities within the more commonly studied temperate zone, fieldwork is implemented in this research. The fieldwork creates a better understanding of the differences in UGS and Socioeconomic Status (SES) across Paramaribo. The relationship between the LST and air temperature is analysed to complete the study. So, a city-wide study with information on the cooling effect in wet and dry season is provided that can be used in future city planning of Paramaribo. This will provide valuable information for urban planners, not only in Paramaribo but also in other tropical cities, about what steps can be taken to optimally design their urban green structure to lower the temperature in their city.

The research aim is divided in the following research sub-objectives:

1. Identify the spatial distribution of LST and UGSs in the Greater Paramaribo Region in the wet and dry season.
2. Identify the UHI effect within the city of Paramaribo in the wet and dry season.
3. Identify relationships of LST with UGS and socioeconomic status in the city of Paramaribo in the wet and dry season.
4. Identify the relationship of LST with air temperature in the wet and dry season.
5. Analyse the differences in observed cooling effect of UGS within the wet and dry season.

1.3. Research questions

To achieve the research objectives set in section 1.2. the following research questions need to be answered.

Research question: What is the UHI effect in the tropical city of Paramaribo, and what is the cooling effect of UGS on the urban temperatures during the wet and dry season?

Sub questions:

1. *Sub-objective:* Identify the spatial distribution of LST and UGS in the Greater Paramaribo Region in the wet and dry season.
 - a. What is the spatial distribution of LST in the Greater Paramaribo Region?
2. *Sub-objective:* Identify the UHI effect of the city of Paramaribo in the wet and dry season.
 - a. What do different indicators for the SUHI report on the UHI effect in Paramaribo?
3. *Sub-objective:* Identify relationships between LST and the composition and configuration of UGS in the city of Paramaribo in the wet and dry season.
 - a. What is the relationship of LST with NDVI?
 - b. What is the relationship of LST with the different classified types of urban green, based on a classified Sentinel green cover map?
 - c. What is the relationship of LST with the configuration of UGS, based on classified Sentinel green cover map?
 - d. What are the influences on LST of the distance to the urban centre, the Atlantic Ocean and the Suriname River?
 - e. What are the characteristics of typical green features, cold spots and neighbourhoods differing in socioeconomic status in the city of Paramaribo and how do they relate to the LST?
4. *Sub-objective:* To identify the relationship between LST and air temperature in the wet and dry season.
 - a. What is the relationship between air and LST on different types of UGS?
 - b. What is the relationship between the urban-rural LST difference and the urban-rural air temperature difference?
5. *Sub-objective:* To analyse the differences in observed cooling effect of UGS within the wet and dry season.
 - a. Is there an observed cooling effect of UGS in both wet and dry season?
 - b. In what way does this cooling effect differ between wet and dry season?

2. Materials and methods

2.1. Case study description

2.1.1. Study Area

The study area, Paramaribo (5° 50' 21.8328" N and 55° 11' 56.7204" W), is the capital of Suriname. Suriname is located on the north-eastern coast of South America and has a population of approximately 575,000, of which more than half live in Paramaribo and its surroundings (The World Bank, 2018; Tropenbos Suriname, 2019). The city of Paramaribo is situated along the northern coast of Suriname just west of the estuary of the Suriname river in the Atlantic Ocean. Paramaribo covers

an area of approximately 174 km². The surrounding area of the city, the Greater Paramaribo Region, includes the districts Paramaribo, Wanica, and part of Commewijne, and covers approximately 863 km² (**Figure 2**) (Fung-Loy, Van Rompaey, & Hemerijckx, 2019). The urban pull effect of the city of Paramaribo on rural populations has resulted in a population increase of 14% in the Greater Paramaribo Region in the period from 2000 to 2015, with a total conurbation of Paramaribo of around 380,000 inhabitants (Fung-Loy et al., 2019). The population increase resulted in a largely unplanned and uncontrolled urban sprawl. Suriname lacks the needed coherent system of land registration, finances, technology, data, and expertise within the government to adequately oversee this spatial planning (Fung-Loy et al., 2019; Verrest, 2010). Due to this somewhat incoherent governing system no proactive urban green policy is in place in Paramaribo (oral communication workshop 'Beboste en Urbane Landschappen: naar een climate smart Suriname', dd 26 November 2019).

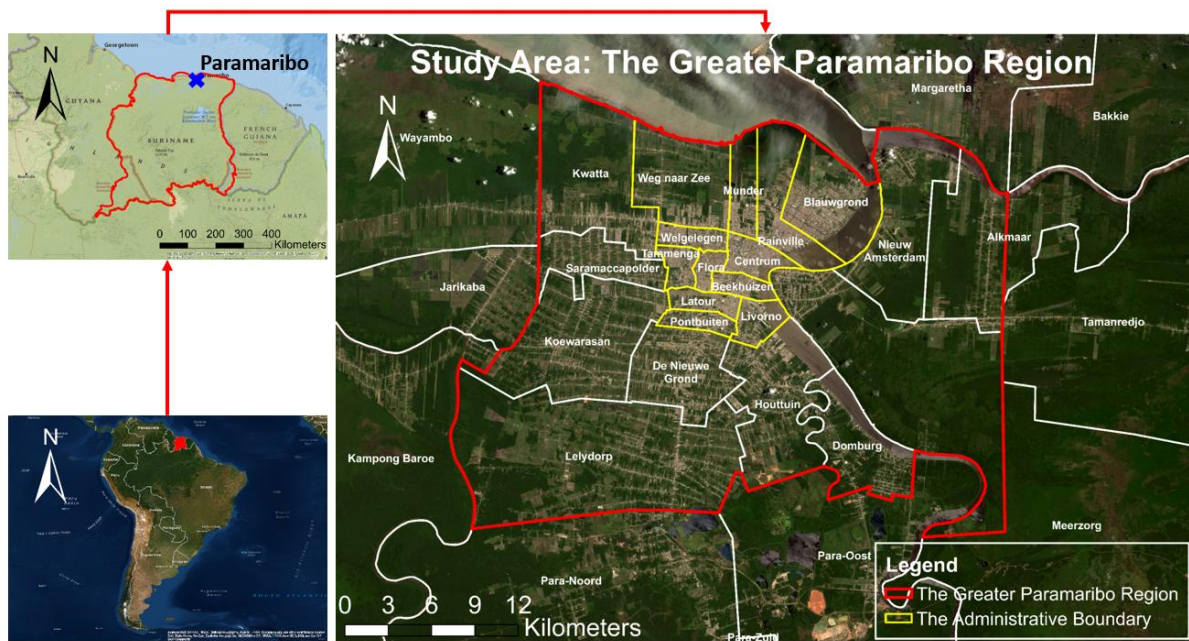


Figure 2. Lower left: The location of Suriname in South America. Upper left: The location of Paramaribo in Suriname. Right: The Study area: The administrative boundary of Paramaribo (yellow) and its surrounding Greater Paramaribo Region (red) including all its districts (white).

Suriname is situated in the inter tropical convergence zone and is therefore experiencing an Af-tropical rainforest climate according to the Köppen climate classification system. This leads to the fact that Suriname experiences four seasons, namely (GBS, 2016):

1. The short rainy season (early December to late January).
2. The short dry season, (early February to mid-April).
3. The rainy season, (mid-April to mid-August).
4. The dry season, (mid-August to early December).

The months with the lowest levels of precipitation are September and October and the months with the highest levels of precipitation are May and June (GBS, 2016). This is also seen in **Figure 3**, which shows the monthly precipitation values for the years 2011-2015 in millimetres. The annual average temperatures in Suriname are between 26°C and 28°C, and do not vary considerably throughout the seasons (**Figure 3**). Through global warming, an average temperature rise of 0.3 to 1.3°C every 10 years is projected (Tropenbos Suriname, 2019).

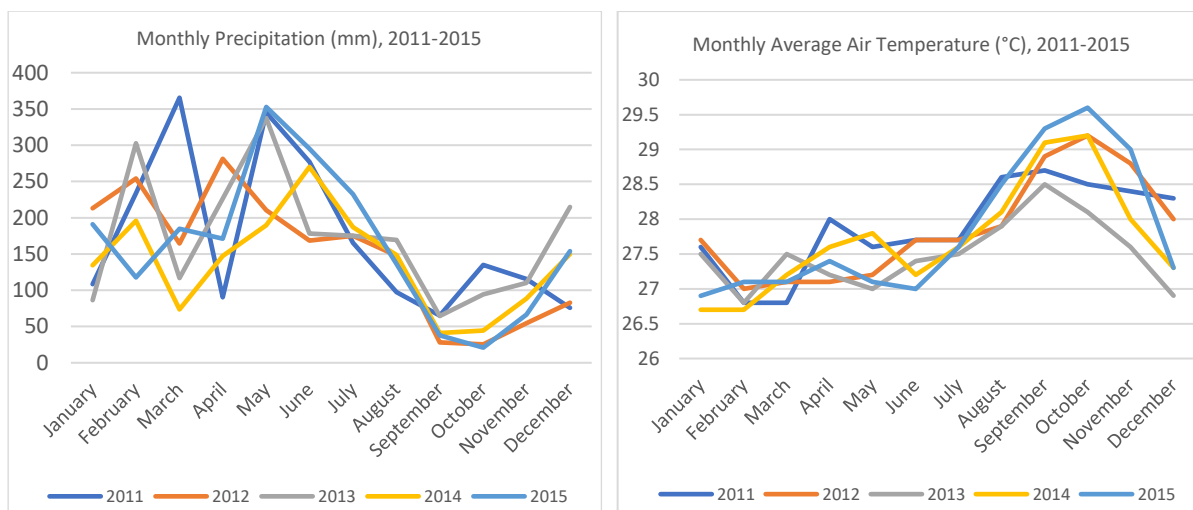


Figure 3. Monthly precipitation values in mm in Suriname from 2011 to 2015 (left), monthly average air temperatures in °C in Suriname from 2011 to 2015 (right) (GBS, 2016).

2.1.2 Project: Towards a Green and more Liveable Paramaribo

This study is part of the project “Towards a Green and more Liveable Paramaribo”, which is a twinning project, sponsored by the UTSN twinning facility. The project is run by the knowledge based non-governmental organization Tropenbos Suriname and the Faculty of Geo-information Science and Earth Observation of the University of Twente (UT-ITC) in the Netherlands. The goal of that project is to promote a green Paramaribo in which ecosystem services contribute to a healthy and more liveable environment for its inhabitants (Tropenbos Suriname, 2019). The project believes that UGS is undervalued and not included within the planning of the city of Paramaribo. This undervaluation of UGS in combination with the rising demand for built-up surfaces, leads to an increased replacement of UGS by built-up surfaces. To alleviate this trend, the “Towards a Green and more Liveable Paramaribo” project wants to create more awareness of the benefits that UGS provides among the residents of Paramaribo. One of these benefits is the cooling effect that UGS provides. More insight into this cooling effect in the recently warming climate can provide valuable information for planners in the city of Paramaribo.

2.2. Data

Most of the data used in this study consisted of secondary data and are summarised in

Table 1. Aside from the satellite data, most of the data was obtained through the overarching project. The primary data used in the study was obtained during fieldwork. This fieldwork data consisted of detailed descriptions of several selected UGSs and was produced by means of ground truthing.

Table 1. Secondary data used in this study.

Data	Format	Data Source
Landsat 8 OLI/TIRS imagery	Raster	(USGS, 2019)
World imagery base map	Raster	(Esri, 2018)
Land cover map	Raster	(Taus, 2019)
Administrative boundary	Vector	(Tropenbos Suriname, 2019)
Greater Paramaribo region	Vector	(Tropenbos Suriname, 2019)
Road network	Vector	Open street map
River network	Vector	Open street map
Air temperature data of outdoor temperature loggers	Table	(Kalpoe, 2019)
Air temperature data stations	Table	Meteorological Service Suriname
Socioeconomic status neighbourhoods	Raster	(Fung-Loy et al., 2019)

2.2.1. Satellite imagery

The satellite images used in this study, summarized in **Table 2**, are from the Landsat 8 OLI/TIRS (Operational Landsat Imager/Thermal Infrared Sensor) satellite and were obtained from the United States Geological Survey (USGS). The Landsat 8 OLI/TIRS satellite is the most recently launched Landsat satellite and resultingly the most used in recent remote sensing studies that assess the UHI effect (e.g. Amorim, 2018; Estoque, Murayama, & Myint, 2017; Marando, Salvatori, Sebastiani, Fusaro, & Manes, 2019; Mushore et al., 2018; Richard et al., 2018; Simanjuntak, Kuffer, & Reckien, 2019). The satellite images used for this study are all geometrically corrected by the USGS. They are also georeferenced to the WGS1984 datum and Universal Transverse Mercator (UTM) Zone 21N coordinate system. As a result, all the vector datasets obtained and created in this study were projected into the UTM Zone 21N. In this study, 30m resolution Landsat 8 OLI/TIRS images were downloaded from the USGS website for the area of Paramaribo (pat/row 229/056, WGS84 UTM21 S reference system). The thermal bands 10 and 11 of the Landsat 8 OLI/TIRS satellite originally have a spatial resolution of 100 meters, but these bands have been resampled to 30m resolution by the USGS (U.S. Geological Survey, 2019).

To investigate the difference in cooling effects of urban green between dry and wet season, four images obtained in the dry season (Mid-August to early December) and three obtained in the wet season (mid-April to mid-August) were selected. Only images that originate from the last five years were selected, because it can be assumed within reason that the vegetation cover of the study area has not changed drastically within this period. Finally, cloud coverage was the determining criterion for selecting the satellite images. Cloud coverage over the study area needed to be limited to a minimum to ensure valid and reliable information extraction of the earth's surface (Tseng, Tseng, & Chien, 2008). A common threshold for maximum cloud coverage is ten percent (Simwanda et al., 2019; Wardana, 2015). Within the dry season, the four images were selected with the least cloud cover over land. These images had a cloud coverage of well below ten percent and were evenly distributed over a period of four years, from October 2015 to October 2019. However, within the wet season, the only three available images with acceptable and workable cloud cover over the study area were selected. The details of these Landsat images are shown in **Table 2**. Note that although some of the images obtained in the wet season had substantially high cloud coverage on land, well over ten percent, the cloud cover above the study area was sufficiently low.

Table 2. Details of Landsat 8 OLI/TIRS imagery used.

Scene ID	Cloud coverage on land (%)	Acquisition date	Acquisition time	Season
LC82290562015288LGN02	1.02	15 October 2015	13:58:11	Dry
LC82290562016275LGN01	2.83	01 October 2016	13:58:25	Dry
LC82290562018264LGN00	3.80	21 September 2018	13:57:50	Dry
LC82290562019251LGN00	5.62	08 September 2019	13:58:25	Dry
LC82290562016211LGN01	20.76	29 July 2016	13:58:11	Wet
LC82290562017165LGN00	23.57	14 June 2017	13:57:53	Wet
LC82290562018216LGN00	26.28	04 August 2018	13:57:31	Wet

2.2.2. Land cover map

The land cover map used in this study shown in **Figure 4** was produced within the project (Taus, 2019). It was produced based on a 10m resolution, cloud free Sentinel 2 image. The image was classified into 8 different land cover classes, using the support vector machine classifier in QGIS. The classification was based on 313 training sample polygons created using high-resolution drone imagery from March 2019 in combination with Google Earth imagery for 2019. An accuracy assessment on the basis of 230 ground truthing polygons, resulted in an overall accuracy of 84%. The maps shown in **Figure 4** show the eight different land cover types according to

Table 3 for two different areas (Greater Paramaribo Region versus administrative boundary). All the obtained Landsat information was clipped to the Greater Paramaribo Region for further analysis.

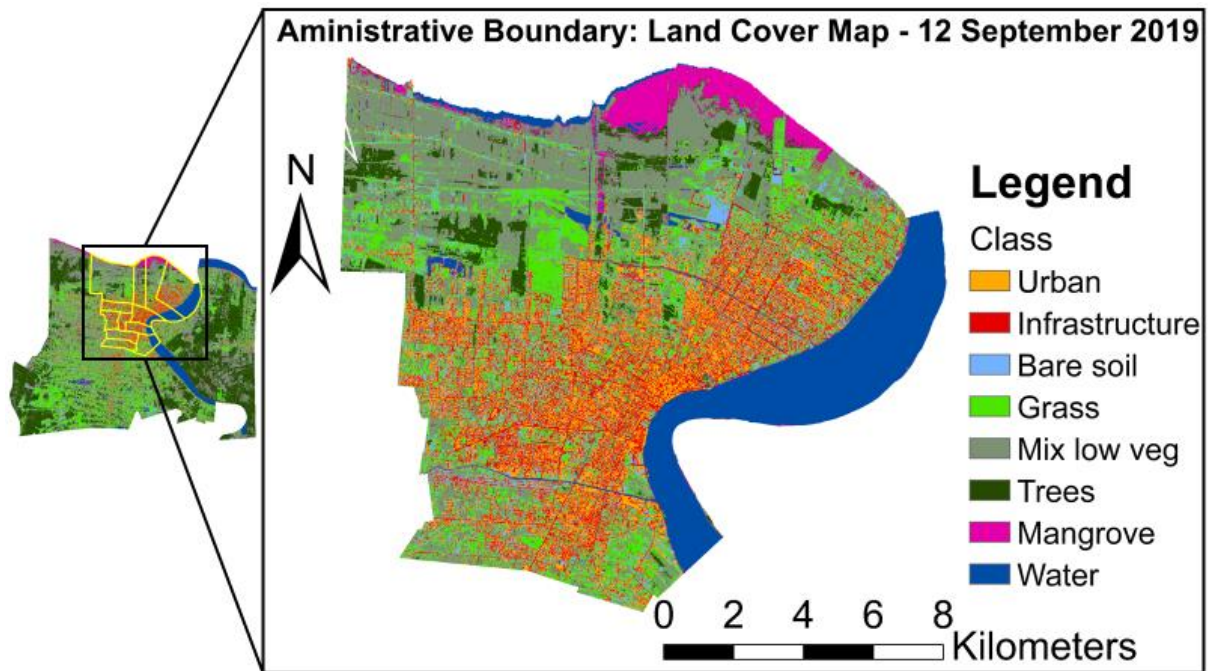


Figure 4. Land cover maps of the Greater Paramaribo Region (left) and the administrative boundary (right) on 12 September 2019.

Table 3. Area covered per land cover type in the Greater Paramaribo Region and the administrative boundary

Land cover	The Greater Paramaribo Region		Administrative Boundary	
	Area (km ²)	Proportion	Area (km ²)	Proportion
Urban	39.77	5%	22.11	13%
Infrastructure	47.02	5%	24.72	14%
Bare soil	66.03	8%	19.34	11%
Grass	180.27	21%	29.67	17%
Mixed low vegetation	244.90	28%	39.03	22%
Trees	220.92	26%	8.57	5%
Mangrove	10.86	1%	6.50	4%
Water	53.16	6%	23.57	14%
Total	862.93	100%	173.51	100%

2.2.3. Neighbourhood SES classification

The SES of different neighbourhoods across Paramaribo was retrieved from a 30m resolution raster provided by Fung-Loy et al. (2019), that divided the administrative boundary of Paramaribo in neighbourhoods classified on their SES. The factor used by Fung-Loy et al. (2019) to represent SES in this study was the type of dominant residential class present in a neighbourhood. As a result the SES was divided into four residential classes: rich, middle, middle to low and poor (**Figure 5**) (Fung-Loy et al., 2019). The spatial criteria upon which the four residential classes were based are shown in

Table 4.

Residential Class of Neighbourhoods in Paramaribo - 2015

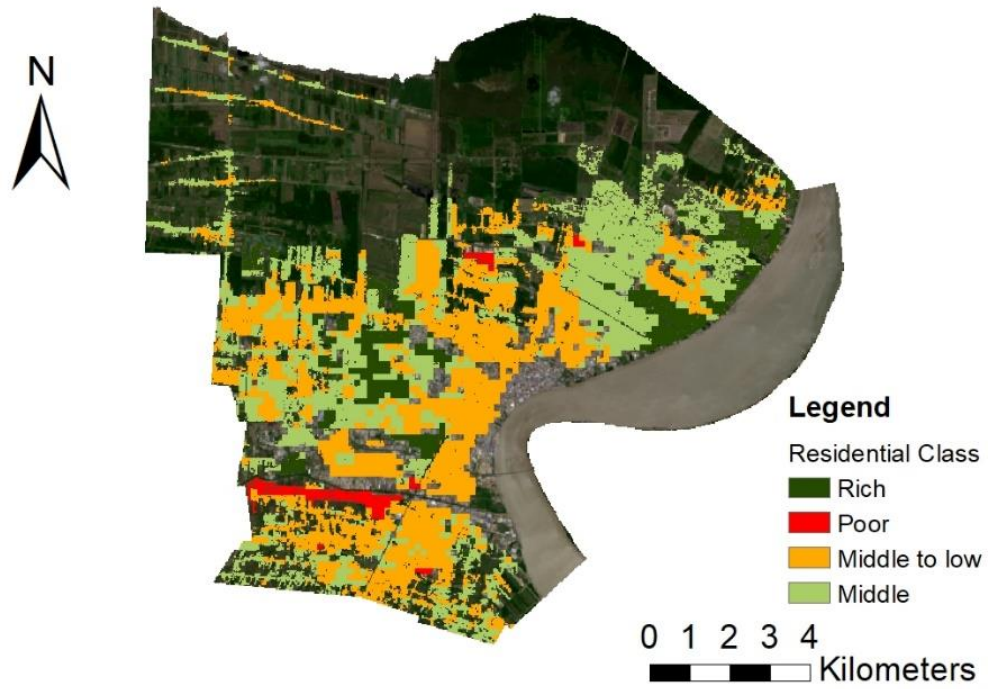


Figure 5. Neighbourhoods in Paramaribo sorted by SES based on residential class (Fung-Loy et al., 2019).

Table 4. Distinction between residential groups, based on spatial criteria (Fung-Loy et al., 2019).

Criteria	Rich	Middle	Middle to low	Poor
Average size of plot	> 600 m ²	350 < plot < 600 m ²	300 < plot < 350 m ²	< 300 m ²
Average size of house	> 300 m ²	150 < house < 300 m ²	100 < house < 150 m ²	< 100 m ²
Street type	Asphalt	Asphalt/street tiles	Asphalt/street tiles/sand	Sand (narrow)/no street
Private swimming pool	Yes	No	No	No
Clear demarcation of plot	Yes	Yes	Yes	No

2.3. Temperature extraction

2.3.1. Cloud correction

Remaining cloud cover present on the Landsat images were removed via cloud removal using the Landsat Quality Assessment (QA) ArcGIS Toolbox which removes clouds, cirrus clouds and cloud shadows on the basis of information in the quality assessment band of the Landsat 8 satellite (Roy et al., 2002; U.S. Geological Survey, 2017). The light clouds that still remained after usage of the QA Toolbox were removed manually to create satellite images which were as cloud-free as possible. This was a process based on visibility, in which polygons were manually drawn over pixels covered with clouds. Afterwards these polygons were erased from the Landsat satellite images, leaving only cloudless surface pixels. On the satellite images that were taken in the wet season, the extra manually erased pixels could amount to about thirty thousand pixels (~3%). However, after the manual LST extraction, the created LST maps still showed patterns of colder temperatures around clouds that had previously been removed. These 30m x 30m cells were probably only partly covered by clouds and therefore not identified as clouds by neither the Landsat QA toolbox nor the manual method. Therefore, to get rid of these edge effects, an additional cloud removal method was performed. This was done with the use of a threshold method that erased pixels with an LST value below a certain threshold value of the image. This threshold value was increased until a pixel was erased that was not situated at the edge of a removed cloud, so that the surface cooling pattern was not affected. This threshold method deleted fewer extra pixels than the manual method, but it was still around fifteen thousand pixels (~1.5%) for some images in the wet season.

2.3.2. Atmospheric corrections and radiometric calibrations

The electromagnetic radiation received by the Landsat satellite is typically a mixture of two kinds of energy. It is a mixture of the reflectance of the earth's surface, in which we are interested, and of reflectance of the atmosphere itself (Themistocleous & Hadjimitsis, 2008). Therefore, atmospheric corrections were applied to correct for the different atmospheric conditions present at the different dates of the satellite images. In this process, Digital Number (DN) values of thermal band 10 were converted into Top Of Atmosphere (TOA) spectral radiance values (1) (Amorim, 2018; Estoque et al., 2017; Marando et al., 2019; U.S. Geological Survey, 2019). Only thermal band 10 is used in this study for the LST extraction since on Jan. 6, 2014, the U.S Geological Survey state in an TIRS calibration notice that it is recommended to use Band 10 instead of Band 11 due to larger calibration uncertainty associated with TIRS Band 11 (U.S. Geological Survey, 2014). Subsequently, TOA radiance values were used to derive the TOA brightness temperature (2). TOA brightness temperature assumes that the earth is a blackbody and so has an unity emissivity (Chander, Markham, & Helder, 2009; Estoque et al., 2017). This derivation was done using prelaunch calibration constants (Chander et al., 2009; U.S. Geological Survey, 2019). The conversion of DN values into TOA planetary spectral reflectance is the second atmospheric correction that was done before the LST could be extracted

(3) (U.S. Geological Survey, 2019; Wardana, 2015). All calculations were performed using the raster calculator in ArcGIS Desktop.

- Conversion of DN values into TOA spectral radiance (U.S. Geological Survey, 2019):

$$L_{\lambda} = M_L \times Q_{cal} + A_L \quad (1)$$

Where:

- L_{λ} = TOA spectral radiance ($W/(m^2 * sr * \mu m)$)
- M_L = Radiance multiplicative scaling factor for the band ($W/(m^2 * sr * \mu m)$)
(RADIANCE_MULT_BAND_n from the Landsat metadata)
- Q_{cal} = Quantified and calibrated pixel value of the standard product (DN)
- A_L = Radiance additive scaling factor for the band ($W/(m^2 * sr * \mu m)$)
(RADIANCE_ADD_BAND_n from the Landsat metadata)

- Conversion of TOA spectral radiance to TOA brightness temperature (U.S. Geological Survey, 2019):

$$T_B = \frac{K_2}{\ln\left(\frac{K_1}{L_{\lambda}} + 1\right)} \quad (2)$$

Where:

- T_B = TOA brightness temperature (K)
- L_{λ} = TOA spectral radiance ($W/(m^2 * sr * \mu m)$)
- K_1 = Band-specific thermal conversion constant from the Landsat metadata
($W/(m^2 * sr * \mu m)$)
(K1_CONSTANT_BAND_x, where x is the thermal band number)
- K_2 = Band-specific thermal conversion constant from the Landsat metadata (K)
(K2_CONSTANT_BAND_x, where x is the thermal band number)

- Conversion of DN values to TOA planetary spectral reflectance (U.S. Geological Survey, 2019).

$$\rho_{\lambda} = \frac{(M_{\rho} \times Q_{cal} + A_{\rho})}{\sin(\theta_{SE})} \quad (3)$$

Where:

- ρ_{λ} = TOA planetary spectral reflectance (unitless)
- M_{ρ} = Reflectance multiplicative scaling factor for the band (unitless)
(REFLECTANCEW_MULT_BAND_n from the metadata)
- Q_{cal} = Quantified and calibrated pixel value of the standard product (DN)
- A_{ρ} = Reflectance additive scaling factor for the band (unitless)
(REFLECTANCE_ADD_BAND_n from the metadata)
- θ_{SE} = Local sun elevation angle (degrees)

2.3.3. LST extraction

To derive the LST from the satellite images, the TOA brightness temperature needed to be adjusted based on surface emissivity (7) (Estoque et al., 2017; Simwanda et al., 2019; Sobrino, Jiménez-Muñoz, & Paolini, 2004; Wardana, 2015). The emissivity was obtained using the NDVI Threshold

Method, which bases emissivity on NDVI value (4) (5) (6) (Sobrino et al., 2004). This method considers pixels with an NDVI value < 0.2 as bare soil, resulting in an emissivity value of 0.97. Pixels with an NDVI value > 0.5 are considered to be completely vegetated and are assigned an emissivity value of 0.99. Pixels with an NDVI value equal or in between 0.2 and 0.5 are considered to have a land cover containing both bare soil and vegetation.

- The resulting emissivity of these pixels with $0.2 \leq NDVI \leq 0.5$ was obtained using the following equation:

$$\varepsilon = 0.004P_v + 0.986 \quad (4)$$

Where:

$$P_v = \left(\frac{NDVI - NDVI_{min}}{NDVI_{max} - NDVI_{min}} \right)^2 \quad (5)$$

Where:

$$NDVI = \frac{\rho_{NIR} - \rho_{Red}}{\rho_{NIR} + \rho_{Red}} \quad (6)$$

Where:

- ε = Land surface emissivity (unitless)
- P_v = Vegetation proportion (unitless)
- $NDVI_{max}$ = 0.5 (unitless)
- $NDVI_{min}$ = 0.2 (unitless)
- ρ_{NIR} = TOA spectral reflectance value in Near Infrared Band 5 (unitless)
- ρ_{Red} = TOA spectral reflectance value in Red Band 4 (unitless)

- Conversion of brightness temperature to LST (Artis & Carnahan, 1982; Estoque et al., 2017; Marando et al., 2019; Simwanda et al., 2019; Wardana, 2015)

$$LST = \frac{T_B}{1 + (\lambda \times T_B / \rho) \ln \varepsilon} - 273.15 \quad (7)$$

Where:

- LST = Land surface temperature (°C)
- T_B = Landsat 8 Band 10 brightness temperature (K)
- λ = Wavelength of emitted radiance = 10.8 (μm), the centre wavelength of Landsat 10
- ρ = hc/σ (1.438×10^{-2} mK)
- h = Planck's constant (6.626×10^{-34} Js)
- c = Velocity of light (2.998×10^8 m/s)
- σ = Boltzmann's constant (1.38×10^{-23} J/K)

2.3.4 LST standardization and seasonal composition procedure

To ensure comparability and better establishment of the SUHI between satellite images obtained during different months and weather conditions, the LST maps were standardized (8) (Walawender, Szymanowski, Hajto, & Bokwa, 2014). Technically, standardization of a LST raster determines by how many standard deviations the LST value of every pixel lies above or below the mean LST value of the whole LST raster sample (Walawender et al., 2014). Therefore, in this study the standardized LSTs were calculated by the following equation:

$$LST_s = \frac{LST_x - LST_\mu}{LST_\sigma} \quad (8)$$

Where:

- LST_s = The standardized LST pixel value (°C)
- LST_x = The LST pixel value (°C)
- LST_μ = The mean LST of the Greater Paramaribo Region (°C)
- LST_σ = The standard deviation of the LST raster of the Greater Paramaribo (°C)

After standardization, the distribution of every LST_s raster was characterized by a mean value of 0 and a standard deviation of 1 (Walawender et al., 2014). This conversion to LST_s meant that the LST values of all the seven individual images were shown in comparison to the mean sample LST on that particular day. This increased the comparability of the cooling effect of the separate images. Standardisation enabled the possibility to create seasonal composites that formed a general representation per season. The seasonal composites were also created to cope with the high cloud coverage on the satellite images in the wet season. The removal of the high cloud coverage resulted in three highly disrupted LST maps, which are shown in Appendix 1 and 2. So, to perform a sufficient analysis on the cooling effect, these three LST_s were combined in a composite to create a more continuous LST_s raster.

These LST_s seasonal composites of the wet and dry season were created by selecting the maximum LST_s value of all the inputs for each pixel location using the Maximum function in cell statistics in ArcGIS Desktop. The Maximum function was used because some cloud edge pixels containing low LST_s remained even after removal of the cloud edge effects in the three images of the wet season. As a result, an edge effect pixel value only prevailed in the outcoming raster if that edge effect pixel value was the only pixel value present on that particular location in all of the input rasters. Consequentially, the influence of cloud pixels was minimized in the resultant seasonal $LST_{s, \max}$ rasters. These $LST_{s, \max}$ rasters together with the classified land cover map formed the basis of this research.

2.4. Analysis

2.4.1. Analysis of the SUHI effect

The SUHI was analysed on two different scales. First, in the Greater Paramaribo Region to show the LST developments between the city core and the rural hinterland (Appendix 1). Secondly, the SUHI was analysed within the administrative boundary, to show the intra-SUHI of the city of Paramaribo (Appendix 2).

On the basis of LST_{\max} values per land cover type, the SUHI effect was scaled using the most reported SUHI indicators in literature (Schwarz et al., 2011; Schwarz, Schlink, Franck, & Großmann, 2012). These indicators are summarized in **Table 5**. We followed the procedure as reported by the referenced studies closely, with the following exceptions. First, in the referenced studies in **Table 5** the mean LST value per land cover type of one satellite image was used for all of the mentioned indicators. However, in this study the mean LST_{\max} value was used instead, since seasonal composites were used to calculate the SUHI indicators as opposed to a single satellite image. Secondly, in this study a distinction was made between urban land cover and infrastructure, while in some of the referenced studies this difference was absent. In these studies, a combined built-up land cover class was used instead, which served as the urban land cover class needed to calculate

the several indicators that use urban temperatures. Therefore, for comparison reasons, in this study the SUHI indicators that include “urban” temperatures, were once calculated by only using the land cover type urban, and once by using a reclassified and combined land cover class termed “built-up” (combination of urban and infrastructure).

Table 5. SUHI indicators used in this study.

Indicator	Units	Quantification	Related references
Difference urban - other	K	Difference in mean LST _{max} between urban area and all other areas	(Dousset & Gourmelon, 2003), (Gallo et al., 1993), (Tomlinson, Chapman, Thornes, & Baker, 2012) (Zhou, Li, & Yue, 2010)
Difference urban - water	K	Difference in mean LST _{max} between urban area and water surface	(Chen, Zhao, Li, & Yin, 2006)
Difference core - rural	K	Difference in mean LST _{max} between urban core (> 67% urban land use in 9 km ²) and rural areas (< 25% urban land use in 25 km ²) in the Greater Paramaribo Region	(Verburg, van Berkel, van Doorn, van Eupen, & van den Heiligenberg, 2010)
Hot island area	km ²	Area with LST _{max} higher than the mean plus one standard deviation	(Zhang & Wang, 2008)
Magnitude	K	Difference between maximum and mean of LST _{max}	(Rajasekar & Weng, 2009)
Micro-UHI	%	Percentage of area (without water surfaces) with LST _{max} higher than the warmest LST _{max} associated with tree canopies	(Aniello, Morgan, Busbey, & Newland, 1995)
Standard deviation	K	Standard deviation of LST _{max}	(Schwarz et al., 2011)

Note: All LST_{max} values, except for the rural LST_{max}, were measured within the administrative boundary.

After the Greater Paramaribo Region SUHI was analysed, the intra-SUHI within the administrative boundary was analysed to study the cooling effect of UGSs. A non-parametric Kruskal-Wallis test was performed on the LST_{s, max} values per land cover class, to assess whether LST_{s, max} values were significantly different across different land cover types. The Kruskal-Wallis test was chosen to ensure robustness. Results of this statistical test were adjusted by the Bonferroni correction for multiple tests. To check if the LST_{s, max} per land cover type significantly differed between the wet and dry season, a non-parametric Wilcoxon signed-rank test was performed. All statistics in this study were performed using IBM SPSS Statistics 25, on a randomly taken sample of raster pixel values created with the CLUE modelling framework file converter 3 (Verburg & Overmars, 2009). A minimum distance of 90 meters between sample pixels was used in the sample to reduce autocorrelation and ensure independency.

2.4.2. Analysis of the cooling effect of UGS

2.4.2.1. The relationship between the LST and NDVI

In previous research focusing on the relationship between LST and green vegetation, green vegetation is mostly represented by NDVI (e.g. Anniballe et al., 2014; Cui & Shi, 2012; Estoque et al., 2017; Simanjuntak et al., 2019; Wardana, 2015). Thus, the relationship between LST and NDVI is of interest, as NDVI is a fast and easily applicable measure that reflects the intensity of green in a landscape. The relation analysis between LST and NDVI was performed twice, once on a random sample of pixels taken from the administrative boundary and once on a random sample taken from the administrative boundary after water surface was excluded. This was done because NDVI values range from -1 to 1, increasing with the greenness of the landscape. Negative values and values close to zero generally correspond to barren or constructed areas, while low positive values generally represent shrub and grassland. High values approaching one indicate very dense green land cover, such as temperate and tropical rainforest. However, the lowest NDVI values approaching -1 (very

low intensity of green) generally correspond to water (Sentinel Hub, n.d.). This is due to the fact that water has a relatively low reflection in both the near infrared spectral band and the red spectral band. The main aim of this study is to explore the relationship between UGSs and LST, this relationship, using NDVI as an indicator for UGS, showed that in general UGSs have a high NDVI value and a low LST. Since water, like UGS, in general has a low LST but unlike UGS, it has a very low NDVI, water interfered strongly with the correlation between LST and NDVI, when NDVI was used as an indicator of UGS. (Cai, Han, & Chen, 2018; Zhang, Estoque, & Murayama, 2017). As a result, a substantial amount of low LST values also corresponded with water (low NDVI values), while we were mainly interested in the relationship between UGS (high NDVI values) and LST.

A Pearson's correlation analysis was performed to test for a statistically significant relationship between the LST and NDVI and to measure the strength of this relationship. A linear regression analysis was conducted to describe the impact of a unit NDVI change on the $LST_{s, \max}$. The correlation and regression were performed on a random sample, with a minimal distance of 90 meters between the sample points.

2.4.2.2. The relationship between the LST and land cover type

In this study of the relationship between UGS and the SUHI, landscape metrics were used to study the composition and configuration of UGS in the landscape. (Du et al., 2019; Li, Zhou, & Ouyang, 2013; Maimaitiyiming et al., 2014; Simanjuntak et al., 2019). The landscape metrics of different land cover classes were calculated from the classified land cover map shown in **Figure 4**, using Fragstats 4.2 (McGarigal, Cushman, & Ene, 2012).

The influence of the eight different land cover classes on the LST was studied using the Percent of Landscape (PLAND) metric. PLAND is a class metric, describing how much area of a landscape is covered by a certain class (McGarigal, 2015). This metric generated land cover density maps, using a moving window method with a circular kernel for a certain radius around a pixel. The PLAND metric was used instead of the pixel land cover type, because with the PLAND also the influence of the land cover in the environment of a pixel on the LST on that pixel is taken into account. This is in line with several studies that used the PLAND metric and thereby addressed this influence from the environment on LST (Du et al., 2019; Li et al., 2013; Maimaitiyiming et al., 2014; Simanjuntak et al., 2019; Wardana, 2015). The radius of optimal influence was determined through a Pearson's correlation analysis between $LST_{s, \max}$ and different PLAND radii that used UGS as land cover class (following Wardana, 2015). The optimal radius was chosen based on the highest Pearson's correlation coefficient. In this calculation UGS is a reclassified land cover class containing all four green land cover types, grass, mixed low vegetation, mangrove and trees. Since the main goal of this research was to determine the cooling effect of UGS, the combined UGS class was used to determine the optimal influence radius.

Thereafter this optimal radius for UGS was used as radius for the moving kernel in the PLAND metric for each individual land cover type. As a result, eight different 30m resolution rasters of the administrative boundary were created, with each cell displaying a percentage of a particular land cover type in its surrounding. These eight-land cover density rasters were then associated with the $LST_{s, \max}$ values in the wet and dry season. This analysis was done on the same random sample as was used for the NDVI analysis. The analysis on the influence of the individual land cover types on LST comprised of Pearson's correlations and simple linear regressions.

However, before each individual land cover was correlated against the $LST_{s, \max}$ the 0% values were filtered out of the sample. The PLAND percentage only gives information on the presence of the selected land cover type. So, a 0% PLAND value only meant that there was 0% of the selected land

cover present, but not what land cover was present instead. This caused a large scatter in the correlation of all land cover types with $LST_{s, \max}$ around the 0% value, also influencing regression results. Therefore, the sample points with a 0% PLAND value of the selected land cover type were filtered out before the correlation analysis was performed.

The individual simple linear regressions were carried out in order to provide insight into the individual relationships between land cover types and LST. However, even after filtering out the 0% values, a substantial part of the land cover at the lower percentages remained unexplained in the individual analyses. This results in an unclear relationship between $LST_{s, \max}$ and PLAND around the lower PLAND values. To overcome these disturbances and in order to provide a complete overview of the relationship between land cover percentages and LST, the PLAND's of the land cover types were combined in a multiple linear regression against $LST_{s, \max}$. The PLAND values of the eight land cover types are fractional data that together sum up to a hundred percent. Therefore, in order to fully investigate the influence of the different land-cover types, the multiple linear regression models tested consisted of all combinations of all eight land-cover types minus one. From these models the best representative model was selected on the basis of the proportion of variance was explained by the models (R^2). In addition, in order to select the best model, the number of times was counted that the coefficient of each land cover switched sign. The ones that switched sign least were the most evident heaters and coolers, and so needed to be included in the model the most.

2.4.2.2. The relationship between the configuration of UGS and its cooling effect

Next to the question whether UGS cool the surface, this study aimed to analyse the influence of the spatial configurations of UGS on this cooling effect. This relationship between spatial configurations of UGS and temperature was analysed on the basis of the most widely used spatial metrics (e.g. Du et al., 2019; Estoque et al., 2017; Li et al., 2013; Maimaitiyiming et al., 2014; McGarigal et al., 2012; Simwanda et al., 2019; Wardana, 2015). The selected class metrics were: Aggregation index (AI), Landscape shape index (LSI), Edge density (ED) and Patch Density (PD). These were selected because they are the most commonly used metrics in previous research, and when combined they provide a complete overview of the shape complexity and distribution of UGS. The detailed descriptions and computing equations of these metrics are listed in **Table 6**.

Table 6. Class metrics used in this study.

Metric (abbreviation)	Description	Equation	Units
Percent landscape (PLAND)	Proportion of the landscape occupied by corresponding class.	$PLAND = \frac{\sum_{j=1}^n a_{ij}}{A} (100)$	%
Aggregation index (AI)	AI equals the number of like adjacencies involving the corresponding class, divided by the maximum possible number of like adjacencies involving the corresponding class.	$AI = \left[\frac{g_{ii}}{\max \rightarrow g_{ii}} \right] (100)$	%
Landscape shape index (LSI)	Perimeter of patch divided by the minimum perimeter possible for a maximally aggregated class.	$LSI = \frac{.25 \sum_{k=1}^m e_{ik}^*}{\sqrt{A}}$	-
Edge density (ED)	Total length of all edge segments of corresponding class divided by the total landscape area per hectare.	$ED = \frac{\sum_{k=1}^m e_{ik}}{A} (10,000)$	m/ha
Patch density (PD)	Number of patches per unit area of corresponding class	$PD = \frac{n_i}{A} (10,000)(100)$	Number per km ²

a_{ij} = area of class ij (m^2); A = total landscape area (m^2); g_{ii} = number of like adjacencies between pixels of class i based on single count method; $\max-g_{ij}$ = maximum number of possible like adjacencies between pixels of class i ; e_{ik} = total length of edge of class i in landscape (m); n_i = number of patches in the landscape of class i . (McGarigal, 2015)

These class metrics were calculated for the combined UGS class using the same optimal radius of influence that was used for the PLAND metric. Afterwards, the values of the several class metrics

were associated with the $LST_{s, \max}$ values of the different seasons. This was done again performing Pearson's correlations and simple regressions on a random sample.

2.4.2.3. Influences of major thermal centres on LST

In order to finally predict the LST within the city of Paramaribo on the basis of several land cover characteristics, the influence of the major thermal centres on LST needed to be analysed. This was necessary because previous research pointed out that for example distances from thermal centres as the city centre or the sea also had a substantial influence on the LST (Cai et al., 2018; Estoque et al., 2017; Marando et al., 2019; Simwanda et al., 2019; Wardana, 2015). Subsequently, distance rasters originating from thermal centres were created, using the Euclidean distance tool in ArcGIS Desktop, to study their thermal influence on their environment (Estoque et al., 2017; Marando et al., 2019; Simwanda et al., 2019; Wardana, 2015). The thermal centres that were selected in this study are the urban city centre, the coastline and the Suriname river. For the urban city centre, the Vaillantssquare was selected because of its central position in the economic centre of the city and its recognizability due to the monument for the colonial parliament that is situated on the square. These distance rasters were related to $LST_{s, \max}$ values from different seasons within a random sample through individual Pearson's correlations and simple regressions.

2.4.2.4. The effect on LST of all land cover features combined.

After all variables were analysed individually, three multiple linear regressions were applied on a restricted number of selected variables. The number of variables was restricted in this process to ensure better variable analysis within the regression models. The multiple linear regression models investigated how changes in land cover features could best describe the LST during the research period while testing one of the formed hypotheses. The dependent variable used to test the three hypotheses formed was $LST_{s, \max}$. The input variables for each model were selected on the basis of the hypothesis that the model tested. Based on the original research questions and the results of the individual simple regression analyses, three central hypotheses were formulated, to confirm these results in multiple linear regression analyses.

1. Impervious urban surface increases surface temperatures.
2. UGS cools the surface.
3. Trees are the UGS type that cools the surface most effective.

By means of the multiple linear regressions, it was tested whether the main findings of the individual relationships with $LST_{s, \max}$ found were still valid when the influence of other indicators was added. As variables for each model, the combination of the least possible variables was chosen that still test the hypothesis well while minimizing loss of explanatory power when compared to the model including all 18 variables. In the selection process all land cover types, class metrics, distances from thermal centres and NDVI were considered. In this selection process the maximum correlation between model variables allowed was 0.7 to prevent multicollinearity, a threshold value which is applied in studies that performed comparable analyses (Van Der Zanden, Verburg, & Múcher, 2013).

2.4.2.5. Detailed analysis on LST across several geographical specifics in Paramaribo

Due to the tropical climate, Paramaribo has a different site-specific vegetation than most of the cities whose UHI effect was analysed, as they are generally located in temperate zones. (Perera & Emmanuel, 2018). To obtain more knowledge on these UGSs that are specific to the tropics, a fieldtrip was conducted as part of this research. During the fieldtrip typical green features for the city of Paramaribo were determined. These typical green features were subdivided into 13 groups differing in vegetation characteristics. The locations of these green features were documented, as was their land cover, in detail using the ESRI Collector app for ArcGIS. Afterwards, the $LST_{s, \max}$ values

of the green features were extracted. As a result, an analysis was done on the cooling effects on the LST of these 13 different green feature groups on the LST. Results of this analysis provides the city council with a good overview of the cooling effect of the different UGSs across the city.

To extend the analysis of which vegetation type most effectively cooled the land surface in the city of Paramaribo, cold spots were selected in addition to the selected green features. These were selected purely on the lowest $LST_{s, \max}$ values within the administrative boundary. Thus, based on the LST data, considered in this study, these sites had proven to effectively reduce local LST over time. LST. During the fieldtrip the land cover characteristics on these selected cold spots were documented.

After all green spaces and cold spots were selected, located and visited, they were grouped according to their size and vegetation characteristics. Next, LST values were extracted from all pixels on the different groups of green features and cold spots. In addition to these descriptive analyses of all pixels, a random sample was taken and analysed for both green features and cold spots. This sample analysis consisted of a Kruskal-Wallis test to check whether the $LST_{s, \max}$ distribution between the groups was statistically different. The Kruskal-Wallis test was followed by a Wilcoxon signed-rank test that checked whether the LST within the groups differed significantly between the wet and dry seasons. This analysis was performed once for the selected green feature groups and once for the selected cold spot groups.

Lastly, different neighbourhoods were also visited that differed in SES of their inhabitants. This was carried out to check if the amount and type of UGS differed between these neighbourhoods and so indirectly between levels of SES. This potential differentiation of UGS between different levels of SES, would then also reflect in different average LST values. This relation was tested on the basis of the 30m resolution raster that divided the administrative boundary of Paramaribo in neighbourhoods classified on their SES (**Figure 5**). The $LST_{s, \max}$ differences between the residential classes were analysed in the same manner as the green features and cold spots, using a Kruskal-Wallis and a Wilcoxon signed-rank test.

2.4.3. Analysis of the relationship between LST and air temperature

2.4.3.1. SUHI vs CLHI

The SUHI between the urban core of the city and its rural surrounding was determined in LST according to the criteria stated in **Table 5**. In addition, within the overarching “Towards a Green and more Liveable Paramaribo” project, the difference in air temperature between the urban core and its rural hinterland was also obtained. This data was collected via an outdoor temperature logger that was placed on the most rural location that was available. Available, meaning a location that was under supervision from someone known within the project, to prevent it from being stolen. As a result, the outdoor temperature logger was placed just outside the Greater Paramaribo Region, see Appendix 3 for the exact location on the map. This rural outdoor temperature logger was only operational since December 7th, 2019, meaning that none of the analysed Landsat images were obtained in the same period. However, December 7th, 2019, is around the same period of the start of the short rainy season (early December – late January). So, to still provide a good overview of the CLHI, the hourly air temperatures of the outdoor temperature loggers from December 7th, 2019 to January 31st, 2020 were averaged, to create some reference air temperatures for the LST values from the wet season. Outdoor temperature loggers 1 and 2, of which an example is shown in Appendix 4, were placed on locations within the urban core and therefore provided the urban core air temperatures during the same short rainy season to subsequently calculate the CLHI. The resulting

CLHI was then compared to the SUHI in the wet season that was obtained through LST extraction from remote sensing data.

2.4.3.2. Relationship between LST and air temperature found in the city of Paramaribo

The relationship between LST and air temperature was analysed through a comparison between air temperature measurements performed by outdoor temperature loggers placed on different locations within the administrative boundary and LST values on the same locations (**Figure 6**). The outdoor temperature loggers were placed at different heights that were on average about two meters above the ground and mostly out of the sun. The comparison between LST and air temperature was done on air temperature data obtained by the outdoor temperature loggers at 2 pm on 8 September 2019. This was due to the fact that this was the only time that one of the analysed LST images was taken within the operational period of the outdoor temperature loggers.

In addition, through the meteorological service of Suriname, air temperature records were obtained for the measuring stations Cultuurtuin and Zorg en Hoop (**Figure 6**). At these two locations, comparisons were performed for all seven acquisition dates of the Landsat images.

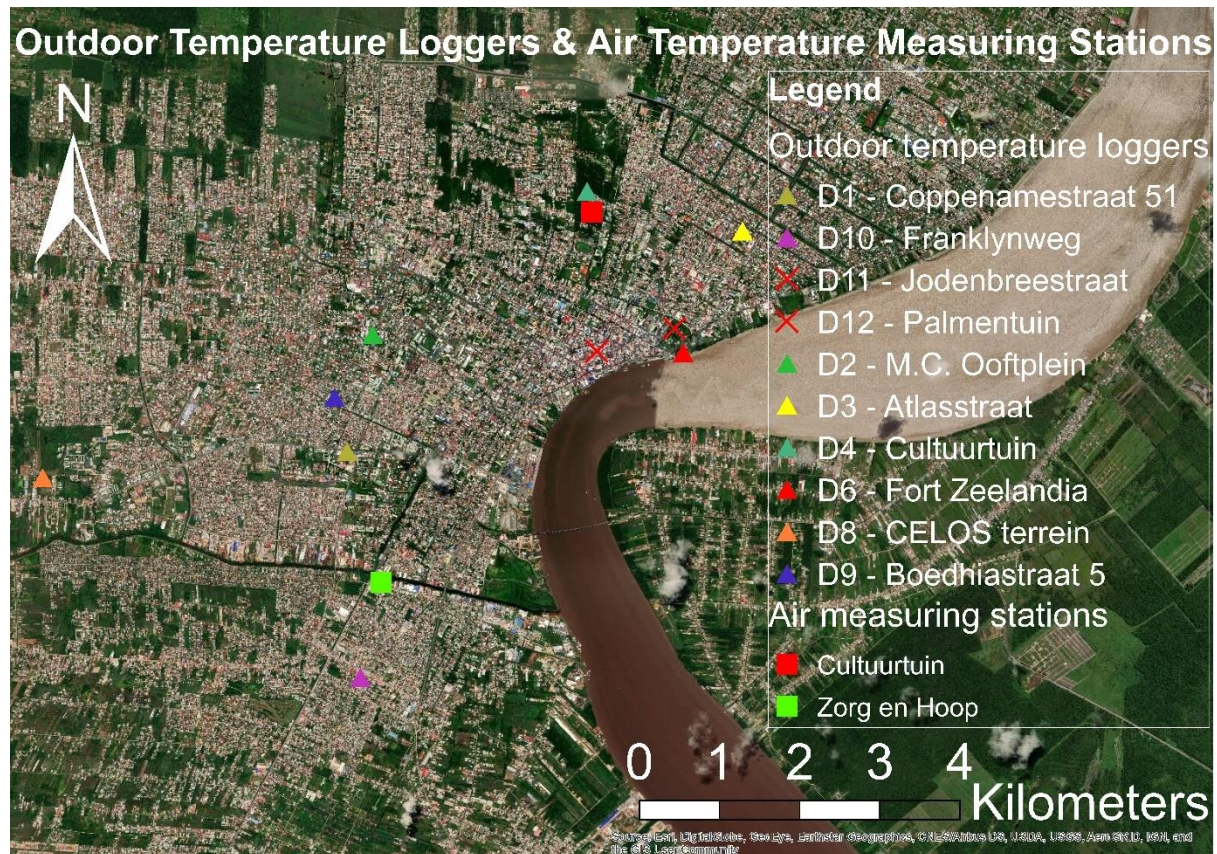


Figure 6. Locations of the outdoor temperature loggers and of the two air measuring stations of the meteorological service.

2.5. Workflow

To provide a complete overview, the methods used in this study are summarized in a flow diagram shown in **Figure 7**.

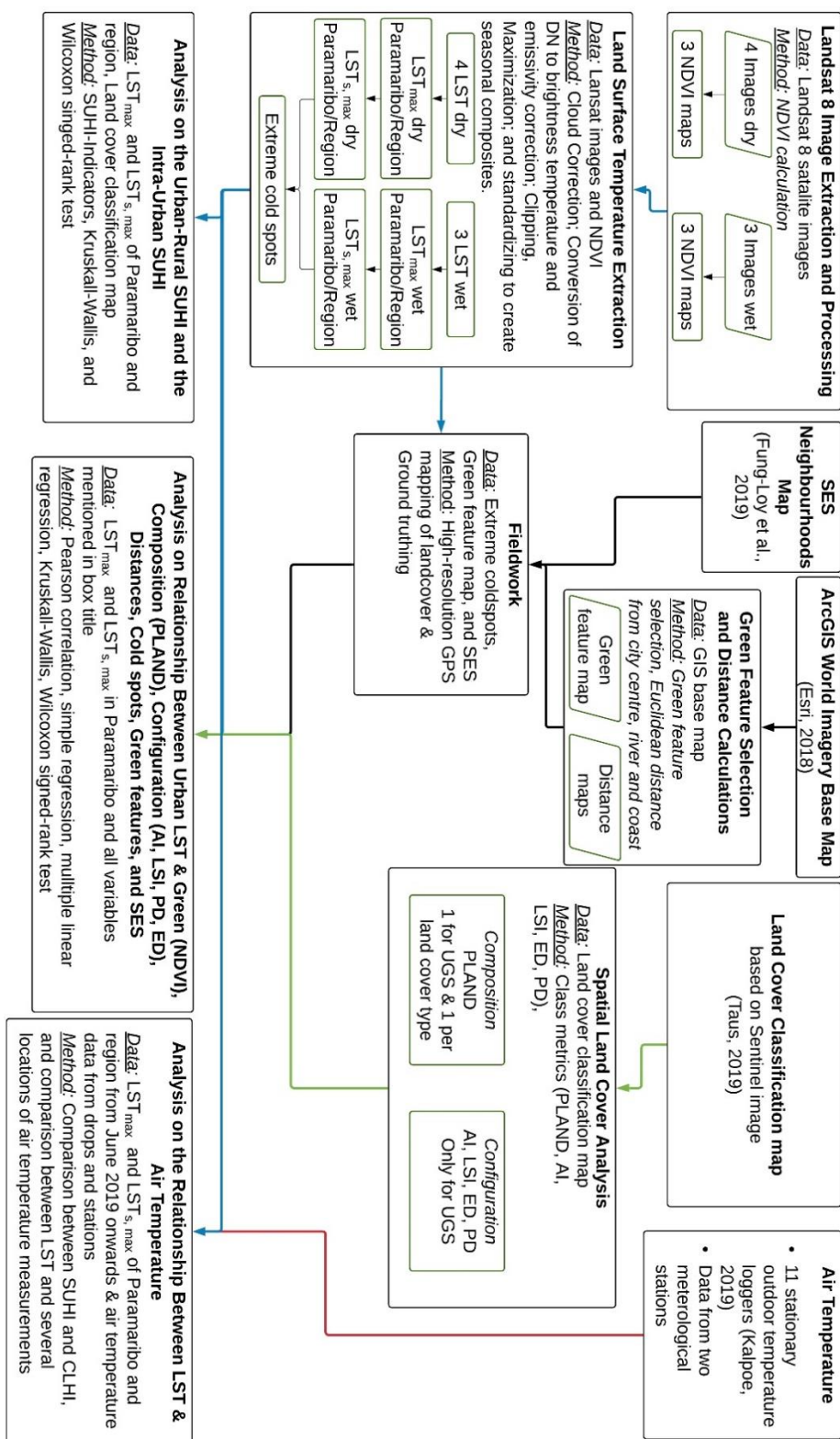


Figure 7. Workflow of methods used in this study. Each box provides the input data and methodology used for a given task. The flow paths (lines) start at boxes on the top (right) that contain the input data, then they proceed to a processing box in the middle to end in an analysis box at the bottom (left). The line colours separate main subjects of the research: LST (blue), local detailed Paramaribo specifics (black), land cover-based analysis (green), and air temperature (red).

3. Results

3.1. Analysis of the SUHI

3.1.1. Spatial characteristics of the SUHI in the Greater Paramaribo Region

Table 7 gives an overview of the LST in the Greater Paramaribo Region on the dates that the satellite images were taken. The table shows an average LST of 27.2 °C for the dry season and an average LST of 25.7 °C for the wet season. The seasonal average minimum LST within the dry and wet season were of equal magnitude (23.6 and 23.7 °C), but the average seasonal maximum LST within the Greater Paramaribo Region was higher in the dry season (36.7 °C) than in the wet season (33.4 °C). This resulted in a larger range of LST values in the Greater Paramaribo Region in the dry season than in the wet season. This is an indication of a larger UHI effect within the dry season than within the wet season. The detailed LST maps of the Greater Paramaribo Region on the separate dates of acquisition are shown in Appendix 1.

Table 7. LST of the Greater Paramaribo Region extracted from Landsat images, including minimum, maximum, range, mean and standard deviation.

The Greater Paramaribo Region						
Season	Date Landsat Image	LST (°C)				
		Min.	Max.	Range	Mean	S.D.
Dry	15/10/2015	24.4	41.4	17.0	28.8	2.2
	01/10/2016	23.6	35.3	11.7	27.1	1.8
	21/09/2018	23.6	36.2	12.6	27.5	1.9
	08/09/2019	22.8	33.8	11.0	25.5	1.7
	Average dry	23.6	36.7	13.1	27.2	1.9
Wet	29/07/2016	24.4	34.5	10.1	26.6	1.5
	14/06/2016	21.9	30.1	8.2	23.6	1.2
	04/08/2018	24.8	35.7	10.9	26.8	1.6
	Average wet	23.7	33.4	9.7	25.7	1.4

The two seasonal maximum LST (LST_{max}) maps are shown in **Figure 8** (a & b). In addition of the LST_{max} maps also the corresponding standardized maximum LST ($LST_{s,max}$) maps are shown in **Figure 8** (c & d).

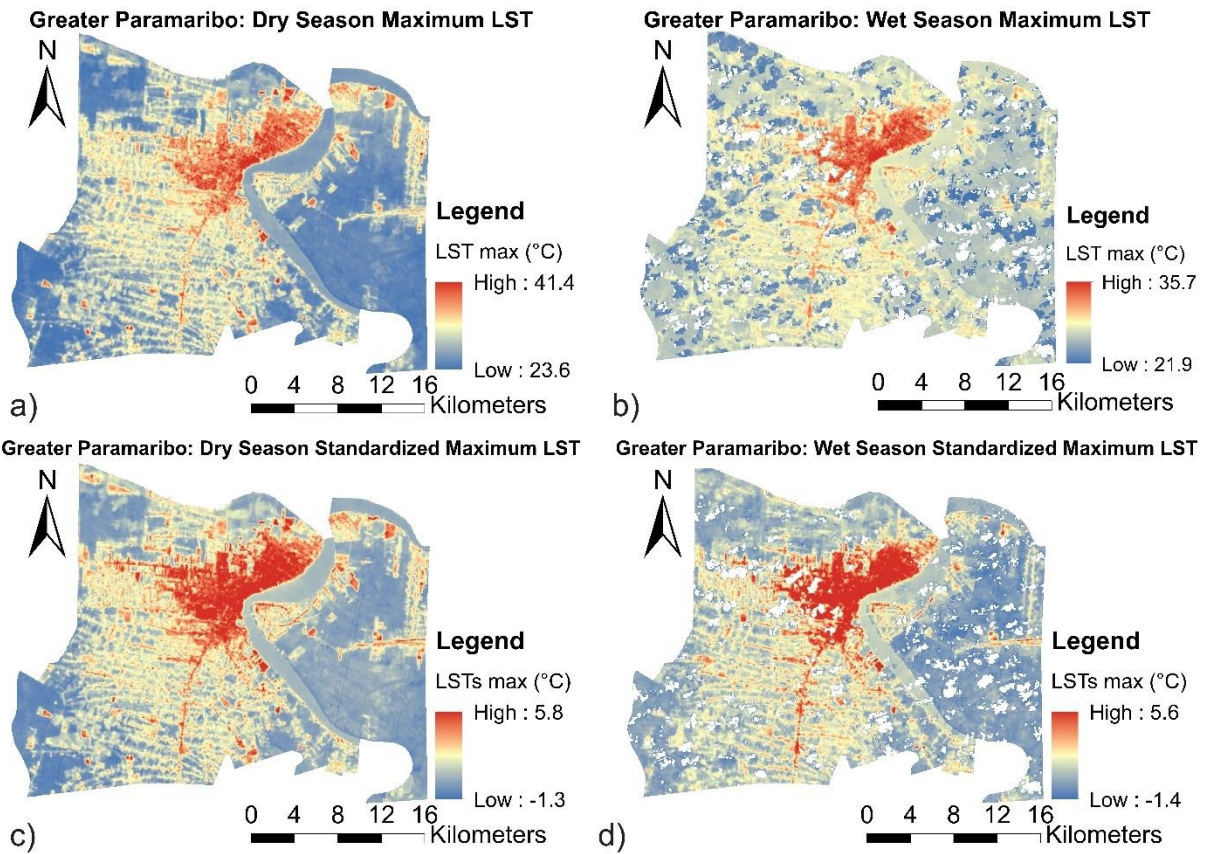


Figure 8. Spatial pattern of LST_{max} in the dry (a) and wet (b) season and $LST_{s, max}$ in the dry (c) and wet (d) season in the Greater Paramaribo Region.

Note: White spots are areas where clouds were present in all the images used to create the seasonal composites, these clouds were removed. Therefore, the white spots in the seasonal images indicate no data.

3.1.2. Spatial characteristics of the intra-SUHI in the administrative boundary

3.1.2.1. Temperature distribution in the administrative boundary of Paramaribo

The intra-SUHI was studied on the basis of LST maps within the administrative boundary. The results of these LST maps are summarized in

Table 8. The table shows an average LST of 29.1 °C for the dry season and an average LST of 26.9 °C for the wet season. Therefore, the average LST in the administrative boundary was 1.9 °C higher in the dry season and 1.3 °C higher in the wet season compared to the Greater Paramaribo Region (**Table 7**). In the wet season, the seasonal average minimum LST within the administrative boundary was 1.1°C higher in the dry season (24.8 °C) than in the wet season (23.7 °C). The average seasonal LST_{max} within the administrative boundary was the same as for the Greater Paramaribo Region in both seasons, indicating that all of the LST_{max} values within the Greater Paramaribo Region occurred within the administrative boundary. This resulted in a slightly smaller range in LST values in the dry season within the administrative boundary than within the Greater Paramaribo region. This indicates an UHI effect between the city of Paramaribo and its rural hinterland. The detailed LST maps of the administrative boundary on the individual acquisition dates are set out in Appendix 2.

Table 8. LST extracted from Landsat images within the administrative boundary.

Administrative Boundary						
Season	Date Landsat Image	LST (°C)				
		Min.	Max.	Range	Mean	S.D.
Dry	15/10/2015	25.6	41.4	15.8	30.6	2.5
	01/10/2016	25.0	35.3	10.3	28.8	2.2
	21/09/2018	25.8	36.2	10.4	29.5	2.2
	08/09/2019	22.9	33.8	10.9	27.4	2.2
	Average dry	24.8	36.7	11.9	29.1	2.3
Wet	29/07/2016	24.4	34.5	10.1	28.0	2.2
	14/06/2016	21.9	30.1	8.2	24.5	1.7
	04/08/2018	24.8	35.7	10.9	28.1	2.2
	Average wet	23.7	33.4	9.7	26.9	2.0

Seasonal composition of the LST_{max} values of the individual images resulted in two seasonal LST_{max} maps shown in **Figure 9** (a & b). Again, for comparability reasons two seasonal $LST_{s,max}$ maps were created **Figure 9**, (c & d) which, in combination with the classified land cover map, formed the basis of this research.

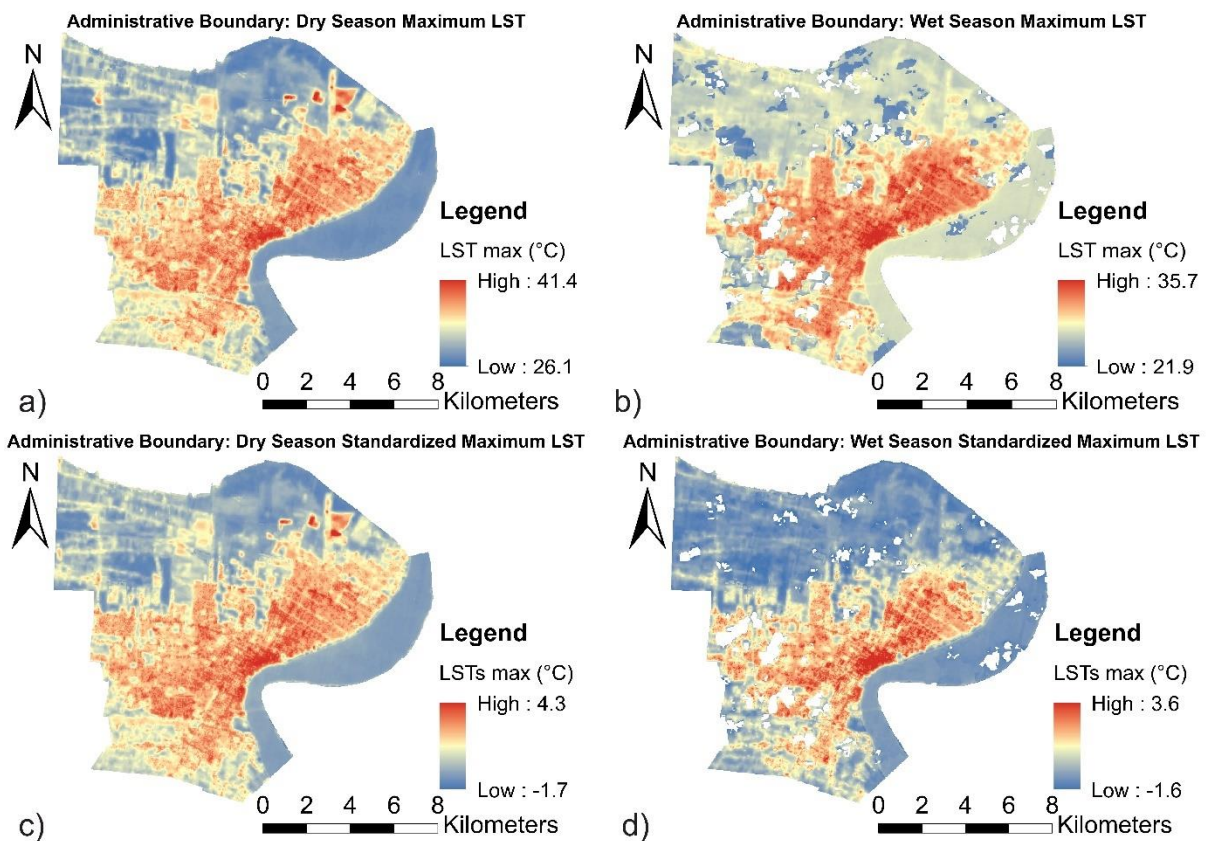


Figure 9. Spatial pattern of LST_{max} in the dry (a) and wet (b) season and $LST_{s,max}$ in the dry (c) and wet (d) season in the administrative boundary.

Note: White spots are areas where clouds were present in all the images used to create the seasonal composites, these clouds were removed. Therefore, the white spots in the seasonal images indicate no data.

3.1.2.2. Land cover based descriptive pixel analysis of LST in the administrative boundary

The mean $LST_{s, \max}$ values and the standard deviations of the different land cover classes in the administrative boundary are shown in **Figure 10**. The corresponding descriptive analysis, including a figure similar to **Figure 10**, of the Greater Paramaribo region is shown in Appendix 5. The full descriptive analysis of the Greater Paramaribo Region and the administrative boundary are shown in Appendix 6 and 7, respectively.

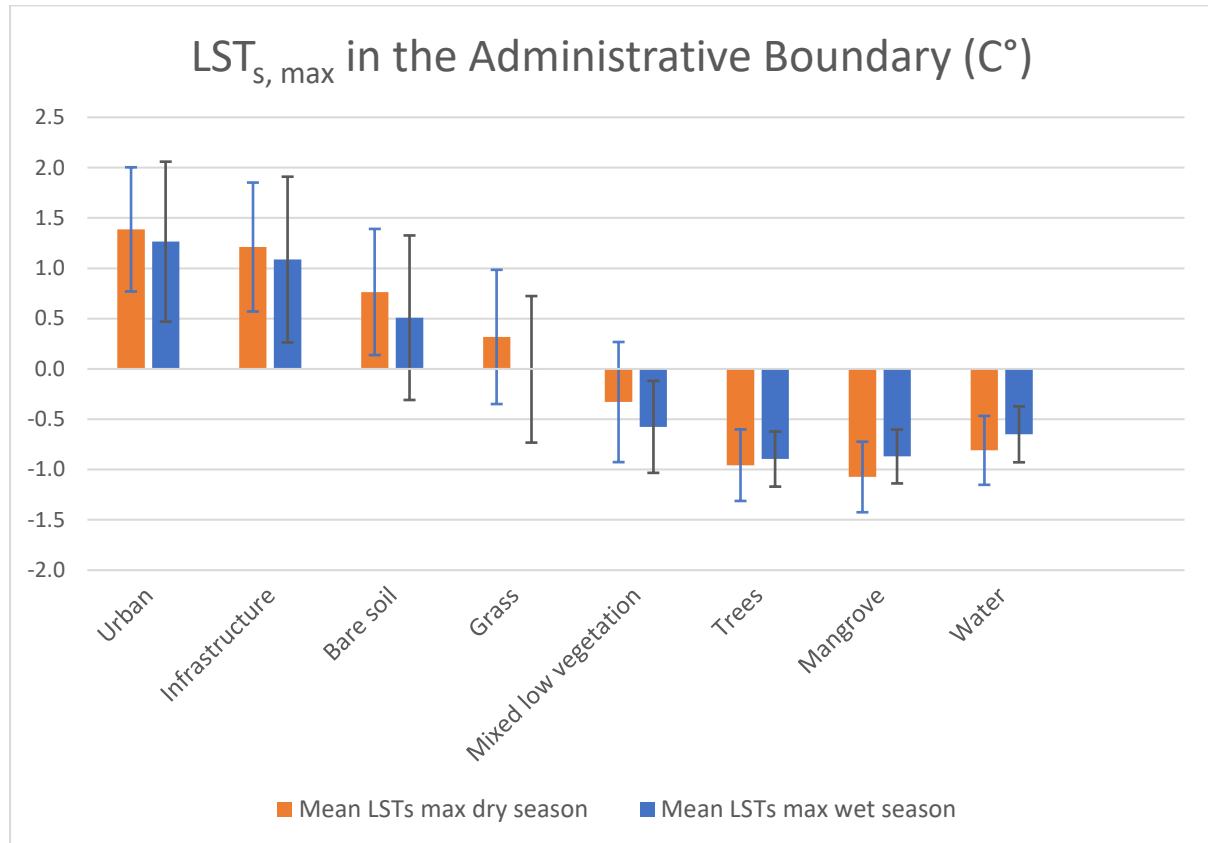


Figure 10. Mean $LST_{s, \max}$ values per land cover class, including error bars displaying the standard deviation, in the administrative boundary in the dry and wet season.

The results show that in general the $LST_{s, \max}$ values for the different land cover types were either lower or higher than average in both the wet and the dry season. This means that every land cover type either heated or cooled the surface independent of the season. The order of magnitude of this heating or cooling effect was dependent on the land cover type and the season. The highest temperatures in both seasons prevailed on the most sealed and constructed land cover types, specifically urban (1.4 ± 0.6 & 1.3 ± 0.8 °C) and infrastructure (1.2 ± 0.6 & 1.1 ± 0.8 °C). The $LST_{s, \max}$ values were lower, but still higher than the average temperature, for the land cover type bare soil (0.8 ± 0.6 & 0.5 ± 0.8 °C). Land covered with grass showed on average slightly higher than average LST values within the dry season (0.3 ± 0.7 °C) and exactly average LST values within the wet season (0 ± 0.7 °C). The rest of the land cover types had an average LST value that was below the average LST value of the administrative boundary and so had a cooling effect on the LST. Mixed low vegetation showed the smallest cooling effect (-0.3 ± 0.6 & -0.6 ± 0.5 °C). This cooling effect was larger on land covered by trees (-1 ± 0.4 & -0.9 ± 0.3 °C), but was largest on land covered by mangrove (-1.1 ± 0.4 & -0.9 ± 0.3).

The Kruskal-Wallis test showed that both the dry season $LST_{s, \max}$ values and the wet season $LST_{s, \max}$ values were significantly affected by land cover type ($H_{dry}(7) = 2691.87$, $p < .001$ & $H_{wet}(7) = 2245.27$,

$p < .001$). To follow up on these findings pair-wise comparisons were performed using Mann-Whitney tests. The detailed results of the Kruskal-Wallis test and the pair-wise comparisons are shown in Appendix 8. These resulted in the conclusion that almost all groups had significantly different $LST_{s, \max}$ values within the dry season, when compared to each other. Only the differences in $LST_{s, \max}$ between the land cover types mangrove and trees ($U = 10251$, $r = -.22$), water and trees ($U = 31334$, $r = -.29$), and infrastructure and urban ($U = 113511$, $r = -.14$) were non-significant. In the wet season it appeared that $LST_{s, \max}$ values were not significantly different between the land cover types trees and mangrove ($U = 11664$, $r = -.093$), water and mixed low vegetation ($U = 196156$, $r = -0.0016$), and infrastructure and urban ($U = 109577$, $r = -.098$). Except for these three combinations of land cover, all other possible combinations of land cover types had significantly different $LST_{s, \max}$ values in the wet season. This conclusion is in line with the mean values of $LST_{s, \max}$ values of the different land cover types displayed in **Figure 10**.

Besides the differences between different land covers the results also showed differences in $LST_{s, \max}$ on the same land cover type between seasons. A larger heating effect was visible on the constructed land cover types, bare soil and grass in the dry season than in the wet season. On the contrary, larger cooling effects were also observed for the vegetated land cover types in the dry season than in the wet season. To check if these seasonal differences per land cover type were statistically significant, a non-parametric Wilcoxon signed-rank test was performed. The results of this test, displayed in detail in Appendix 9, point out that these seasonal differences per land cover type were all statistically significant.

3.1.2.3. Analysis of the SUHI in the city of Paramaribo according to widely used SUHI-indicators

The results of the SUHI indicators are shown in

Table 9. They reveal that the SUHI indicators are quite similar when either using the urban land cover type or the combined built-up land cover. The LST_{max} on urban land was clearly higher than all other classes of land use in both the dry and wet season. This temperature difference was even larger when not all other land use was considered but just land covered by water. Moreover, the difference between urban and water surfaces was about 2 K larger in the dry season than in the wet season, indicating a larger SUHI effect in the dry season. The slightly higher value of the Magnitude indicator in the dry season than in the wet season supports this indication. The Micro-UHI indicator, on the other hand, showed a slightly higher UHI effect in the wet season. This was due to the fact that in the dry season, 12.3 % of the total area had a higher LST_{max} value than the maximum LST_{max} value on the tree-covered land, whereas in the wet season this was 15.3 %. The difference between the mean LST_{max} in the urban core and the rural hinterland in the Greater Paramaribo Region was around the same magnitude in the dry and wet season. In conclusion, when comparing all SUHI indicators, most indicators show a slightly larger SUHI in the dry than in the wet season, however these differences are small.

Table 9. SUHI indicators at 14:00 hrs, local time, for both seasons, once taking only the urban land cover type as "urban" and once using a combination of urban and infrastructure in the form of a reclassified built-up land cover class as "urban"

SUHI Indicators						
Indicator	Units	Quantification	Dry season		Wet season	
			Urban	Built-up	Urban	Built-up
Difference urban - other	K	Difference in mean LST _{max} between urban area and all other areas	3.1	3.5	2.8	2.8
Difference urban - water	K	Difference in mean LST _{max} between urban area and water surface	5.4	5.3	3.7	3.5
Difference core - rural	K	Difference in mean LST _{max} between urban core (> 67% urban land use in 9 km ²) and rural areas (< 25% urban land use in 25 km ²) in the Greater Paramaribo Region	5.3		5.1	
Hot island area	km ²	Area with LST _{max} higher than the mean plus one standard deviation	33.4		32.6	
Magnitude	K	Difference between maximum and mean of LST _{max}	10.9		8.1	
Micro-UHI	%	Percentage of area (without water surfaces) with LST _{max} higher than the warmest LST _{max} associated with tree canopies	12.3		15.3	
Standard deviation	K	Standard deviation of LST _{max}	2.5		2.4	

Note: All areas and LST_{max} values, except for the rural areas and LST_{max}, are measured within the administrative boundary.

3.2. Analysis of the cooling effect of UGS

3.2.1. Relationship between the LST and NDVI within the administrative boundary.

The results of the correlation analysis between the LST_{s, max} and the NDVI are shown in **Table 10**.

Table 10. Pearson's correlation (*r*) of seasonal LST_{s, max} values and NDVI once using a sample of the whole administrative boundary and once using a sample after water was excluded from the administrative boundary. *N* = number of pixels in sample.

NDVI	Pearson's Correlation			
	Dry season		Wet season	
	N	r	N	r
NDVI (all)	12064	-.264*	11364	-.364*
NDVI (no water)	10516	-.813*	9902	-.805*

* Statistically significant at the .001 level (2-tailed).

The results in **Table 10** show the interference of water in the relationship between LST and NDVI. When all land cover was considered, there was only a small to medium negative correlation between LST and NDVI in the dry (-.264) and wet (-.364) season. This indicates that when the NDVI increased,

$LST_{s, \max}$ decreased, or vice versa since Pearson's correlation does not indicate the direction of causality (Field, 2009). The correlation disturbance is seen in the large increase in correlation coefficient when water was excluded from the analysis. This exclusion resulted in a notably strong negative relationship between LST and $NDVI$ in both the dry (-.813) and wet (-.805) season.

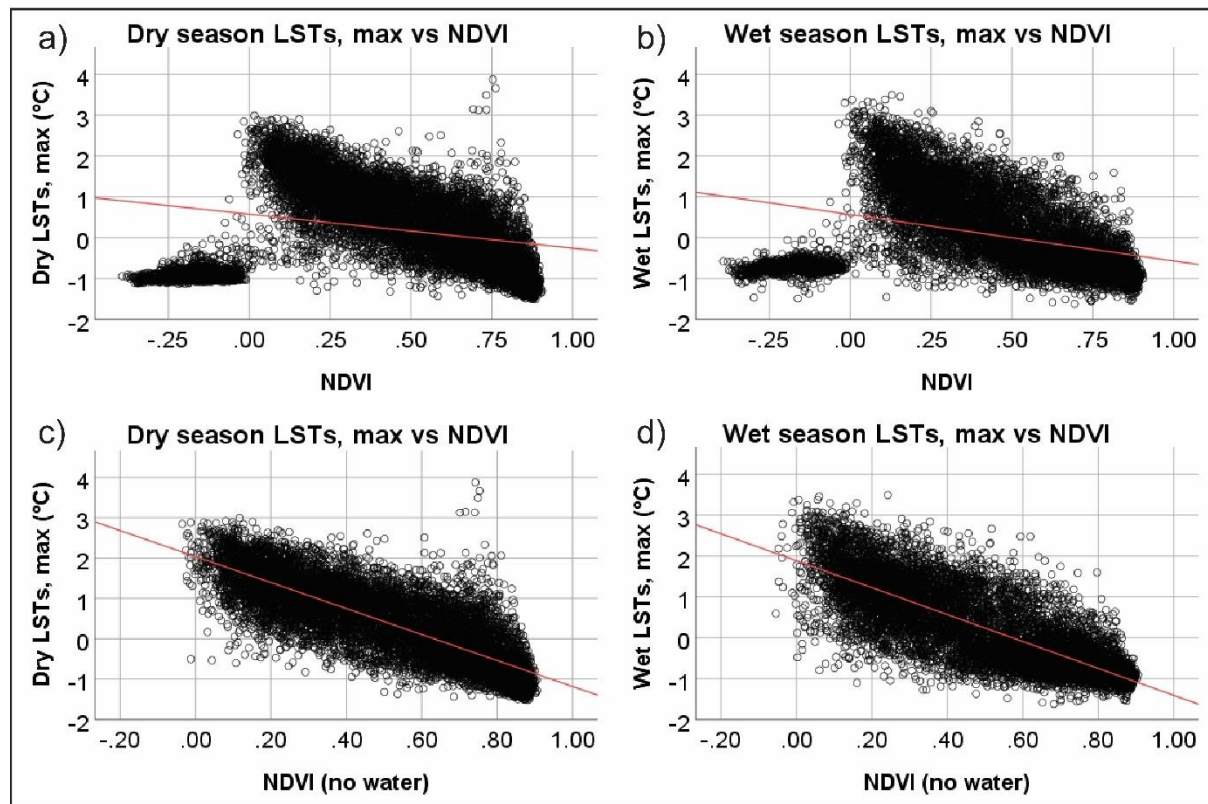


Figure 11. Scatterplots, including regression line, of $LST_{s, \max}$ vs $NDVI$ with water in the dry (a) and wet (b) season, and of $LST_{s, \max}$ vs $NDVI$ without water in the dry (c) and wet (d) season.

The disturbance of the relationship due to water was also clearly visible in the scatterplots, shown in **Figure 11**. Scatterplots a and b in **Figure 11** show a substantial point cloud in the lower left corner of the grid. These values are clearly influencing the general downward pattern of the values. The regression lines are therefore also highly influenced in both the dry ($y = 0.577 - 0.833x$, $R^2 = 0.007$, $p < .001$) and wet ($y = 0.568 - 1.138x$, $R^2 = 0.133$, $p < .001$) season. The disturbing values are also those with the lowest $NDVI$ values. When water was excluded from the sample, these values did not show on the scatterplots anymore, proving that these disturbing points were points on water. The two scatterplots c and d in **Figure 11** show a significant and strong relationship between $LST_{s, \max}$ and $NDVI$ in both the dry ($y = 2.038 - 3.221x$, $R^2 = 0.660$, $p < .001$) and wet ($y = 1.889 - 3.296x$, $R^2 = 0.648$, $p < .001$) season.

3.2.2. Relationship between the LST and the land cover composition in the surrounding area within the administrative boundary.

There was a statistically significant negative correlation between the $LST_{s, \max}$ values and the percentage of UGS for every radius in both the wet and dry season (**Table 10 & Table 11**). So, this means that when the density of green cover around a pixel increased, the $LST_{s, \max}$ on that pixel tended to decrease. The Pearson's correlation coefficient was highest when the radius of the moving window was about 90 meters ($r_{dry, 90} = -.508$, $p < 0.01$ & $r_{wet, 90} = -.614$, $p < 0.01$), **Table 11**. These 90 meter correlation coefficients for the dry and the wet season both show that $LST_{s, \max}$ and UGS

density have a large and negative relationship (Cohen, 1988). Since the correlation coefficient was lower when the radius of the moving window surpassed 90 meters and started decreasing when the radius increased to 200 meters, the process was stopped.

Table 11 shows the results of the Pearson’s correlations between the pixel $LST_{s, \max}$ value and the PLAND of UGS for an increasing radius. The results showed a statistically significant negative correlation between the $LST_{s, \max}$ values and the percentage of UGS for every radius in both the wet and dry season. So, this means that when the density of green cover around a pixel increased, the $LST_{s, \max}$ on that pixel tended to decrease. Averaging over the wet and dry season it is seen in **Table 11** that the Pearson’s correlation coefficient was highest when the radius of the moving window was about 90 meters ($r_{\text{dry}, 90} = -.508, p < .01$ & $r_{\text{wet}, 90} = -.614, p < .01$). Both of these correlation coefficients show that $LST_{s, \max}$ and UGS density have a large and negative relationship (Cohen, 1988). Since the correlation coefficient flattened out when the radius of the moving window surpassed 90 meters and started decreasing when the radius increased to 200 meters, the process was stopped.

Table 11. Pearson’s correlation (r) of seasonal $LST_{s, \max}$ values and PLAND for different radii used in the focal analysis.

Pearson’s Correlation Coefficient		
Radius (m)	Dry season	Wet season
10	-.477*	-.564*
20	-.486*	-.575*
30	-.496*	-.589*
40	-.502*	-.597*
50	-.506*	-.604*
60	-.508*	-.608*
70	-.509*	-.611*
80	-.509*	-.613*
90	-.508*	-.614*
100	-.507*	-.614*
110	-.506*	-.614*
120	-.505*	-.614*
130	-.504*	-.613*
140	-.502*	-.613*
150	-.500*	-.612*
160	-.499*	-.611*
170	-.497*	-.610*
180	-.477*	-.564*
190	-.493*	-.607*
200	-.491*	-.605*
Number of observations	12064	11364

* Statistically significant at the .001 level (2-tailed).

After the optimal radius of influence was determined at 90 meters by using the combined UGS class, the individual relationship of all eight land cover classes with the LST was analysed. This was done by running the PLAND metric, using a moving window of 90 meters, for each class individually. This resulted in eight different rasters within the administrative boundary, with each pixel displaying the percentage of land covered by a certain land cover type in a 90-meter radius around the pixel. **Figure 12** shows the result of this process for the combined land cover class UGS in the dry and wet season.

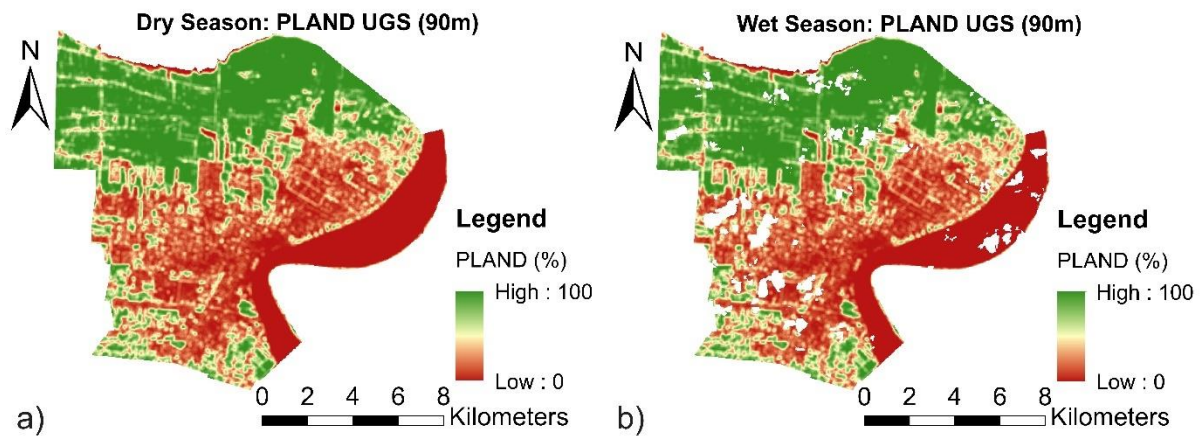


Figure 12. Percentage of UGS in a 90-meter radius around focal cell in the Administrative boundary in the dry (a) and wet (b) season.

Note: White spots are areas where clouds were present in all the images used to create the seasonal composites, these clouds were removed. Therefore, the white spots in the seasonal images indicate no data.

The results of Pearson’s correlations of LST with the PLAND values of the individual land cover types, after 0% values were filtered out, are shown in **Table 12**.

Table 12. Pearson’s correlation (r) of seasonal $LST_{s, \max}$ values and PLAND values of the combined land cover class UGS and of all individual land cover types, after 0% values were filtered out. N = number of pixels in sample.

Pearson's Correlation										
Land cover		UGS	Urban	Infra	Bare soil	Grass	Mixed low veg	Trees	Mangrove	Water
Dry Season	N	10723	7210	8222	8695	9674	9669	3399	1933	2830
	r	-.822*	.772*	.792*	.247*	-.146*	-.576*	-.475*	-.553*	-.670*
Wet Season	N	10120	6772	7707	8177	9144	9134	3238	1855	2695
	r	-.848*	.789*	.816*	.155*	-.258*	-.611*	-.392*	-.409*	-.514*

* Statistically significant at the .001 level (2-tailed).

To correctly interpret the results shown in **Table 12** scatterplots were produced for each of the individual relationships between the land cover PLAND (90m) values and the $LST_{s, \max}$ values. These scatterplots for the dry season are shown in **Figure 13**, and for the wet season in Appendix 10. **Table 12** shows that $LST_{s, \max}$ and the PLAND values for the different land cover types correlated in approximately the same direction and magnitude in the dry and wet season. The $LST_{s, \max}$ and the PLAND of the land cover UGS, mixed low vegetation, trees, mangrove and water showed a large negative relationship. If these land cover types increased around a pixel the LST on that pixel tended to decrease, or vice versa. **Table 12** indicates that several types of UGS cool the surface. The PLAND of the land cover types urban and infrastructure showed a very strong positive relationship with $LST_{s, \max}$ since if these land cover types increased in a 90-meter radius around a pixel, the LST value on that pixel tended to increase, or vice versa. This result confirmed the basis of the SUHI effect, namely that impervious man-made urban surfaces heat the surface. The PLAND of the grass showed a small to medium negative effect on the LST, while the PLAND of bare soil showed a small to medium positive effect on LST. These land cover types were not correlated that strongly with LST which is also clearly seen in the scatterplots in **Figure 13**. It is clearly visible that there were as many pixels around bare soil (d) and grass (e) that had a higher than average $LST_{s, \max}$, as pixels that had a lower than average $LST_{s, \max}$.

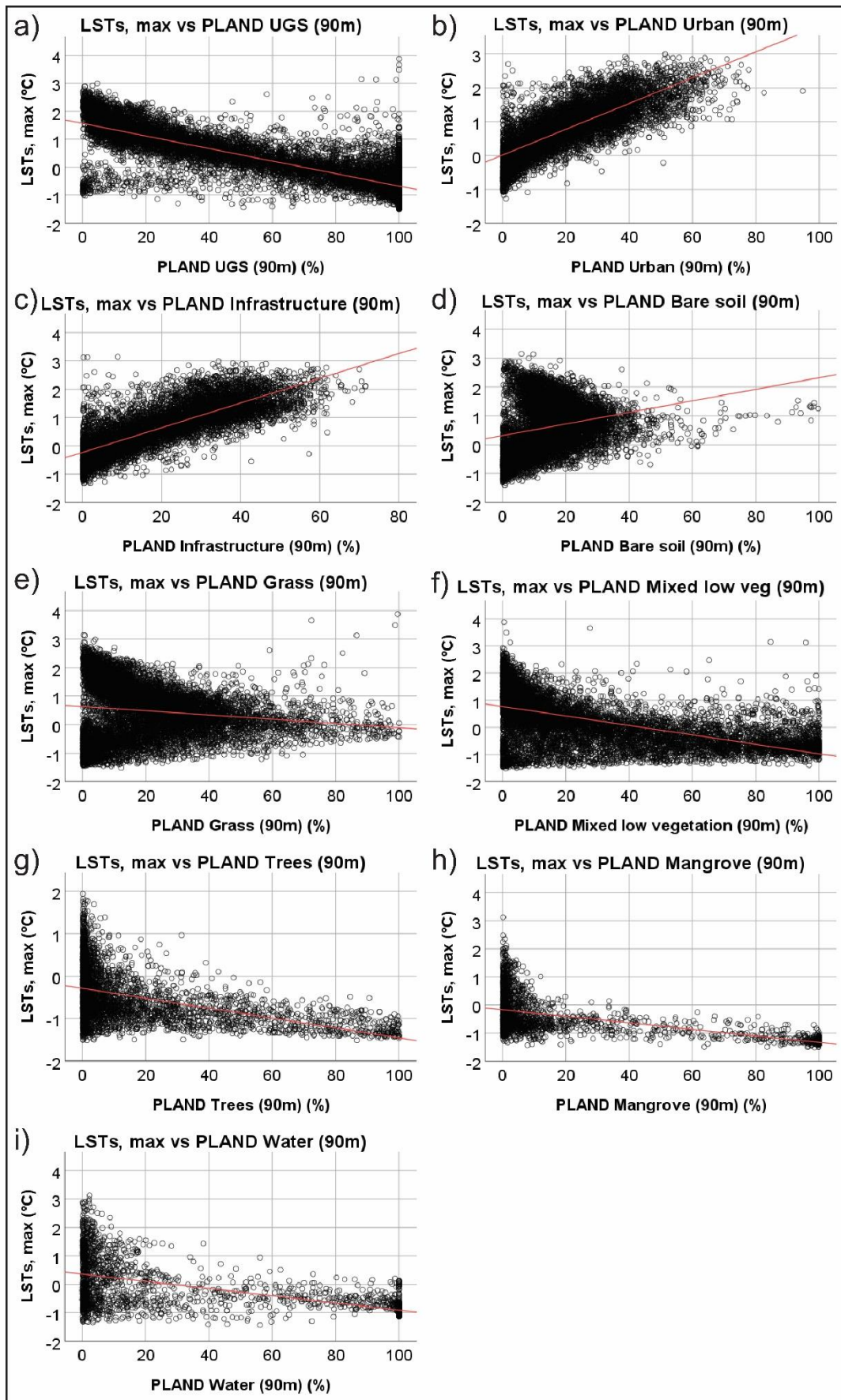


Figure 13. Scatterplots, including regression line, of $LST_{s,max}$ vs PLAND (90m) values of the combined land cover class UGS and of all individual land cover types in the dry season after the 0% PLAND values were filtered out.

To assess the heating or cooling effect of the different land cover types in more detail, linear regressions were performed on the $LST_{s, \max}$ ($^{\circ}C$) values and the individual PLAND (%) values. These linear regressions predicted the $LST_{s, \max}$ value (y) from the PLAND value (x) of a land cover type. The results of these linear regressions are shown as a red line in the scatterplots in **Figure 13** and as equation in **Table 13**. From the coefficient in the regression equation, the difference in $LST_{s, \max}$ value on a pixel can be predicted when the coverage, of the land cover in question, in a 90-meter radius around that pixel increased by 1%. The R^2 , as a percentage, represents the amount of variation in the $LST_{s, \max}$ that can be explained by the model.

Table 13. Linear regression results of $LST_{s, \max}$ and PLAND values of the combined land cover class UGS and of all the individual land cover types.

PLAND Land Cover	Dry Season		Wet Season	
	Equation	R^2	Equation	R^2
a) PLAND UGS (90m)	$y = 1.566 - 0.022x$.676*	$y = 1.456 - 0.024x$.720*
b) PLAND Urban (90m)	$y = 0.012 + 0.038x$.596*	$y = -0.324 + 0.045x$.623*
c) PLAND Infrastructure (90m)	$y = -0.234 + 0.044x$.628*	$y = -0.588 + 0.051x$.666*
d) PLAND Bare soil (90m)	$y = 0.317 + 0.020x$.061*	$y = 0.187 + 0.014x$.024*
e) PLAND Grass (90m)	$y = 0.637 - 0.007x$.021*	$y = 0.556 - 0.014x$.067*
f) PLAND Mixed low vegetation (90m)	$y = 0.768 - 0.017x$.331*	$y = 0.613 - 0.019x$.373*
g) PLAND Trees (90m)	$y = -0.289 - 0.012x$.225*	$y = -0.467 - 0.008x$.153*
h) PLAND Mangrove (90m)	$y = -0.171 - 0.012x$.306*	$y = -0.330 - 0.007x$.167*
i) PLAND Water (90m)	$y = 0.360 - 0.013x$.449*	$y = 0.147 - 0.009x$.264*

* Statistically significant at the .001 level (2-tailed).

Table 13 shows that much of the variation in $LST_{s, \max}$ could be explained by the variation in UGS ($R^2_{\text{dry}} = .68$ & $R^2_{\text{wet}} = .72$), urban (.60 & .62) and infrastructure (.63 & .67). However, variation in mixed low vegetation, trees, mangrove and water also accounted for substantial amounts of variation in $LST_{s, \max}$. Bare soil and grass did not show a substantial influence on the LST. The coefficients of the regression equations in **Table 13** showed that infrastructure and urban land cover were the largest heaters of the surface. An increase of 1% in infrastructure coverage in a 90-meter radius around a pixel would increase the $LST_{s, \max}$ on that pixel with 0.044 $^{\circ}C$ in the dry season and with 0.051 $^{\circ}C$ in the wet season. When the different types of UGS are considered, **Table 13** indicates that mixed low vegetation (-0.017 & -0.019) was the biggest cooler of the surface, followed by trees, mangroves and grass. However, observation of the scatterplots in **Figure 13** reveals that the average temperature on land covered with trees and mangrove is on average cooler than land covered with mixed low vegetation.

Due to the lack of information on land covered by a different land cover type than the selected one, the relationships between LST and land cover types were disturbed at lower PLAND percentages. Therefore, in order to test the influence of different land cover types on LST more extensively, all possible combinations of seven out of the eight land cover type densities (PLANDs) were combined in seven multiple linear regression models. During the selection process for the best model, it appeared that the model had to explain two patterns, namely a heating pattern and a cooling pattern. When one of the heating variables was left out of the regression model (infrastructure or urban), then the cooling variables had a very strong influence and the model explained the cooling pattern. However, the influence of the other heater became negligible. When one of the strong cooling variables (trees or mangrove) was left out of the model, the model explained the heating pattern and the heating variables had a very strong influence, while the influence of the other strong cooling variable became negligible.

For all seven land cover combinations, the proportion of variance in $LST_{s, max}$ explained by the model (R^2) was around the same value. The land cover types which switched signs most were grass and bare soil. Consequentially, the best explaining model was that without the inclusion of grass or bare soil. The best model between the two was then selected based on the coefficient of each land cover minus the average coefficient of that land cover in all the possible models of 7 land cover types. As a result, the model did not contain the PLAND value for bare soil. The results of these multiple linear regression models are shown in **Table 14**.

Table 14. Multiple linear regressions to predict $LST_{s, max}$ in the dry (upper) and wet season (lower) based on PLAND for all land cover types except bare soil.

Land Cover Model Dry Season	Coefficients Dry Season					R ²
	Unstandardized coefficients		Standardized coefficients	t	Sig.	
	B	Std. Error	β			
Constant	0.221	0.035		6.242	.000	.862
PLAND Urban (90m)	0.018	0.001	0.287	34.997	.000	
PLAND Infrastructure (90m)	0.018	0.001	0.288	32.450	.000	
PLAND Grass (90m)	-0.002	0.000	-0.042	-4.841	.000	
PLAND Mixed low vegetation (90m)	-0.008	0.000	-0.222	-20.437	.000	
PLAND Trees (90m)	-0.016	0.000	-0.246	-39.428	.000	
PLAND Mangrove (90m)	-0.014	0.000	-0.229	-34.531	.000	
PLAND Water (90m)	-0.011	0.000	-0.356	-30.039	.000	

Land Cover Model Wet Season	Coefficients Wet Season					R ²
	Unstandardized coefficients		Standardized coefficients	t	Sig.	
	B	Std. Error	β			
Constant	-0.622	0.035		-17.888	.000	.871
PLAND Urban (90m)	0.029	0.001	0.461	56.452	.000	
PLAND Infrastructure (90m)	0.029	0.001	0.461	52.220	.000	
PLAND Grass (90m)	0.001	0.000	0.011	1.263	.207	
PLAND Mixed low vegetation (90m)	-0.002	0.000	-0.053	-4.885	.000	
PLAND Trees (90m)	-0.005	0.000	-0.071	-11.361	.000	
PLAND Mangrove (90m)	-0.003	0.000	-0.051	-7.608	.000	
PLAND Water (90m)	-0.001	0.000	-0.024	-2.075	.038	

The results in **Table 14** show that when all land cover types except for bare soil were taken into account, urban and infrastructure had a similar heating effect in both seasons ($B_{dry} = 0.018$ & $B_{wet} = 0.029$). Land covered with grass showed a very small cooling effect in the dry season (-0.002) and a non-significant influence in the wet season. Water (-0.011 & -0.001) and mixed low vegetation (-0.008 & -0.002) were significant coolers of the surface in both seasons, although this effect was larger in the dry than in the wet season. The second most effective cooling UGS type was mangrove (-0.016 & -0.003). However, the land cover type that cooled the surface most was trees (-0.016 & -0.005).

3.2.3. Relationship between the LST and configuration of UGS

The previous sections showed that the presence of UGS cooled the surface. This cooling effect was investigated in more detail via analysis of the configurational class metrics AI, LSI, ED and PD. By means of Pearson's correlations and regression analyses the relation between LST and the distribution of UGS was studied. The statistical analysis was performed only on pixels that contained some UGS in their environment. The results of the Pearson's correlation are shown in **Table 15**.

Table 15. Pearson's correlation of seasonal $LST_{s, \max}$ values and the used configurational class metrics, after 0% UGS values were filtered out.

Configurational Class Metric	Pearson's Correlation	
	Dry season	Wet season
Aggregation index (90m)	-.712*	-.745*
Landscape shape index (90m)	.560*	.521*
Edge density (90m)	.406*	.336*
Patch density (90m)	.598*	.599*
Number of observations	10723	10120

* Statistically significant at the .001 level (2-tailed).

The results show that all relations were statistically significant, and that there was a significant, strong and negative relationship between $LST_{s, \max}$ and AI in both the wet and dry season. This implies that if the aggregation of UGS increased then the LST would tend to decrease. The class metrics LSI and PD showed a large positive correlation with $LST_{s, \max}$ in both seasons while the $LST_{s, \max}$ and ED showed a medium correlation with each other. However, to correctly interpret the results of the Pearson's correlation, scatterplots were also created and compared to the correlation results.

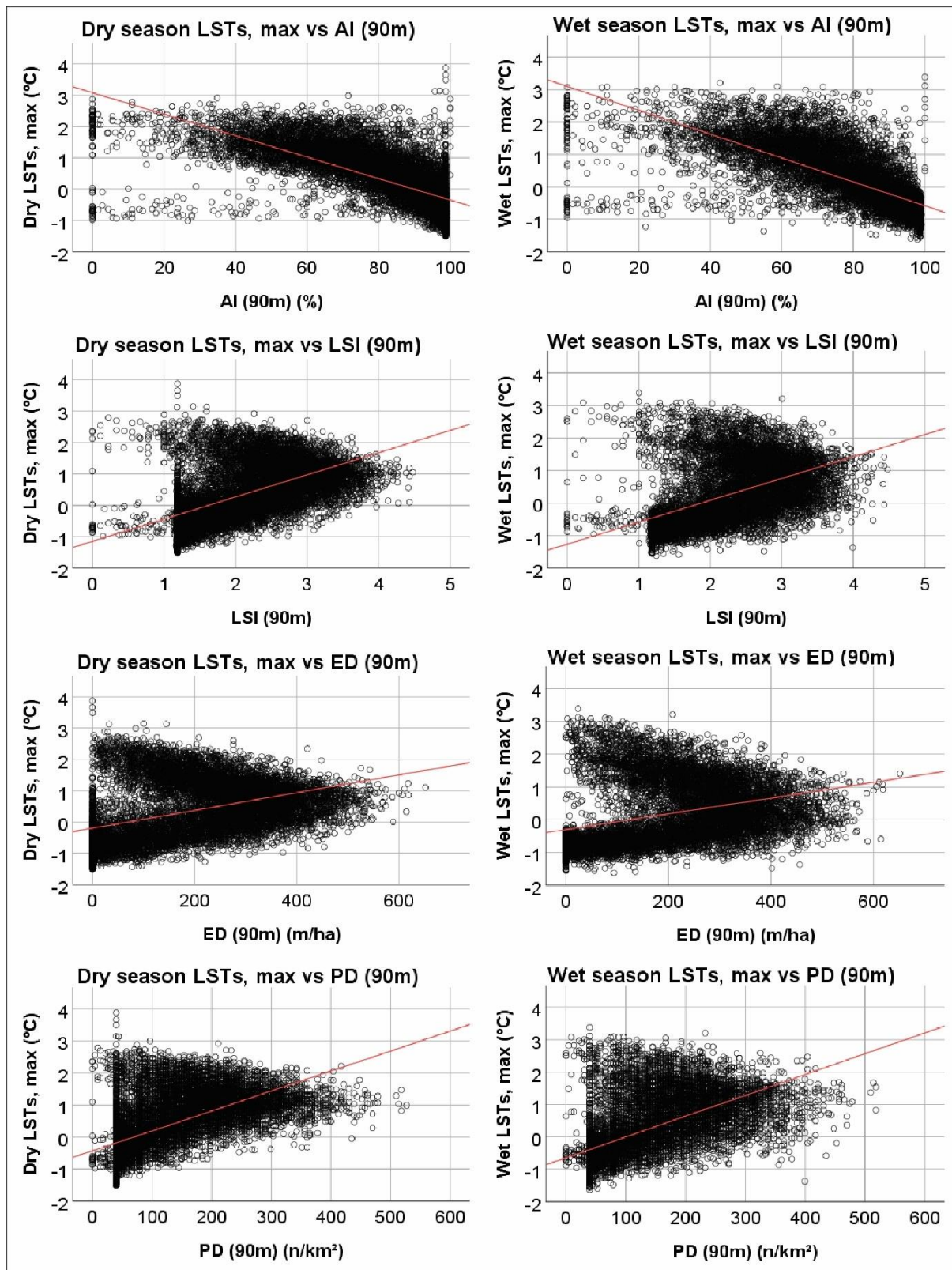


Figure 14. Scatterplots, including regression line and equation, of $LST_{s,max}$ by the several configurational class metrics for the dry (left) and wet (right) season after the 0% PLAND UGS values were filtered out.

The scatterplots in **Figure 14** show a linear relationship between LST and aggregation index. This relationship was specified by a linear regression analysis, resulting in significant negative relationships between AI and $LST_{s,max}$ in both the dry ($y = 3.083 - 0.034x$, $R^2 = 0.507$) and wet ($y =$

$3.098 - 0.037x$, $R^2 = 0.555$) season. This means that the more aggregated an UGS is, the better it cools the land surface. More aggregated UGS partly results from a higher presence of UGS in the pixels 90-meter radius environment, since the AI was highly correlated ($r = 0.853$).

On the contrary, the scatterplots of $LST_{s, \max}$ by LSI, ED and PD in **Figure 14** do not show a linear relationship between the three class metrics and LST, even though the Pearson's correlations indicated otherwise. However, the scatterplots all show a sort of V-shape to some extent. These can be explained based upon the nature of the different class metrics and their relationship with the presence of UGS in the 90-meter radius on which they were calculated:

The equation in **Table 6** shows that the minimum LSI value of one was reached when the shape of a UGS was as simple as possible. The LSI value does not say anything about the size of this UGS. So, both an UGS that totally covered the total 90-meter radius environment around a pixel, and the smallest UGS of just one, simply square-shaped pixel, have LSI values equal or very close to one. It could therefore be either very cold or very hot at a low LSI value, due to the difference in presence of UGS. When higher LSI are reached there needs to be at least a certain amount of UGS pixels and a certain amount of non-UGS pixels to be present in the 90-meter radius for a complex shape to be formed. As a result, a V-shape is displayed in **Figure 14** representing high and low $LST_{s, \max}$ for low LSI values and average $LST_{s, \max}$ values for higher LSI values.

The V-shape displayed in the scatterplot of the class metric ED can be explained in a similar way. A very low value for ED can be a result of just one pixel of UGS in the whole radius. But when the total 90-meter environment is covered by one large UGS there is no border length present at all, resulting in an ED of zero. So as with LSI, a low value of ED can either mean a high quantity of UGS or very little UGS. An increase in the border length could therefore mean both a decrease and an increase in UGS abundance. As a result, a V-shaped pattern emerged.

The minimum PD value is reached when just one patch of UGS was present in the 90-meter radius environment of a pixel. However, as with ED this could be an UGS patch that exists of just one pixel or an UGS patch that covered the whole 90-meter radius environment. So, an increase in PD from an UGS of one pixel could indicate an increase in UGS abundance. But an increase in PD from an UGS covering the whole 90-meter radius environment, means that there also needs to be non-UGS pixels present to separate the patches. As a result, the UGS abundance in the pixel environment decreases, leading to an increase of $LST_{s, \max}$. High values of PD are most likely reached when around 50% of the 90-meter radius environment consists of UGS. This resulted in the V-shaped scatterplot between PD and $LST_{s, \max}$ displayed in **Figure 14**.

3.2.4. Analysis of thermal centres and the effect on LST of all land cover features combined.

3.2.4.1. Influence of thermal centres

To complete the influence of individual land cover features, the influence of selected thermal centres was analysed. The results of the Pearson's correlations are shown in **Table 16**. The results indicate that there was a medium to large negative correlation between $LST_{s, \max}$ and distance to centre, and a small negative relation between $LST_{s, \max}$ and distance to river. Furthermore, there was a small to medium correlation visible between $LST_{s, \max}$ and distance to coast.

However, observation of the scatterplots shown in Appendix 11 reveals that there is a lack of pattern visible in the plots of $LST_{s, \max}$ by all three distance variables in both seasons. As a result, for the city of Paramaribo these thermal centres did not clearly influence the LST.

Table 16. Pearson's correlation of seasonal $LST_{s, \max}$ values and distances between interesting thermal centres.

Distances	Pearson's Correlation	
	Dry season	Wet season
Distance centre	-.468*	-.563*
Distance coast	.261*	.460*
Distance river	-.110*	-.244*
Number of observations	12064	11364

* Statistically significant at the .001 level (2-tailed).

3.2.4.2. The effect on LST of all land cover features combined.

After the relationships between all variables and LST were analysed, the three stated hypotheses were tested. When all 18 variables were combined in a multiple linear regression model, this resulted in an adjusted R^2 of .878 for the dry season (Appendix 12) and .882 for the wet season (Appendix 13), respectively. As a result, all 18 variables combined explained around 88% of the variance in $LST_{s, \max}$.

Variable selection revealed that the PLAND of water, urban and a green indicator (PLAND UGS or NDVI) turned out to be essential variables in all three of the models. The PLAND of water was essential for the variance explained by the model because of the vast Suriname river that runs through the administrative boundary. All river pixels located further than 90-meters from the riverbank only contained a PLAND value for water and were zero for all other land covers. Thus, only the PLAND value of water correlated to $LST_{s, \max}$ values in the river in both the wet and dry season. The PLAND of urban turned out to be essential, because it provided the heating counterpart for the mostly cooling UGS and water variables that explained $LST_{s, \max}$ on urbanized land cover. Therefore, it made sure that the variance explained by the model increased, since not only the lower values of $LST_{s, \max}$ but also the higher were explained. Vice versa, the same argument applies to the inclusion of a green indicator in the model to provide a cooling counterpart. Moreover, during the variable selection it became clear that after the essential variables to test the hypotheses were included, adding one of the configurational class metrics or distance to thermal centre variables did not explain any extra variance in $LST_{s, \max}$. This negligible additional influence can also be seen in the total multiple linear regression models shown in Appendices 12 and 13. Therefore, they have been omitted in all three models.

As a result, the following variable combinations were found to best describe $LST_{s, \max}$ in both seasons, while testing the hypotheses:

Model 1: PLAND Urban (90m), PLAND Water (90m), NDVI

Model 2: PLAND UGS (90m), PLAND Urban (90m), PLAND Water (90m)

Model 3: PLAND Trees (90m), PLAND Mixed low vegetation (90m), PLAND Grass (90m),
PLAND Urban (90m), PLAND Water (90m)

The results of the first model to test if impervious urban surface heats the surface in the dry season are shown in

Table 17.

Table 17. Multiple linear regression model 1, used to test the hypothesis: Impervious urban surface heats the surface in the dry season.

Model 1: Urban Heats	Coefficients Dry Season					R ²
	Unstandardized coefficients		Standardized coefficients	t	Sig.	
	B	Std. Error	B			
(Constant)	0.937	0.021		44.228	.000	.781
PLAND Urban (90m)	0.026	0.000	0.422	59.004	.000	
PLAND Water (90m)	-0.021	0.000	-0.671	-74.128	.000	
NDVI	-1.797	0.029	-0.569	-62.172	.000	

*Dependent variable: dry season $LST_{s, max}$

The R² value shows that the model variables accounted for 78.1% of the variation in LST in the dry season. So, the explained variance that was lost by just using these three variables instead of all 18, only amounted to 9.7%. The adjusted R² of model one was equal to R², meaning that the model generalizes very well. Because there is a unit difference between the PLAND values and the NDVI, the standardized β -coefficients have been considered for the sake of comparability.

Table 17 shows that urban land cover in a 90-meter environment of a pixel has a significantly strong positive effect on the $LST_{s, \max}$ on that pixel. So, model one confirmed the first hypothesis, that impervious urban land cover does heat the surface.

Table 18. Multiple linear regression model 2, used to test the hypothesis: UGS cools the surface in the dry season.

Model 2: UGS Cools	Coefficients Dry Season					R ²
	Unstandardized coefficients		Standardized coefficients	t	Sig.	
	B	Std. Error	B			
(Constant)	1.458	0.021		68.767	.000	.822
PLAND UGS (90m)	-0.021	0.000	-0.792	-87.061	.000	
PLAND Urban (90m)	0.008	0.001	0.123	14.580	.000	
PLAND Water (90m)	-0.023	0.000	-0.756	-97.795	.000	

*Dependent variable: dry season $LST_{s, \max}$

Table 18 shows the results of model two which was used to test the second hypothesis: UGS cools the surface. As in model one, the variance of $LST_{s, \max}$ in the dry season explained by model two (R^2), was close to the amount of variance explained by the total model containing all 18 variables. Again, the adjusted R^2 was equal to R^2 meaning that the model generalizes well. The standardized β -coefficient of UGS points out that the presence of UGS in a 90-meter radius has a strong and significant cooling effect on $LST_{s, \max}$ in the dry season. The coefficients of urban land cover were also positive in this model indicating a heating effect.

Table 19. Multiple linear regression model 3, used to test the hypothesis: Trees are the UGS type that cools the surface most effective in the dry season.

Model 3: Trees Cool Most	Coefficients Dry Season					R ²
	Unstandardized coefficients		Standardized coefficients	T	Sig.	
	B	Std. Error	β			
(Constant)	-0.014	0.018		-0.768	.442	.774
PLAND Trees (90m)	-0.015	0.000	-0.225	-44.034	.000	
PLAND Mixed low vegetation (90m)	-0.005	0.000	-0.157	-23.063	.000	
PLAND Grass (90m)	0.003	0.000	0.054	9.159	.000	
PLAND Urban (90m)	0.039	0.000	0.616	82.457	.000	
PLAND Water (90m)	-0.009	0.000	-0.282	-38.793	.000	

*Dependent variable: dry season $LST_{s, max}$

Table 19, shows the results of model 3 that was used to test the third hypothesis, that trees are the UGS type that cool the surface most effectively. The model’s explanatory power was still high with an R² of .774. However, it lost some of the explanatory power compared to model two. This was a consequence of the exclusion of mangrove in the model, whereas it was included in the combined land cover class UGS in model two. The standardized β-coefficient in **Table 19** show that from the three different types of UGS included in the model, trees had the strongest significantly negative relationship with $LST_{s, max}$ in the dry season. Mixed low vegetation showed to have a smaller but still negative effect on the $LST_{s, max}$, where land covered with grass showed a slight heating effect in the dry season.

From the results of the three models, all of the stated hypotheses were confirmed for the dry season. Three models were ran containing the same variable combinations, only this time from within the wet season and predicting $LST_{s, max}$ in the wet season. The results of these models are shown in Appendix 14. The results slightly differ in value, but resulted in the same conclusions.

3.2.5. Detailed cooling effects of green features specific for Paramaribo

3.2.5.1. Green features

The location of the 32 selected typical green features for the city of Paramaribo, based on remote sensing imagery and field work experience, are shown in **Figure 15**.

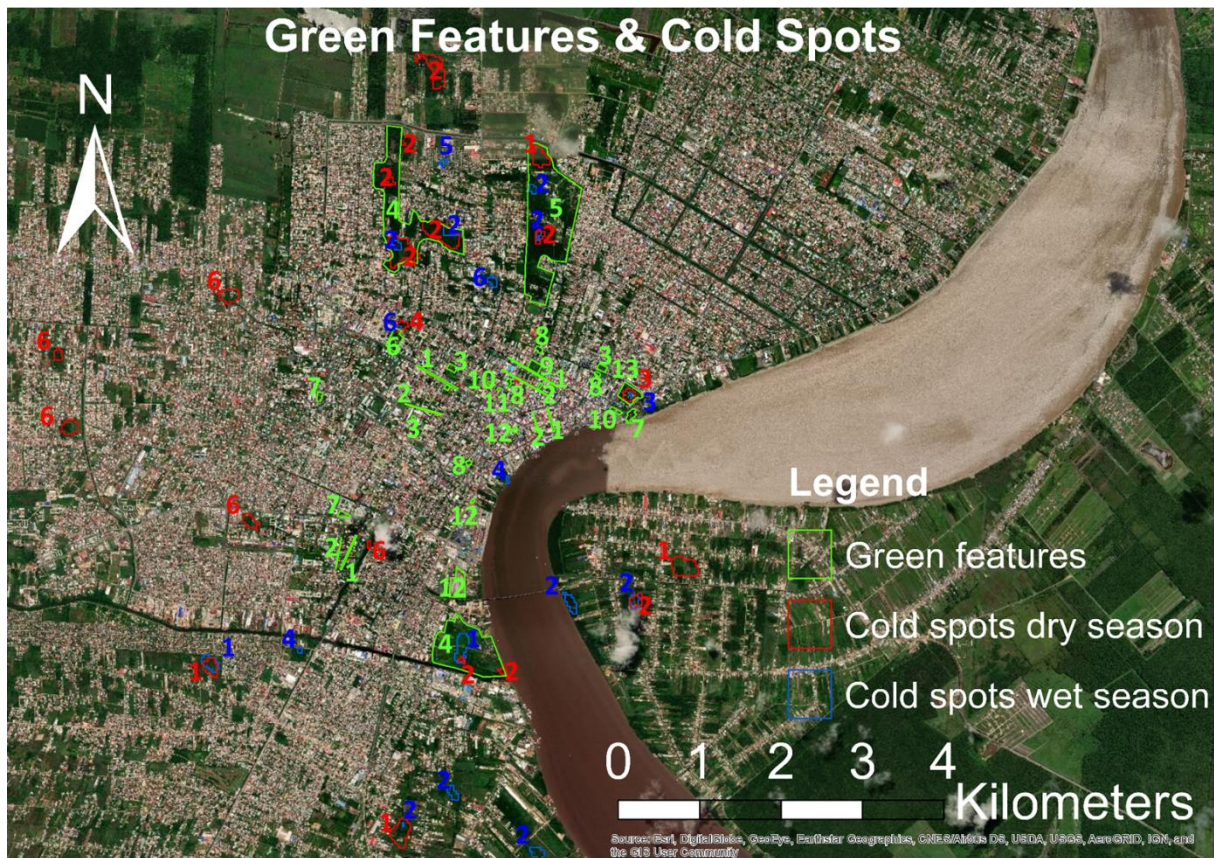
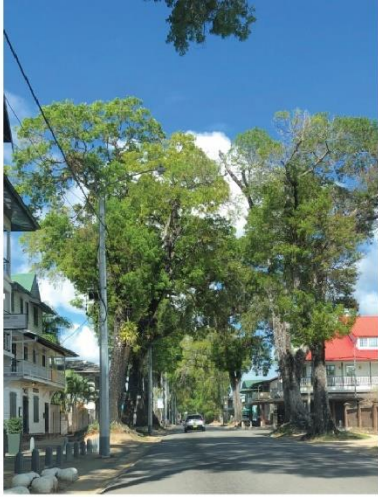


Figure 15. Location of selected green features and cold spots, including their group number (explained in **Figure 16**, **Figure 18** and **Appendix 15**) in the city of Paramaribo.

Figure 16 shows six images taken at green features belonging to six green feature groups. These pictures were selected because they give a good representation of the land cover that is common for each green feature group. The green features groups differed in vegetation cover. In addition, some green feature groups did not differ in vegetation cover but only in size. These green features are indicated with either small (0 – 1,300 m²), moderate (3,400 – 4,500 m²) or large (4,100,00 m² - 8,320,00 m²). **Appendix 15** shows similar representative images for all the other groups of green features that were studied.



1 - Street with trees



4 - Large green area with trees



5 - Large park with trees



7 - Small park with trees



12 - Bare land



13 - Moderate park with palm trees

Figure 16. Typical land cover for six of the thirteen selected green feature groups.

The average $LST_{s, \max}$ value in the dry and wet season for all the groups of selected typical green features for the city of Paramaribo are shown in **Figure 17**.

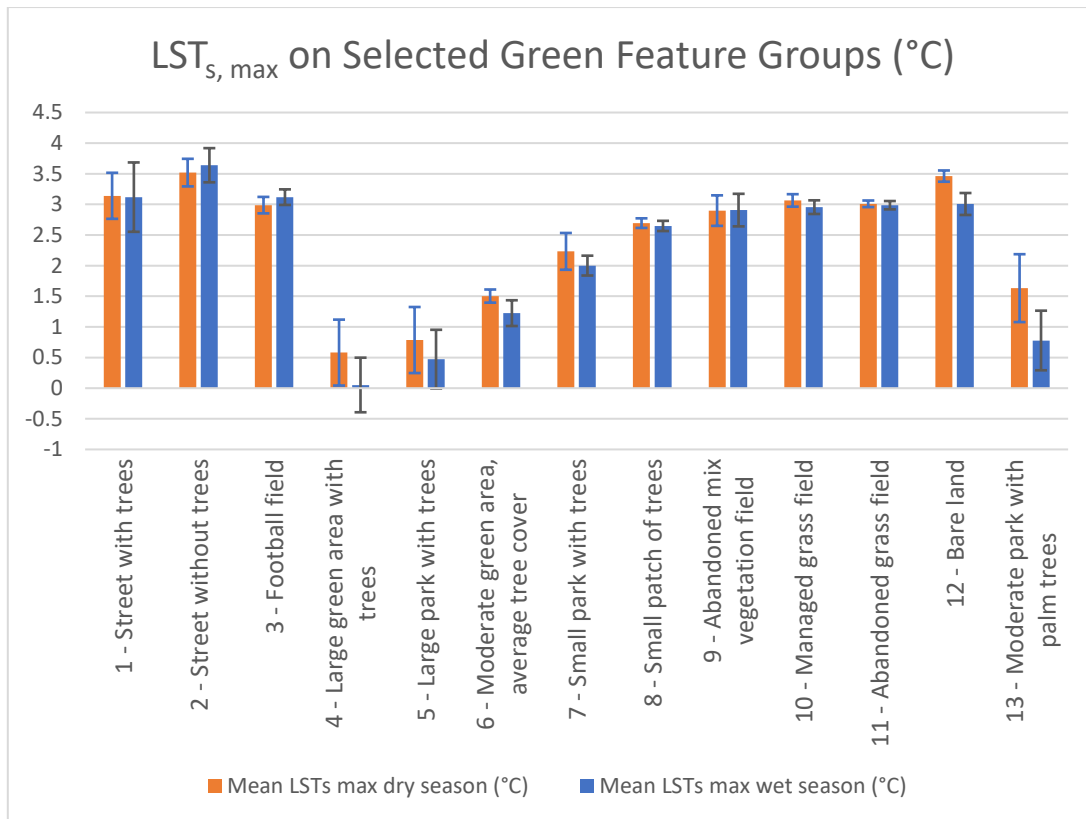


Figure 17. Average $LST_{s, \max}$ on the selected green feature groups, including error bars displaying the standard deviation, in the city of Paramaribo.

Figure 17 shows the average $LST_{s, \max}$ values per green feature group of all the pixels that were contained in the polygons that were drawn around the green features of the same group. The results showed that the size of a green feature was pivotal for the obtained cooling effect as it was seen that all the lowest $LST_{s, \max}$ values prevailed on groups existing of the larger green features. In addition, **Figure 17** shows that trees had a larger cooling effect than mixed vegetation and grass. When considering tree type, there is a slightly stronger cooling effect visible on land covered by deciduous trees than land covered by palm trees. This is likely because of the larger leaf area index of deciduous trees. In terms of cooling effect, it does not matter if a grass field was properly managed or abandoned according to the results. Lastly, **Figure 17** shows that although the effect was small with regard of cooling the surface it was beneficial to plant trees along streets.

After this descriptive analysis, a random point sample ($N = 448$) was taken of $LST_{s, \max}$ pixels on the selected green features. The Kruskal-Wallis test on the sample showed that there was a statistically significant difference in $LST_{s, \max}$ between different green feature groups in the dry season and wet season, $H_{dry}(12) = 177.62$, $p < .001$ and $H_{wet}(12) = 214.32$, $p < .001$. After which a post-hoc Bonferroni correction was applied on the pair-wise comparisons that were performed using Mann-Whitney tests, of which detailed results are shown in Appendix 16. The tests showed that in the dry season the $LST_{s, \max}$ was significantly lower on a very big green area with trees than on all the other green features except for very big parks with trees and abandoned grass fields, and that $LST_{s, \max}$ was significantly lower on a very big park with trees than on bare land and on streets with and without trees.

The Wilcoxon signed-rank test, showed in detail in Appendix 9, showed that the differences between $LST_{s, \max}$ in the wet and dry season were only significant for the following green features: Very big green area with trees ($z = -8.64$, $p < .001$, $r = -.44$), Big green area moderate tree cover ($z = -2.03$, $p <$

.05, $r = -.54$), and Bare land ($z = -3.11$, $p < .01$, $r = -.61$). These results are also visible when looked at **Figure 17**, where temperature differences between the wet and dry season were generally very small.

3.2.5.2. Cold spots

The land cover was documented on the 37 cold spots that were selected purely based on the lowest $LST_{s, \max}$ values that prevailed within the administrative boundary. The locations of these cold spots are shown on the World Imagery ArcGIS base map in **Figure 15** and on the two seasonal $LST_{s, \max}$ in Appendix 17. **Figure 19** shows the average $LST_{s, \max}$ on the cold spots after they were grouped based on land cover characteristics. Representative images of the characteristic land cover defining each group are shown in **Figure 18**.



1 - Mixed vegetation in large green area



2 - Patch of high-density trees in large green area



3 - Patch of high-density palm trees in large green area



4 - Patch of high-density trees in urban



5 - Mixed vegetation in urban



6 - Patch of trees in urban

Figure 18. Representative land cover for each of the cold spot groups.

The $LST_{s, \max}$ values in **Figure 19** show that the coldest spots in Paramaribo were all covered by vegetation. The cold spot results also confirmed the conclusions drawn on the analysis of green features, that size of green area is an essential contribution to the cooling effect of an UGS. Besides size, **Figure 19** also confirms that within the cold spots the coldest areas were found on land covered with trees over land covered with other vegetation.

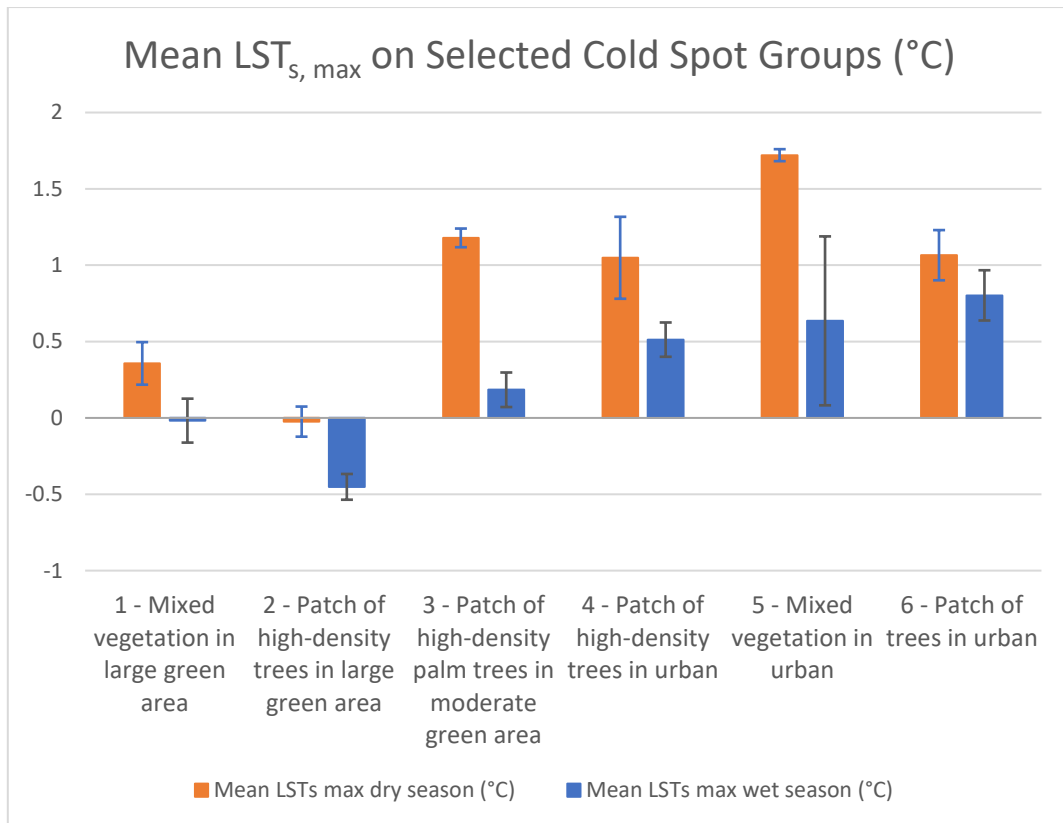


Figure 19. Average LSTs, max on the selected cold spot groups, including error bars displaying the standard deviation, in the city of Paramaribo.

A non-parametric Kruskal-Wallis test was performed on a randomly taken sample of 156 points within the selected cold spots. The detailed results of this test are shown in Appendix 18, but in conclusion this test showed that the distribution of dry and wet season $LST_{s, \max}$ was not the same across the six different groups of cold spots, $H_{\text{dry}}(5) = 96.09$, $p < .001$ and $H_{\text{wet}}(5) = 87.12$, $p < .001$. Following this, a post-hoc Bonferroni correction was applied on the pair-wise comparisons that were performed using Mann-Whitney tests. The test showed that in the dry season there were statistically significant differences between the groups:

1. Patch of high-density trees in big green area
 - a. Patch of high-density palm trees in big green area
 - b. Mixed vegetation in big green area
 - c. Patch of high-density trees in urban
 - d. Mixed vegetation in urban
 - e. Patch of trees in urban
2. Patch of high-density palm trees in big green area
 - a. Patch of trees in urban
3. Mixed vegetation in big green area
 - a. Patch of trees in urban

In the wet season differences in $LST_{s, \max}$ between the same groups were significant except for the differences between, patch of high-density trees in big green area and mixed vegetation in urban.

A Wilcoxon signed-rank test, Appendix 9, showed that the difference between $LST_{s, \max}$ in the wet and dry season were only significant for the cold spot categories: Patch of high-density trees in big green area ($z = -2.75$, $p < .01$, $r = -.32$) and Patch of trees in big green area ($z = -3.22$, $p < .01$, $r = -.42$).

Only two of the cold spot categories were significantly different, even though differences seem large between seasons in more categories. This was a consequence of the small sample size which was unevenly distributed between groups.

3.2.5.3. Neighbourhoods

Fieldwork pointed out that vegetation type did differ in neighbourhoods of different SES. Vegetation patterns that were typical for each neighbourhood type are shown in **Figure 20**.



Top SES (Rich)



Middle SES



Middle to low SES



Low SES (Poor)

Figure 20. Characteristic street image, including vegetation pattern, in neighbourhoods of different SES based on residential class.

The associated differences in $LST_{s, \max}$ between neighbourhoods differing in SES based on residential class are shown in **Figure 21**. A Kruskal-Wallis ($H_{\text{wet}}(3) = 407.25, p < .001$ & $H_{\text{dry}}(3) = 342.06, p < .001$), pointed out that differences in $LST_{s, \max}$ in both the wet and dry season between neighbourhoods of different residential class were all significant except for the difference between residential classes middle and rich (details in Appendix 19).

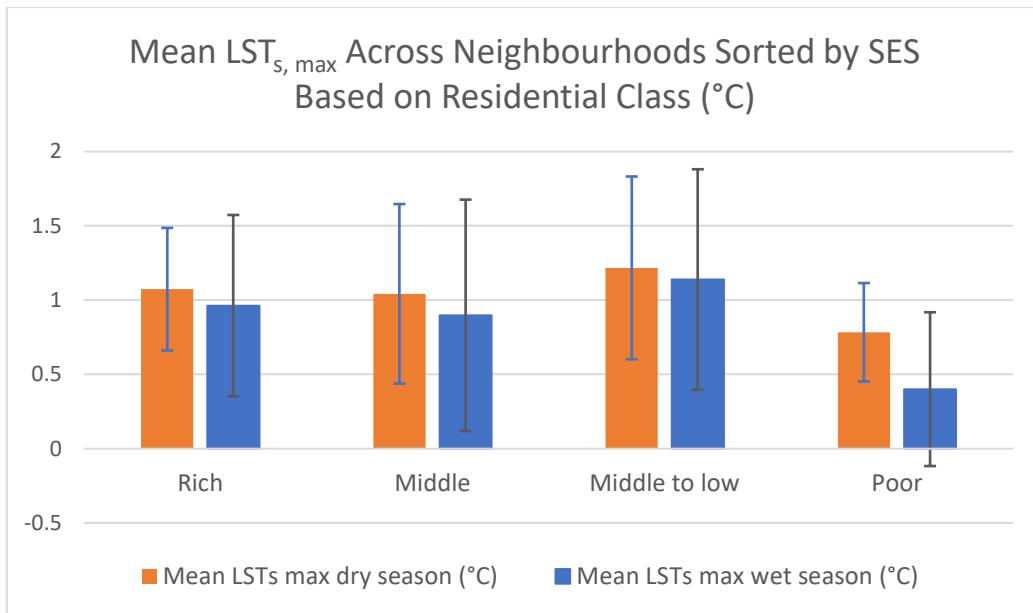


Figure 21. Mean $LST_{s,max}$ in neighbourhoods, including error bars displaying the standard deviation, in Paramaribo differing in SES once based on residential class.

The results from both graphs in **Figure 21** show that both seasonal average $LST_{s,max}$ values were significantly highest in neighbourhoods with a middle to low SES and significantly lowest within low SES neighbourhoods. The differences in $LST_{s,max}$ between neighbourhoods of middle and top SES on the other hand were negligible.

3.3. Analysis of the relationship between the LST and air temperature

3.3.1. SUHI vs CLHI

The comparison between the larger SUHI and the CLHI, was based on the urban “core – rural” indicator value shown in

Table 9 and on air temperature data from the urban core outdoor temperature loggers 1 and 2, and rural outdoor temperature logger 13 (Appendix 3 & 20). Outdoor temperature loggers 1 and 2 serve as the urban core reference, since these outdoor temperature loggers are the only two that are situated at a location with more than 67 percent of urban cover in its 9 km² surroundings. This is the same definition as was used for the urban core in the SUHI indicator.

Since, the rural outdoor temperature logger was not operational at the time when the Landsat images were obtained, a direct comparison on the same dates was not possible. Thus, was chosen to compare mean air temperature results from the short rainy season (early December 2019 – late January 2020) to mean LST values from the wet season. The resulting CLHI during this short rainy season is shown in **Figure 22**.

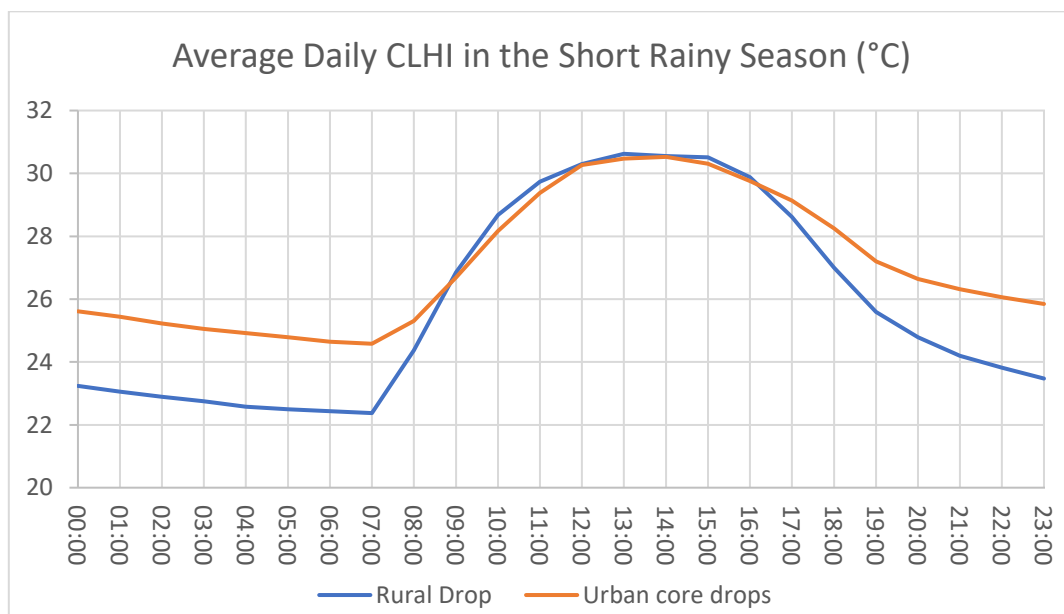


Figure 22. The average daily CLHI during the short rainy season (07-12-2019 – 31-01-2020) between the urban core (outdoor temperature logger 1 & 2) and rural (outdoor temperature logger 13).

Figure 22 shows that during the short rainy season, according to the outdoor temperature logger results, the CLHI is present during the night, but almost absent during the day. The CLHI reached its maximum of around 2.4 °C at 01:00 a.m., a more or less constant value that prevailed during the night. However, the CLHI decreased quickly to 0 or even slightly negative values after sunrise, to increase again from the late afternoon onwards.

For the comparison with the SUHI, the average difference between the urban core outdoor temperature loggers and the rural outdoor temperature logger was taken at 14:00 hrs, local time. The CLHI during the short rainy season amounted to a negligible negative difference of -0.03 °C. Therefore, air temperatures on average were equal in the rural hinterland and the urban core at 14:00 hrs, local time, during the short rainy season. The SUHI averaged to an amount of 5.14 °C at 14:00 hrs, local time, during the wet season.

3.3.2. Relationship between LST and air temperature found within the administrative boundary of Paramaribo

The results of the air temperature measurements and LST values at the location of the measuring stations Cultuurtuin and Zorg en Hoop on the time when all the analysed Landsat images were taken are shown in **Figure 23**. From the results it can be seen that at both locations and in both seasons the air temperatures were higher than the LST's.

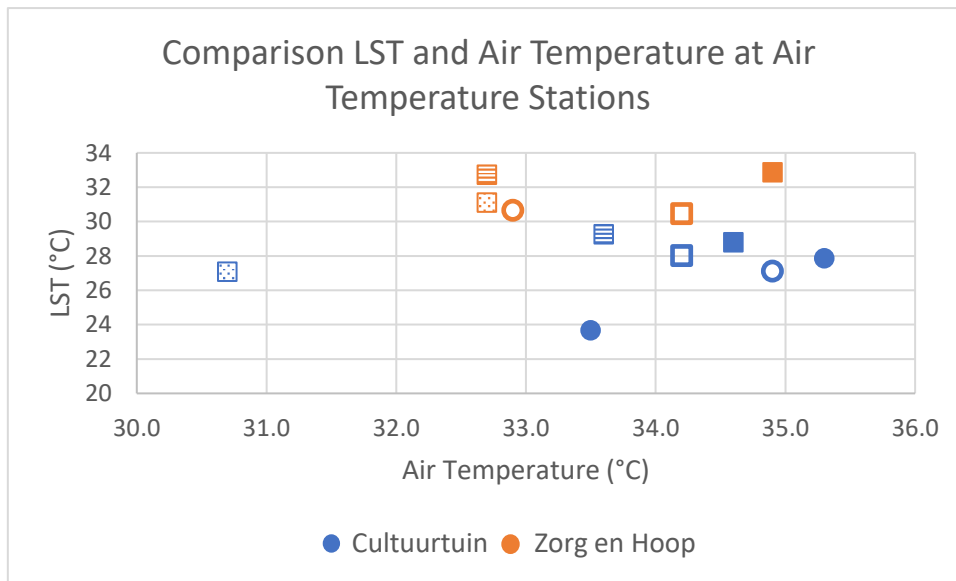


Figure 23. LST and air temperatures measured on 14:00 hrs, local time, at the locations of the measuring stations, Cultuurtuin and Zorg en Hoop, of the meteorological service Suriname. In the figure, air temperatures measured at Cultuurtuin are depicted in blue and temperatures measured at Zorg en Hoop are depicted in orange. Temperatures measured in the dry season are depicted with squares, while temperatures measured in the wet season are depicted in circles.

The magnitude of the temperature difference between air temperature and LST seems to be related to both season and location. Firstly, LST values were higher for all dates on the industrial location Zorg en Hoop than on the highly vegetated and green station Cultuurtuin, while the difference in air temperature between the two locations was not that obvious in the dry season. Although it seemed that air temperatures in the wet season tended to be lower at Zorg en Hoop (avg. 32.6°C) than at the Cultuurtuin (avg. 34.6°C). Secondly, the results showed that differences between LST and air temperature were larger on the highly vegetated and green location at the Cultuurtuin (avg. 6.3°C) than on the industrial site Zorg en Hoop (avg. 1.9°C). Lastly, the temperature differences between surface and air temperatures were larger in the wet season (avg. 6.8°C) than in the dry season (avg. 3.4°C).

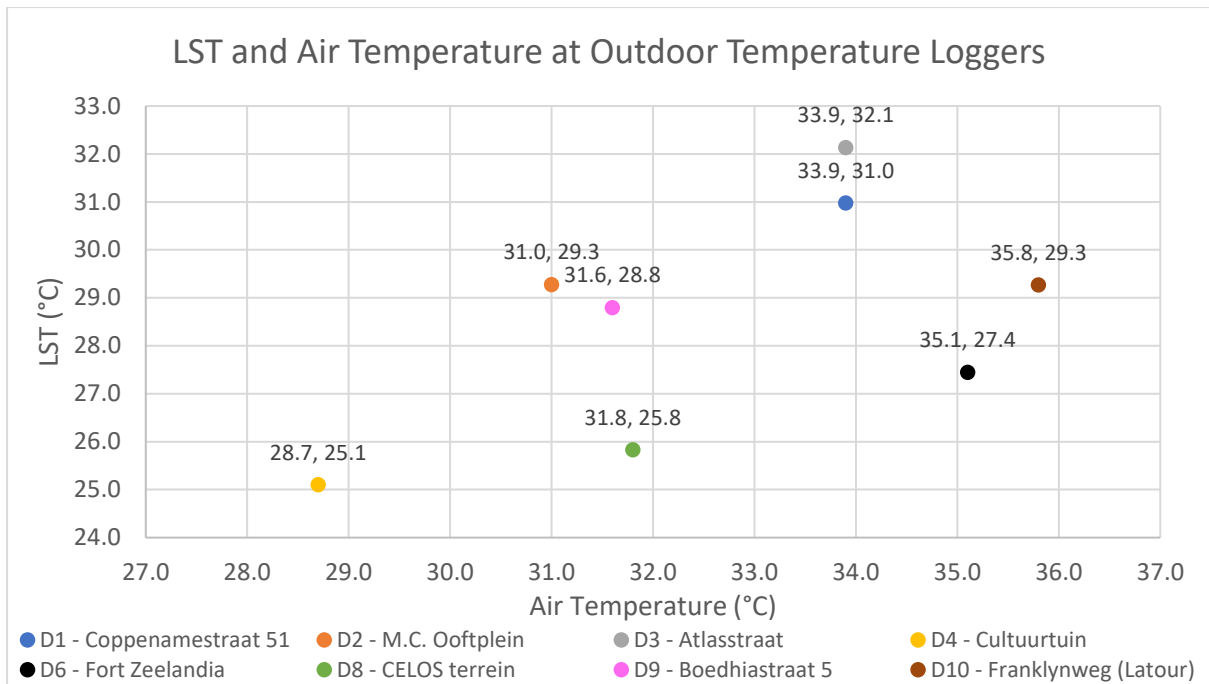


Figure 24. LST and air temperatures on 14:00 hrs, local time, on August 8th, 2019 at the locations of the outdoor temperature loggers.

The results of air temperature measurements of the outdoor temperature loggers are shown in **Figure 24**. Only the temperature values obtained at 14:00 hrs, local time, on the 8th of September, 2019 are displayed, because this was the only time and date that one of the analysed Landsat images was obtained during the operational period of the outdoor temperature loggers. The results showed that at all locations the air temperature was higher than the LST, independent of the landcover. The range across all outdoor temperature logger values was in the same order of magnitude for the LST as for air temperature. However, when looked at the ranks of the individual outdoor temperature loggers when they were ranked from high to low once for LST and once air temperature, only the ranks of the outdoor temperature logger placed in the Cultuurtuin matched as the coldest outdoor temperature logger of all. While, from the air temperature results obtained on all the dates through the air measuring stations of the meteorological service, the Cultuurtuin did not show to be extremely low. This could be a consequence of the difference in exact location of the air measuring station (open grass field within the urban forest) and the outdoor temperature logger (in the middle of highly dense tropical forest). Taking this into account, this temperature difference should still not be so great. All results of both the air temperature measuring stations as the outdoor temperature loggers are displayed in more detail in Appendix 20.

4. Discussion

4.1. Reflection on results

The results showed a mean SUHI at 14:00 hrs, local time, of 5.3 °C in the dry season and of 5.1 °C in the wet season between the urban core in the administrative boundary and the rural hinterland in the Greater Paramaribo region (see section 3.1.). As a result, it is concluded that the SUHI in Paramaribo in the dry season is slightly larger compared to the SUHI in the wet season. Average daily SUHI magnitudes found in the few SUHI studies conducted in the tropics that also included the wet season, range from 3 to 6 °C (Acero & González-Asensio, 2018; Amorim, 2018; Ayanlade, 2016).

However, these studies show different results regarding the difference in SUHI between seasons. Similar to the results of this study, the study of Ayanlade (2016) who studied the SUHI in Lagos, showed a slightly larger SUHI (3.1 °C vs 3.4 °C) in the dry season. According to them this is due to the thermal heating influence of urban surface, which they consider to be larger than the thermal cooling influence of vegetation. This might be explained by the fact that in Lagos, like in Paramaribo, temperatures and the amount of sun hours are larger in the dry season, which leads to a larger increase in the LSTs in urban areas in the dry season compared to the wet season. In the wet season there is more vegetation present, mainly within the rural area, leading to lower LSTs in rural areas. However, this does not outplay the excessive heating influence of the urban surface in the dry season. Together these effects result in a slightly larger SUHI in the dry season in Lagos and in Paramaribo as reported by the present study. However, since the heating influence of urban surface is larger, the SUHI is also slightly larger in the dry season. On the contrary, Amorim (2018) and Acero & González-Asensio (2018) found the SUHI to be larger in the wet season in the city of Presidente Prudente in southern Brazil and San Salvador in El Salvador, respectively. The studies point out that this is caused by the increase of vegetation in the wet season, that subsequently mainly cools the rural surface. This may be explained by differences in distribution of temperature and precipitation across seasons in these cities compared to Paramaribo. As opposed to Paramaribo, temperatures in these cities were higher during the wet season resulting in larger heating of urban surfaces. In addition, the SUHI's in both these studies were based on satellite images taken in the mid-morning, when the influence of vegetation thermal inertia in relation to the loss of heat by latent heat flux is largest and therefore larger than at the time of measurement in this study (14:00 hrs, local time) (Weng, Lu, & Schubring, 2004). Also, the difference in precipitation amount between the dry and the wet season was substantially larger in the two studies than in the present study. When all the SUHI indicator values found in this study are compared to those reported in Schwarz et al. (2011) found at 13:30 on July 2002, across 263 European cities, some are found to differ and some are found equal. However, this is expected due to the difference in climate, vegetation cover and urban design.

To mitigate the heating effect of the SUHI, this study points out that implementing UGS is an effective cooling measure (see section 3.2.2. & 3.2.4.2.). This finding is consistent with a large number of previous studies (Bowler et al., 2010; Demuzere et al., 2014; Huang, Cui, & He, 2018a; Marando et al., 2019; Mirrahimi, Lukman Nik Ibrahim, & Surat, 2015). From the four studied UGS types, trees and mangrove appear to be the most effective coolers of the surface. As a result, the mean LST_{max} measured on land covered with trees was around 5 °C cooler than the mean LST_{max} found on urban surfaces. These differences in LST_{max} were slightly larger than the 4 °C difference found in the study by Du et al. (2019) in Shanghai and the 3 °C difference found in the study of Marando et al. (2019) in Rome. However, the use of LST_{max} in the present study instead of LST makes comparisons of absolute results difficult. In general, however, this finding is consistent with previous research indicating that UGS with higher tree densities reduce LST more than UGS with fewer trees (Brown et al., 2015; Jaganmohan et al., 2016; Kong et al., 2014; Vanos et al., 2012). This results from the fact that shading is the most effective cooling mechanism of UGS (Brown et al., 2015; Kong et al., 2014; Vanos et al., 2012). Therefore, these studies conclude that to cool an urban area focus should be on designing shaded UGS (Brown et al., 2015; Vanos et al., 2012). The lower LST values found on land with deciduous trees compared to palm trees in the city of Paramaribo underline this conclusion.

In addition to the composition of the UGS, this study did not show a clear relationship between LST and most of the configurational characteristics of the UGSs (see section 3.2.3.). Only AI seemed to have a negative relationship with LST, meaning that a single aggregated UGS reduce LST more

effectively than multiple disaggregated UGSs of the same total area. This conclusion is confirmed by the research of Simwanda et al. (2019) and Cao et al. (2010). The study by Kong et al. (2014) concludes that if an UGS of 3.45 ha or larger is present close to disaggregated smaller UGSs the cooling effect of the large UGS can extend to the smaller disaggregated UGSs and so effectively cool a larger area. An UGS of 3.45 ha is larger than the area of the used moving window in the present study, so this negative effect of disaggregated smaller UGSs on LST was not found in the present study. The other class metrics (LSI, PD, ED) did not show a clear relationship with LST in the present study, although relationships between these class metrics and LST were reported in other studies (Du et al., 2019; Maimaitiyiming et al., 2014). In the present study these other class metrics showed an odd V-shaped relationship with LST, which may have been due to the small area (90-meter radius circle) used in this study to calculate these class metrics. Due to the properties of these class metrics they proved to be not suitable for the chosen analysis method. However, the effect of the distribution and shape class metrics on LST in previous studies is also inconclusive. The study by Huang et al. (2018) argues that a simply designed UGS is beneficial for cooling, whereas the study by Maimaitiyiming et al. (2014) indicates that complexly shaped UGS are desirable.

Regardless the shape, this study showed that the size of the UGS is essential for the cooling effect of the UGS. The analysis of the green features and the cold spots showed that the larger the UGS, the lower the LST (see section 3.2.5.1 & 3.2.5.2.). Previous studies confirm this negative relationship between UGS size and LST (Cao et al., 2010; Huang et al., 2018a; Jaganmohan et al., 2016; Kong et al., 2014).

The distances from the selected thermal centres (city centre, Suriname river, Atlantic Ocean) did not have a relationship with LST in the administrative boundary of Paramaribo (see section 3.2.4.1.). The study by Simwanda et al. (2019) also showed no clear relationships between LST and the distance to the city centre in the cities of Addis Ababa and Lusaka. However, these findings are not in line with the study by Cai et al. (2018) that reported a positive relationship between the distance to large waterbodies and the prevailing LST. In addition, the study of Marando et al. (2019) showed a negative relationship between the distance from city centre of Rome and the prevailing LST. The specific situation in the administrative boundary of Paramaribo, where the city centre lies directly on the border of the large Suriname river, may explain why no relation was found between these distances and LST. This makes it plausible that, the positive influence of the city centre on the LST and the negative influence of the water body on LST more or less cancel each other out.

This study found a negative relationship between SES and LST, except for the lowest SES group. The LST distribution across neighbourhoods of different SES showed that LST values were lowest in neighbourhoods of the lowest SES (see section 3.2.5.3.). This is in contradiction with previous studies that point out that when the SES of citizens in a neighbourhood decreases that LST tends to increase (Jenerette et al., 2007; Tang et al., 2017). These studies found that when SES decreased, the amount of impervious surface increased and the amount of vegetation decreased, resulting in a higher LST. This negative relation also holds for the upper three classes of SES in the city of Paramaribo. However, in the developing city of Paramaribo, in contrast to the above-mentioned studies, in the hardly urbanized neighbourhoods of the lowest SES the impervious surface is replaced by a sandy surface. This considerably reduces the albedo and heat capacity of the surface and therefore decreases the LST. In addition, neighbourhoods of low SES were found to have a relatively high amount of green, however this green almost entirely consisted of non-public and unmanaged green space. As a result, it can be concluded that a negative relationship exists between LST and SES in Paramaribo, with the exception of the neighbourhoods with the lowest SES.

One of the main aims of the study was to show the differences in cooling effect of UGS in the dry and wet season. The results showed that all analysed UGS types, except for grass, significantly cooled the surface in both the wet and dry season (see section 3.1.2.2. & 3.2.2.). The results also showed that this cooling effect of the UGS types trees and mangrove is slightly stronger during the dry season in the administrative boundary of Paramaribo, whereas it is found to be slightly stronger during the wet season for the whole Greater Paramaribo Region. This might be a consequence of the fact that evaporative cooling is enhanced by larger temperature rise during the dry season. This only holds if during the dry season, water is available for plant growth in Paramaribo (GBS, 2016). As a result, the rate of evaporation increases as the temperature rises, as warmer air can retain more water vapour (North Carolina Climate Office, n.d.). Since temperatures rise more in the administrative boundary than in the Greater Paramaribo Region this could explain the higher cooling rate of trees and mangrove in the administrative boundary during the dry season. However, another factor that increases UGS cooling is the increase in vegetation, since there is more vegetative growth during the wet season in the Greater Paramaribo Region than in the administrative boundary, the cooling effect also increases more in the Greater Paramaribo Region. However, the excessive vegetative growth during the wet season in the Greater Paramaribo Region compared to the administrative boundary, might be responsible for an extra cooling effect in the Greater Paramaribo Region during that season. The cooling effect of mixed low vegetation is slightly stronger in the wet season in both the administrative boundary and the Greater Paramaribo Region. This might be explained by the fact that mixed low vegetation may be more dependent on the frequent rain supply in the wet season since they have less access to deeper and more stable groundwater supply. However, this explanation is not found in other studies and thus needs further investigation.

Regarding air temperatures, both the magnitude and the pattern of the diurnal CLHI in Paramaribo are in line with the general pattern of the CLHI, found in other studies, that is present during the night but almost absent during the day (Chang, Li, & Chang, 2007; Mutiibwa et al., 2015; U.S. Environmental Protection Agency, 2008; Voogt, 2007). Since the SUHI is present during the day it is surprising that air temperatures at 14:00 hrs, local time, were found to be larger than LSTs at both the measuring station and at all locations of the outdoor temperature loggers in the administrative boundary (U.S. Environmental Protection Agency, 2008; Voogt, 2007). In addition, no relation was found between the land cover and the prevailing air temperature, since air temperatures were higher on the vegetative surface of the Cultuurtuin as on the industrial surface of Zorg en Hoop. This is in contrast with previous research, which investigated the relationship between LSTs and air temperatures (Anniballe et al., 2014; Mutiibwa et al., 2015).

4.2. Methodological strengths and limitations

One of the main strengths of this research is that it is one of the few studies analysing the SUHI in a city located in the tropics (Estoque et al., 2017; Simwanda et al., 2019; Wardana, 2015; Yusuf, Pradhan, & Idrees, 2014). Unfortunately, the tropics are a very clouded region all year round. This high cloud coverage complicates optical remote sensing, making a remote sensing study of the SUHI on a large and continuous surface difficult (see section 2.3.1. & 2.3.4.). Consequently, the few tropical SUHIs that have been studied are most often done during the dry season, where occasional cloudless days occur. (Estoque et al., 2017; Simwanda et al., 2019; Wardana, 2015; Yusuf et al., 2014). This study is one of the first to study the SUHI in both the dry and wet season in the tropics and therefore yields important information. There already exist three studies that provide a link between UGS and LST in a city in the tropics in both the wet and dry season (Acero & González-Asensio, 2018; Amorim, 2018; Ayanlade, 2016). However, these three studies provide this

relationship between UGS and LST only through the use of NDVI, while this study in Paramaribo complements this link by making a distinction in type of UGS. The cloudiness that was present in the wet season did make several methodological adjustments necessary. For instance, a lot of information was lost due to cloud correction and the creation of LST information on a large and continuous surface required the production of seasonal composites. This made it necessary to switch from LST to standardized LST. Moreover, to limit the cloud interference, not the average LST, but the maximum standardized LST values were used for the creation of these composites. These necessary adjustments resulted in composites of the dry and the wet season where the maximum $LST_{s, \max}$ value from four time steps in the dry season and three time steps in the wet season was taken. However, many pixels also just display the only pixel value present, as clouds were present at that location on the other two selected dates. This can result in different patterns between the wet and dry seasons, as in the dry season only nearly cloud-free images were selected and thus almost every composite pixel was maximized out of three. In addition, the use of LST_{\max} in the SUHI indicators and the use of $LST_{s, \max}$ in the correlation and regression analysis make it difficult to compare findings to other studies.

In this study LST values were extracted from the satellite imagery using the most widely used generalized single-channel method by Jiménez-Muñoz and Sobrino (2003) (e.g. Estoque et al., 2017; Maimaitiyiming et al., 2014; Simwanda et al., 2019; Wardana, 2015) (see section 2.3.3.). The main advantage of this method is that in-situ radio soundings or effective atmospheric temperature values are not needed. Instead, this method uses the land surface emissivity to calculate the LST. However, land surface emissivity values are not directly readable from the Landsat satellite information. Instead in the study by Jiménez-Muñoz and Sobrino (2003) a method was developed that estimates the land surface emissivity values based on NDVI values. Therefore, the resulting LST is a priori influenced by NDVI. Since NDVI is highly correlated with UGS, the method of measurement of LST might have influenced the association on LST with UGS. However, after validation to in-situ measured LST, the generalized single-channel method was found to be the most accurate method when compared to the other available methods for LST extraction (Jiménez-Muñoz & Sobrino, 2003). This justifies the use of these values, as well as their use in the majority of studies in the literature, even though the LST values have a quadratic mean root deviation of 1.3 K of the in-situ LST values. (Jiménez-Muñoz & Sobrino, 2003).

In some studies the negative relationship between UGS and LST is mainly based on the strong and negative linear relation found between NDVI and LST (Huang et al., 2018a; Marando et al., 2019; Wardana, 2015; Yue, Xu, Tan, & Xu, 2007). This negative relationship was mainly absent in the present study due to the vast waterbody, the Suriname river, that resides within the study area. Previous research shows that water disturbs the relationship between temperature and NDVI because water is generally cool, but has a very low NDVI value (Cai et al., 2018; X. Zhang et al., 2017). When the Suriname river was excluded from the study area, a negative linear relationship was found between NDVI and LST. This exclusion of large water bodies prior to the relationship analysis between NDVI and LST was also carried out in the SUHI study by Ayanlade (2014), that excluded the Lagos Lagoon prior to the analysis of the SUHI in the city of Lagos. From this it is concluded that NDVI is a better indicator for the cooling effect in an urban environment, when there is little water present.

This study based all UGS composition and configurational variables on a moving window analysis using a circle with a 90-meter radius (see section 2.4.2.2. & 3.2.2.). Since the analysis of the cooling effect of UGS was the main goal of this research, this radius was chosen based on the highest Pearson correlation between $LST_{s, \max}$ and PLAND UGS using multiple radii. However, the results of

this analysis do not show large differences in correlation coefficients. The correlation coefficient difference between the chosen 90-meter radius and a 200-meter radius is just in the order of 0.01 (around 2%). As a result, the radius of the moving window, which determined the area on which all the class metrics were calculated, was determined on small differences. This uncertainty of the best radius to investigate the cooling effect of UGS is also reflected in other studies where the optimal radius varied from 118 to 152 meters (Estoque et al., 2017; Kong et al., 2014; Wardana, 2015). After the optimal radius was determined for UGS, this radius was applied for all other land cover types. This was done for comparability reasons between all the land cover types. However, the optimal radius of influence can differ between the different types of land cover. This may have affected the influence of the different land cover types on LST.

The choice for the relatively small 90-metre radius also had consequences for the effect of the configuration class metric in the study (see section 3.2.3.). The study of Kong et al. (2014) found that to test the influence of forest patches on LST, the choice of window size is pivotal. If the window size is chosen substantially smaller than the mean patch of UGS, the large UGSs will be divided into smaller areas by the analysis window. Therefore, the class metrics AI, LSI, ED and PD in that window are based on UGSs that were adjusted and fragmented by the analysis method. However, if the window size chosen is too large, the smaller UGSs could not show a significant cooling effect, since the cooling effect associated with UGS is weakened by the influence of the surrounding landscape (Kong et al., 2014). As a result, the influence of the different configurational class metrics can only be measured correctly within areas where sufficient UGS is present and all UGSs in their entirety fall within that area. In this study, all measuring points of which at least one percent of their 90-meter radius environment consisted of UGS were analysed. Consequentially, several times the class metrics and their cooling relationship were based on a window with a low percentage of UGS. Since on these windows the LST is determined by other land cover types than UGS, this may have influenced the relationship between the class metrics and LST.

Due to the fact that only one of the seven satellite images was obtained during the operational period of the outdoor data loggers, the relationship between air temperature and LST was based on limited data (see section 3.3.2.). To compare air temperatures and LST correctly, more data is needed that can be obtained through the addition of mobile measurements next to the stationary measurements as is done in the UHI study by Schwarz et al. (2012). Therefore, due to the limited data, the results found in this study of the relationship between air temperature and LST should be interpreted with care.

4.3. Ways forward

This study makes a valuable contribution to the understanding of the spatial characteristics of the SUHI across different land cover types in an urban area located in the tropics. It is one of the first to show differences in UHI between the wet and dry season. However, to improve the understanding of the effect of UGS on the UHI, further research is recommended in the Greater Paramaribo Region. This research should mainly focus on the effect of form complexity of UGS on LST, since, unlike other studies, no clear link was found between the two in this study. In order to study this relationship correctly, it is recommended to select larger areas than the area size used in this study, which contain a sufficient number of UGSs located entirely within the selected areas. Further research into the relationship between LST and air temperature across different land cover types is also recommended, as no relationship between LST and air temperature was found in this study, whereas previous studies did report such a relationship. This will most likely lead to a more complete

understanding of the relationship between the SUHI and the UHI across Paramaribo. This will provide valuable information that could be extrapolated to other tropical cities.

The study provides evidence that both water and UGSs lower the prevailing LST in the city of Paramaribo. Moreover, it shows that forested UGSs are the most effective coolers of the surface during both the wet and dry season. In addition, the study highlights how increasing size of an UGS also increases its cooling effect. Due to the limited amount of UGS, temperatures are highest in neighbourhoods of middle to low SES. Based on these results, the city of Paramaribo can formulate its first comprehensive green policy to mitigate the temperature increase caused by the UHI effect in the city. Other cities in the tropics can also base such a policy on the results of this study in line with the translation in a greening policy of similar results found in the UHI study by Mirrahimi et al. (2015) in Kuala Lumpur. In addition, they can set out to use the present study as an example on how to study the effects of their UHI more specifically.

5. Conclusion

Due to the high cloud coverage in tropical areas during the wet season, are SUHI studies rare in cities in the tropics. The studies that exist only provide information on the influence of UGS based on NDVI. As a result, there exists a knowledge gap regarding the influence of different types of UGS on LST across cities in the tropics. Therefore, the main objectives of this study were to analyse the UHI effect during the wet and dry season in the tropical city of Paramaribo and to analyse the potential cooling effect offered by UGSs to mitigate this UHI effect.

From the results it is concluded that there is an UHI effect present between the rural hinterland and the urban core of Paramaribo. This UHI effect is of approximately of the same magnitude during both the wet and dry season and of similar magnitude as those found across other cities in the tropics. This study showed that the UHI effect was due to the heating relationship between urban land use and LST in Paramaribo. This study did not find a cooling effect of UGS when NDVI was used as an indicator of UGS, due to the presence of a very large waterbody within the administrative boundary of Paramaribo in the form of the Suriname river. However, the results of a land cover-based analysis between the amount of land covered by UGS and the LST did show a strong cooling effect provided by UGS. This cooling effect was strongly dependent on the type of UGS. From this study it can be concluded that trees and mangrove are the most effective surface coolers, while mixed low vegetation provides a smaller cooling effect. Grass, on the other hand, did not show a clear relationship with LST. The cooling effect of UGS was found to be slightly stronger in the dry season as opposed to in the wet season, most likely due to the prevailing lower humidity and slightly higher temperatures in the dry season. In addition to the type of UGS, this study concluded that increasing the size of UGS increases the cooling effect. As a result, a large aggregated UGS is favoured over a number of smaller disaggregated UGSs.

Although earlier studies indicated otherwise, the shape of an UGS did not affect the LST in Paramaribo. The amount of UGS was found to differ between neighbourhoods of different SES, resulting in an indirect negative relationship between SES and LST. This relationship did not apply to the neighbourhoods of the lowest SES, due to the sandy characteristic of the streets in these neighbourhoods, their LST is also low. Unexpectedly, the results of the air temperature analysis do not show the same relationships between temperature and different land cover types as those found in the land cover-based analysis of LST. This unexpected finding was however based on limited data.

References

- Acerro, J. A., & González-Asensio, B. (2018). Influence of vegetation on the morning land surface temperature in a tropical humid urban area. *Urban Climate*, 26, 231–243. <https://doi.org/10.1016/j.uclim.2018.09.004>
- Amorim, M. C. de C. T. (2018). Spatial variability and intensity frequency of surface heat island in a Brazilian city with continental tropical climate through remote sensing. *Remote Sensing Applications: Society and Environment*. <https://doi.org/10.1016/j.rsase.2017.11.001>
- Aniello, C., Morgan, K., Busbey, A., & Newland, L. (1995). Mapping micro-urban heat islands using LANDSAT TM and a GIS. *Computers and Geosciences*. [https://doi.org/10.1016/0098-3004\(95\)00033-5](https://doi.org/10.1016/0098-3004(95)00033-5)
- Anniballe, R., Bonafoni, S., & Pichierri, M. (2014). Spatial and temporal trends of the surface and air heat island over Milan using MODIS data. *Remote Sensing of Environment*. <https://doi.org/10.1016/j.rse.2014.05.005>
- Argüeso, D., Evans, J. P., Pitman, A. J., & Di Luca, A. (2015). Effects of City Expansion on Heat Stress under Climate Change Conditions. *PLOS ONE*, 10(2), e0117066. <https://doi.org/10.1371/journal.pone.0117066>
- Artis, D. A., & Carnahan, W. H. (1982). Survey of emissivity variability in thermography of urban areas. *Remote Sensing of Environment*, 12(4), 313–329. [https://doi.org/10.1016/0034-4257\(82\)90043-8](https://doi.org/10.1016/0034-4257(82)90043-8)
- Ayanlade, A. (2016). Seasonality in the daytime and night-time intensity of land surface temperature in a tropical city area. *Science of the Total Environment*, 557–558, 415–424. <https://doi.org/10.1016/j.scitotenv.2016.03.027>
- Balogun, I. A., & Balogun, A. A. (2014). Urban heat island and bioclimatological conditions in a hot-humid tropical city: The example of Akure, Nigeria. *Erde*, 145(1–2), 3–15. <https://doi.org/10.12854/erde-145-2>
- Barradas, V. L. (1991). Air temperature and humidity and human comfort index of some city parks of Mexico City. *International Journal of Biometeorology*, 35(1), 24–28. <https://doi.org/10.1007/BF01040959>
- Bowler, D. E., Buyung-Ali, L., Knight, T. M., & Pullin, A. S. (2010). Urban greening to cool towns and cities: A systematic review of the empirical evidence. *Landscape and Urban Planning*, 97(3), 147–155. <https://doi.org/10.1016/j.landurbplan.2010.05.006>
- Brown, R. D., Vanos, J., Kenny, N., & Lenzholzer, S. (2015). Designing urban parks that ameliorate the effects of climate change. *Landscape and Urban Planning*, 138, 118–131. <https://doi.org/10.1016/j.landurbplan.2015.02.006>
- Cai, Z., Han, G., & Chen, M. (2018). Do water bodies play an important role in the relationship between urban form and land surface temperature? *Sustainable Cities and Society*, 39, 487–498. <https://doi.org/10.1016/j.scs.2018.02.033>
- Cao, X., Onishi, A., Chen, J., & Imura, H. (2010). Quantifying the cool island intensity of urban parks using ASTER and IKONOS data. *Landscape and Urban Planning*, 96(4), 224–231. <https://doi.org/10.1016/j.landurbplan.2010.03.008>
- Chander, G., Markham, B. L., & Helder, D. L. (2009). Summary of current radiometric calibration coefficients for Landsat MSS, TM, ETM+, and EO-1 ALI sensors. *Remote Sensing of Environment*,

113(5), 893–903. <https://doi.org/10.1016/j.rse.2009.01.007>

- Chang, C. R., Li, M. H., & Chang, S. D. (2007). A preliminary study on the local cool-island intensity of Taipei city parks. *Landscape and Urban Planning*, 80(4), 386–395. <https://doi.org/10.1016/j.landurbplan.2006.09.005>
- Chapman, S., Watson, J. E. M., Salazar, A., Thatcher, M., & McAlpine, C. A. (2017). The impact of urbanization and climate change on urban temperatures: a systematic review. *Landscape Ecology*, 32(10), 1921–1935. <https://doi.org/10.1007/s10980-017-0561-4>
- Chen, X. L., Zhao, H. M., Li, P. X., & Yin, Z. Y. (2006). Remote sensing image-based analysis of the relationship between urban heat island and land use/cover changes. *Remote Sensing of Environment*. <https://doi.org/10.1016/j.rse.2005.11.016>
- Cohen, J. (1988). *Statistical Power Analysis for the Behavioral Sciences Second Edition (2nd ed.)*. New York: Academic Press.
- Cui, L., & Shi, J. (2012). Urbanization and its environmental effects in Shanghai, China. *Urban Climate*, 2, 1–15. <https://doi.org/10.1016/j.uclim.2012.10.008>
- Demuzere, M., Orru, K., Heidrich, O., Olazabal, E., Geneletti, D., Orru, H., ... Faehnle, M. (2014). Mitigating and adapting to climate change: Multi-functional and multi-scale assessment of green urban infrastructure. *Journal of Environmental Management*, 146, 107–115. <https://doi.org/10.1016/j.jenvman.2014.07.025>
- Dousset, B., & Gourmelon, F. (2003). Satellite multi-sensor data analysis of urban surface temperatures and landcover. *ISPRS Journal of Photogrammetry and Remote Sensing*. [https://doi.org/10.1016/S0924-2716\(03\)00016-9](https://doi.org/10.1016/S0924-2716(03)00016-9)
- Du, H., Ai, J., Cai, Y., Jiang, H., & Liu, P. (2019). Combined effects of the surface urban heat Island with landscape composition and configuration based on remote sensing: A case study of Shanghai, China. *Sustainability (Switzerland)*, 11(10). <https://doi.org/10.3390/su11102890>
- Esri. (2018). ArcGIS World Imagery with Metadata. Retrieved March 16, 2020, from <https://www.arcgis.com/home/webmap/viewer.html?webmap=c1c2090ed8594e0193194b750d0d5f83>
- Estoque, R. C., Murayama, Y., & Myint, S. W. (2017). Effects of landscape composition and pattern on land surface temperature: An urban heat island study in the megacities of Southeast Asia. *Science of the Total Environment*, 577, 349–359. <https://doi.org/10.1016/j.scitotenv.2016.10.195>
- Field, A. (2009). *Discovering Statistics Using SPSS (Third edit)*. Los Angeles, London, New Delhi, Singapore, Washington DC: SAGE.
- Fung-Loy, K., Van Rompaey, A., & Hemerijckx, L. (2019). Detection and Simulation of Urban Expansion and Socioeconomic Segregation in the Greater Paramaribo Region, Suriname. *Tijdschrift Voor Economische En Sociale Geografie*, 110(3), 339–358. <https://doi.org/10.1111/tesg.12350>
- Gallo, K. P., McNab, A. L., Karl, T. R., Brown, J. F., Hood, J. J., & Tarpley, J. D. (1993). The use of NOAA AVHRR data for assessment of the urban heat island effect. *Journal of Applied Meteorology*, 32(5), 899–908. [https://doi.org/10.1175/1520-0450\(1993\)032<0899:TUONAD>2.0.CO;2](https://doi.org/10.1175/1520-0450(1993)032<0899:TUONAD>2.0.CO;2)
- GBS. (2016). *Milieu Statistieken*. <https://doi.org/10.1192/bjp.112.483.211-a>
- Giridharan, R., & Emmanuel, R. (2018). The impact of urban compactness, comfort strategies and energy consumption on tropical urban heat island intensity: A review. *Sustainable Cities and*

- Society*, 40(December 2017), 677–687. <https://doi.org/10.1016/j.scs.2018.01.024>
- Huang, M., Cui, P., & He, X. (2018a). Study of the cooling effects of urban green space in Harbin in terms of reducing the heat island effect. *Sustainability (Switzerland)*, 10(4), 1–17. <https://doi.org/10.3390/su10041101>
- Huang, M., Cui, P., & He, X. (2018b). Study of the Cooling Effects of Urban Green Space in Harbin in Terms of Reducing the Heat Island Effect. *Sustainability*, 10(4), 1101. <https://doi.org/10.3390/su10041101>
- IPCC. (2018). *Summary for Policymakers. In: Global Warming of 1.5°C. An IPCC Special Report on the impacts of global warming of 1.5°C above pre-industrial levels and related global greenhouse gas emission pathways, in the context of strengthening the global.*
- Jaganmohan, M., Knapp, S., Buchmann, C. M., & Schwarz, N. (2016). The Bigger, the Better? The Influence of Urban Green Space Design on Cooling Effects for Residential Areas. *Journal of Environmental Quality*, 45(1), 134–145. <https://doi.org/10.2134/jeq2015.01.0062>
- Jenerette, G. D., Harlan, S. L., Brazel, A., Jones, N., Larsen, L., & Stefanov, W. L. (2007). Regional relationships between surface temperature, vegetation, and human settlement in a rapidly urbanizing ecosystem. *Landscape Ecology*, 22(3), 353–365. <https://doi.org/10.1007/s10980-006-9032-z>
- Jiménez-Muñoz, J. C., & Sobrino, J. A. (2003). A generalized single-channel method for retrieving land surface temperature from remote sensing data. *J. Geophys. Res.*, 108(D22), 4688. <https://doi.org/10.1029/2003JD003480>
- Jiménez Cisneros, B. E., Oki, T., Arnell, N. W., Benito, G., Cogley, J. G., Döll, P., ... Nishijima, A. (2014). Freshwater resources. In *Climate Change 2014 Impacts, Adaptation and Vulnerability: Part A: Global and Sectoral Aspects* (pp. 229–270). <https://doi.org/10.1017/CBO9781107415379.008>
- Kalpoe, N. (2019). *Towards a green and more liveable Paramaribo: The Cooling Effect of Urban Green Spaces*. Anton de Kom University.
- Kong, F., Yin, H., James, P., Hutyra, L. R., & He, H. S. (2014). Effects of spatial pattern of greenspace on urban cooling in a large metropolitan area of eastern China. *Landscape and Urban Planning*, 128, 35–47. <https://doi.org/10.1016/j.landurbplan.2014.04.018>
- Li, X., Zhou, W., & Ouyang, Z. (2013). Relationship between land surface temperature and spatial pattern of greenspace: What are the effects of spatial resolution? *Landscape and Urban Planning*, 114, 1–8. <https://doi.org/10.1016/j.landurbplan.2013.02.005>
- Luber, G., & McGeehin, M. (2008). Climate Change and Extreme Heat Events. *American Journal of Preventive Medicine*, 35(5), 429–435. <https://doi.org/10.1016/j.amepre.2008.08.021>
- Maimaitiyiming, M., Ghulam, A., Tiyp, T., Pla, F., Latorre-Carmona, P., Halik, Ü., ... Caetano, M. (2014). Effects of green space spatial pattern on land surface temperature: Implications for sustainable urban planning and climate change adaptation. *ISPRS Journal of Photogrammetry and Remote Sensing*, 89, 59–66. <https://doi.org/10.1016/j.isprsjprs.2013.12.010>
- Marando, F., Salvatori, E., Sebastiani, A., Fusaro, L., & Manes, F. (2019). Regulating Ecosystem Services and Green Infrastructure: assessment of Urban Heat Island effect mitigation in the municipality of Rome, Italy. *Ecological Modelling*. <https://doi.org/10.1016/j.ecolmodel.2018.11.011>
- McGarigal, K. (2015). *FRAGSTATS HELP*. Amherst.
- McGarigal, K., Cushman, S. A., & Ene, E. (2012). *FRAGSTATS v4: Spatial Pattern Analysis Program for*

Categorical and Continuous Maps. Computer software program produced by the authors at the University of Massachusetts, Amherst. Available at the following web site:
<http://www.umass.edu/landeco/research/f>. Amherst.

- Mirrahimi, S., Lukman Nik Ibrahim, N., & Surat, M. (2015). Developing a Sustainable City in a Tropical Area to Create a Balance between Vegetation and Water Bodies. *International Journal of Engineering and Technology*, 7(1), 50–54. <https://doi.org/10.7763/ijet.2015.v7.765>
- Mushore, T. D., Dube, T., Manjowe, M., Gumindoga, W., Chemura, A., Roustia, I., ... Mutanga, O. (2018). Remotely sensed retrieval of Local Climate Zones and their linkages to land surface temperature in Harare metropolitan city, Zimbabwe. *Urban Climate*. <https://doi.org/10.1016/j.uclim.2018.12.006>
- Mutiibwa, D., Strachan, S., & Albright, T. (2015). Land Surface Temperature and Surface Air Temperature in Complex Terrain. *IEEE Journal of Selected Topics in Applied Earth Observations and Remote Sensing*, 8(10), 4762–4774. <https://doi.org/10.1109/JSTARS.2015.2468594>
- North Carolina Climate Office. (n.d.). Evapotranspiration. Retrieved February 21, 2020, from <https://climate.ncsu.edu/edu/Evap>
- Ojeh, V. N., Balogun, A. A., & Okhimamhe, A. A. (2016). Urban-rural temperature differences in Lagos. *Climate*, 4(2), 1–18. <https://doi.org/10.3390/cli4020029>
- Oke, T. R. (1982). The energetic basis of the urban heat island. *Quarterly Journal of the Royal Meteorological Society*, 108(455), 1–24. <https://doi.org/10.1002/qj.49710845502>
- Perera, N. G. R., & Emmanuel, R. (2018). A “Local Climate Zone” based approach to urban planning in Colombo, Sri Lanka. *Urban Climate*. <https://doi.org/10.1016/j.uclim.2016.11.006>
- Rajasekar, U., & Weng, Q. (2009). Urban heat island monitoring and analysis using a non-parametric model: A case study of Indianapolis. *ISPRS Journal of Photogrammetry and Remote Sensing*. <https://doi.org/10.1016/j.isprsjprs.2008.05.002>
- Richard, Y., Emery, J., Dudek, J., Pergaud, J., Chateau-Smith, C., Zito, S., ... Pohl, B. (2018). How relevant are local climate zones and urban climate zones for urban climate research? Dijon (France) as a case study. *Urban Climate*. <https://doi.org/10.1016/j.uclim.2018.10.002>
- Roy, D. P., Borak, J. S., Devadiga, S., Wolfe, R. E., Zheng, M., & Descloitres, J. (2002). *The MODIS Land Product Quality Assessment Approach, Remote Sensing of Environment* (Vol. 83). Retrieved from www.impact-test.co.uk
- Schwarz, N., Lautenbach, S., & Seppelt, R. (2011). Exploring indicators for quantifying surface urban heat islands of European cities with MODIS land surface temperatures. *Remote Sensing of Environment*, 115(12), 3175–3186. <https://doi.org/10.1016/j.rse.2011.07.003>
- Schwarz, N., Schlink, U., Franck, U., & Großmann, K. (2012). Relationship of land surface and air temperatures and its implications for quantifying urban heat island indicators - An application for the city of Leipzig (Germany). *Ecological Indicators*. <https://doi.org/10.1016/j.ecolind.2012.01.001>
- Sentinel Hub. (n.d.). NDVI (Normalized Difference Vegetation Index). Retrieved February 11, 2020, from <https://www.sentinel-hub.com/eoproducts/ndvi-normalized-difference-vegetation-index>
- Simanjuntak, R. M., Kuffer, M., & Reckien, D. (2019). Object-based image analysis to map local climate zones: The case of Bandung, Indonesia. *Applied Geography*. <https://doi.org/10.1016/j.apgeog.2019.04.001>
- Simwanda, M., Ranagalage, M., Estoque, R. C., & Murayama, Y. (2019). Spatial Analysis of Surface

- Urban Heat Islands in Four Rapidly Growing African Cities. *Remote Sensing*, 11(14), 1645. <https://doi.org/10.3390/rs11141645>
- Sobrino, J. A., Jiménez-Muñoz, J. C., & Paolini, L. (2004). Land surface temperature retrieval from LANDSAT TM 5. *Remote Sensing of Environment*, 90(4), 434–440. <https://doi.org/10.1016/j.rse.2004.02.003>
- Tan, J., Zheng, Y., Tang, X., Guo, C., Li, L., Song, G., ... Chen, H. (2010). The urban heat island and its impact on heat waves and human health in Shanghai. *International Journal of Biometeorology*, 54(1), 75–84. <https://doi.org/10.1007/s00484-009-0256-x>
- Tang, J., Di, L., Xiao, J., Lu, D., & Zhou, Y. (2017). Impacts of land use and socioeconomic patterns on urban heat Island. *International Journal of Remote Sensing*, 38(11), 3445–3465. <https://doi.org/10.1080/01431161.2017.1295485>
- Taus, R. (2019). *Analyzing green spaces in Paramaribo and developing a method for monitoring using GIS and Remote Sensing*. Anton de Kom University.
- The Nature Conservancy. (2018). *Nature in the Urban Century*. Stockholm.
- The World Bank. (2018). Population, total - Suriname | Data. Retrieved February 18, 2020, from <https://data.worldbank.org/indicator/SP.POP.TOTL?locations=SR>
- Themistocleous, K., & Hadjimitsis, D. G. (2008). *The importance of considering atmospheric correction in the pre-processing of satellite remote sensing data intended for the management and detection of cultural sites: a case study of the Cyprus area*. Limasol.
- Tomlinson, C. J., Chapman, L., Thornes, J. E., & Baker, C. J. (2012). Derivation of Birmingham’s summer surface urban heat island from MODIS satellite images. *International Journal of Climatology*, 32(2), 214–224. <https://doi.org/10.1002/joc.2261>
- Tropenbos Suriname. (2019). Groen Paramaribo. Retrieved September 20, 2019, from <http://www.groenparamaribo.org/>
- Tseng, D. C., Tseng, H. T., & Chien, C. L. (2008). Automatic cloud removal from multi-temporal SPOT images. *Applied Mathematics and Computation*, 205(2), 584–600. <https://doi.org/10.1016/j.amc.2008.05.050>
- U.S. Environmental Protection Agency. (2008). “Urban Heat Island Basics.” In: *Reducing Urban Heat Islands: Compendium of Strategies. Draft*. Retrieved from <https://www.epa.gov/heat-islands/heat-island-compendium>
- U.S. Geological Survey. (2014). Landsat 8 OLI and TIRS Calibration Notices. Retrieved November 6, 2019, from Landsat 8 Reprocessing Details website: <https://www.usgs.gov/land-resources/nli/landsat/landsat-8-oli-and-tirs-calibration-notice>
- U.S. Geological Survey. (2017). Landsat Quality Assessment ArcGIS Toolbox. U.S. Geological Survey software release. <https://doi.org/10.5066/F7JM284N>
- U.S. Geological Survey. (2019). *Landsat 8 (L8) Data Users Handbook*. Retrieved from https://prd-wret.s3-us-west-2.amazonaws.com/assets/palladium/production/atoms/files/LSDS-1574_L8_Data_Users_Handbook_v4.pdf
- United Nations. (2015). Sustainable Development Goals Knowledge Platform. Retrieved February 18, 2020, from <https://sustainabledevelopment.un.org/#>
- United Nations, Department of Economic and Social Affairs, & Population Division. (2019a). *World Population Prospects 2019: Highlights (ST/ESA/SER.A/423)*.

- United Nations, Department of Economic and Social Affairs, & Population Division. (2019b). *World Urbanization Prospects: The 2018 Revision (ST/ESA/SER.A/420)*. New York: United Nations.
- USGS. (2019). USGS science for a changing world. Retrieved October 5, 2019, from <https://glovis.usgs.gov/app>
- Van Der Zanden, E. H., Verburg, P. H., & Mùcher, C. A. (2013). Modelling the spatial distribution of linear landscape elements in Europe. *Ecological Indicators*, *27*, 125–136. <https://doi.org/10.1016/j.ecolind.2012.12.002>
- Vanos, J. K., Warland, J. S., Gillespie, T. J., Slater, G. A., Brown, R. D., & Kenny, N. A. (2012). Human energy budget modeling in urban parks in Toronto and applications to emergency heat stress preparedness. *Journal of Applied Meteorology and Climatology*, *51*(9), 1639–1653. <https://doi.org/10.1175/JAMC-D-11-0245.1>
- Verburg, P. H., & Overmars, K. P. (2009). *The CLUE model*. *Landscape Ecology* *24*(9) 1167–1181.
- Verburg, P. H., van Berkel, D. B., van Doorn, A. M., van Eupen, M., & van den Heiligenberg, H. A. R. M. (2010). Trajectories of land use change in Europe: A model-based exploration of rural futures. *Landscape Ecology*, *25*(2), 217–232. <https://doi.org/10.1007/s10980-009-9347-7>
- Verrest, H. J. L. M. (2010). Paramaribo. *Cities*, *27*(1), 50–60. <https://doi.org/10.1016/j.cities.2009.07.003>
- Voogt, J. (2007). *How Researchers Measure Urban Heat Islands*. Ontario.
- Voogt, J. A., & Oke, T. R. (2003). Thermal remote sensing of urban climates. *Remote Sensing of Environment*, *86*(3), 370–384. [https://doi.org/10.1016/S0034-4257\(03\)00079-8](https://doi.org/10.1016/S0034-4257(03)00079-8)
- Walawender, J. P., Szymanowski, M., Hajto, M. J., & Bokwa, A. (2014). Land Surface Temperature Patterns in the Urban Agglomeration of Krakow (Poland) Derived from Landsat-7/ETM+ Data. *Pure and Applied Geophysics*, *171*(6), 913–940. <https://doi.org/10.1007/s00024-013-0685-7>
- Wardana, I. K. (2015). Analysis of Urban Surface Temperature for Green Spaces Planning in Bandung City, Indonesia. *Msc. Thesis*, (1), 593–605.
- Weng, Q., Lu, D., & Schubring, J. (2004). Estimation of land surface temperature-vegetation abundance relationship for urban heat island studies. *Remote Sensing of Environment*, *89*(4), 467–483. <https://doi.org/10.1016/j.rse.2003.11.005>
- Yao, L., Chen, L., Wei, W., & Sun, R. (2015). Potential reduction in urban runoff by green spaces in Beijing: A scenario analysis. *Urban Forestry and Urban Greening*. <https://doi.org/10.1016/j.ufug.2015.02.014>
- Yu, Z., Wang, Y., Deng, J., Shen, Z., Wang, K., Zhu, J., & Gan, M. (2017). Dynamics of hierarchical urban green space patches and implications for management policy. *Sensors (Switzerland)*, *17*(6). <https://doi.org/10.3390/s17061304>
- Yue, W., Xu, J., Tan, W., & Xu, L. (2007). The relationship between land surface temperature and NDVI with remote sensing: application to Shanghai Landsat 7 ETM+ data. *International Journal of Remote Sensing*, *28*(15), 3205–3226. <https://doi.org/10.1080/01431160500306906>
- Yusuf, Y. A., Pradhan, B., & Idrees, M. O. (2014). Spatio-temporal Assessment of Urban Heat Island Effects in Kuala Lumpur Metropolitan City Using Landsat Images. *Journal of the Indian Society of Remote Sensing*, *42*(4), 829–837. <https://doi.org/10.1007/s12524-013-0342-8>
- Zhang, J., & Wang, Y. (2008). Study of the Relationships between the Spatial Extent of Surface Urban Heat Islands and Urban Characteristic Factors Based on Landsat ETM+ Data. *Sensors*, *8*(11),

7453–7468. <https://doi.org/10.3390/s8117453>

Zhang, X., Estoque, R. C., & Murayama, Y. (2017). An urban heat island study in Nanchang City, China based on land surface temperature and social-ecological variables. *Sustainable Cities and Society*, 32, 557–568. <https://doi.org/10.1016/j.scs.2017.05.005>

Zhang, Z., Lv, Y., & Pan, H. (2013). Cooling and humidifying effect of plant communities in subtropical urban parks. *Urban Forestry and Urban Greening*, 12(3), 323–329. <https://doi.org/10.1016/j.ufug.2013.03.010>

Zhou, J., Li, J., & Yue, J. (2010). Analysis of urban heat island (UHI) in the Beijing metropolitan area by time-series MODIS data. *International Geoscience and Remote Sensing Symposium (IGARSS)*, 3327–3330. <https://doi.org/10.1109/IGARSS.2010.5651278>

Appendix

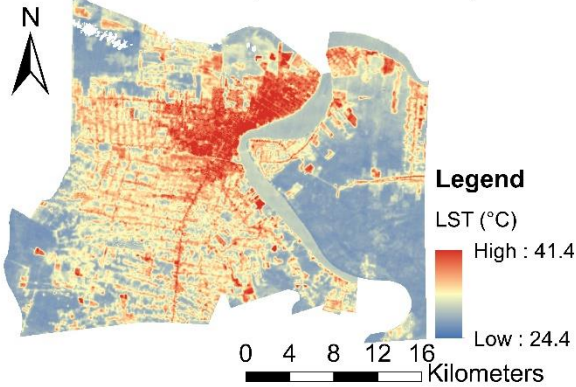
Table of Appendices

Appendix 1 – Spatial pattern of LST in the Greater Paramaribo Region	73
Appendix 2 – Spatial pattern of LST in the administrative boundary	74
Appendix 3 – Rural outdoor temperature logger location	75
Appendix 4 – Example of the outdoor temperature logger air measuring devices used in this study	76
Appendix 5 – Summary of a descriptive seasonal analysis of $LST_{s, \max}$ in the Greater Paramaribo Region.....	77
Appendix 6 – Descriptive seasonal analysis of $LST_{s, \max}$ in the Greater Paramaribo Region	78
Appendix 7 – Descriptive seasonal analysis of $LST_{s, \max}$ in the administrative boundary	79
Appendix 8 – Kruskal-Wallis test: land cover types	80
Appendix 9 – Wilcoxon signed rank test of $LST_{s, \max}$ on different land cover, green features groups, and cold spots groups in the dry and wet season.....	81
Appendix 10 – Scatterplots of wet season $LST_{s, \max}$ vs UGS and individual landcover classes, after the 0% PLAND values were filtered out.	82
Appendix 11 – Scatterplot $LST_{s, \max}$ vs distances	83
Appendix 12 – Total multiple linear regression model for the dry season containing all studied variables	84
Appendix 13 – Total multiple linear regression model for the wet season containing all studied variables	85
Appendix 14 – Multiple linear regression models selected to test hypotheses in the wet season .	86
Appendix 15 – Representative images of green features groups.....	87
Appendix 16 – Kruskal-Wallis test: green features groups.....	88
Appendix 17 – The selected Cold spots depicted on the seasonal $LST_{s, \max}$ maps.	91
Appendix 18 – Kruskal-Wallis test: cold spots groups	92
Appendix 19 – Kruskal-Wallis test: socioeconomic status.....	93
Appendix 20 – Comparison between LST and air temperature at the air temperature measuring stations and outdoor temperature logger locations.....	94

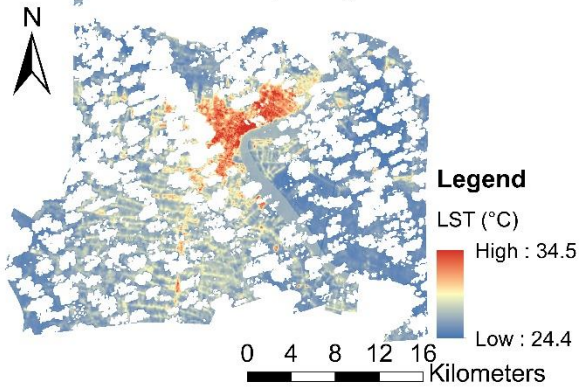
Appendix 1 – Spatial pattern of LST in the Greater Paramaribo Region.

Note: White spots are areas where clouds were present in all the images used to create the seasonal composites, these clouds were removed. Therefore, the white spots in the seasonal images indicate no data.

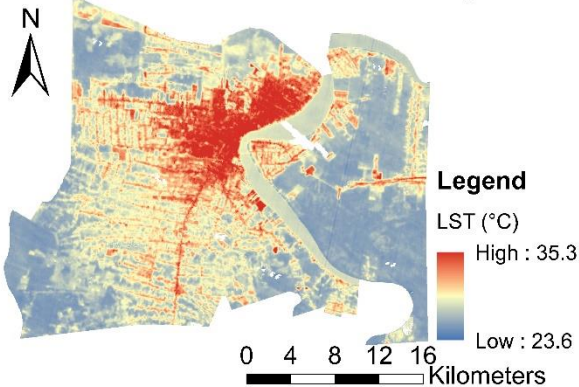
Greater Paramaribo: LST, 15 October 2015 - Dry Season



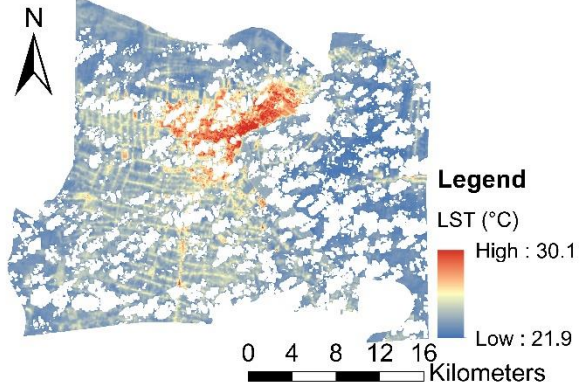
Greater Paramaribo: LST, 29 July 2016 - Wet Season



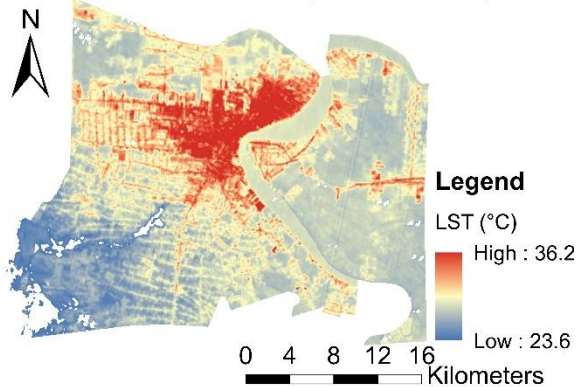
Greater Paramaribo: LST, 1 October 2016 - Dry Season



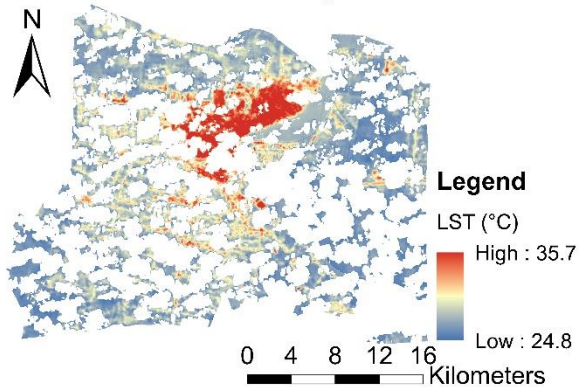
Greater Paramaribo: LST, 14 June 2017 - Wet Season



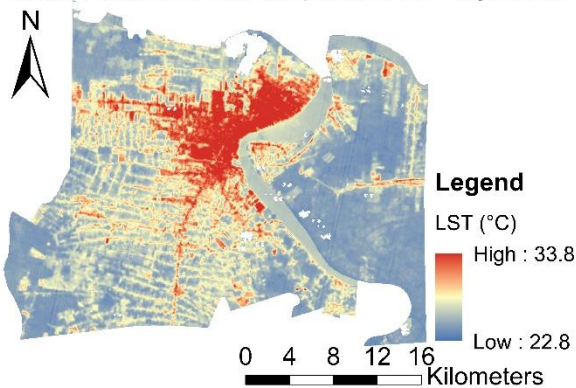
Greater Paramaribo: LST, 21 September 2018 - Dry Season



Greater Paramaribo: LST, 4 August 2018 - Wet Season

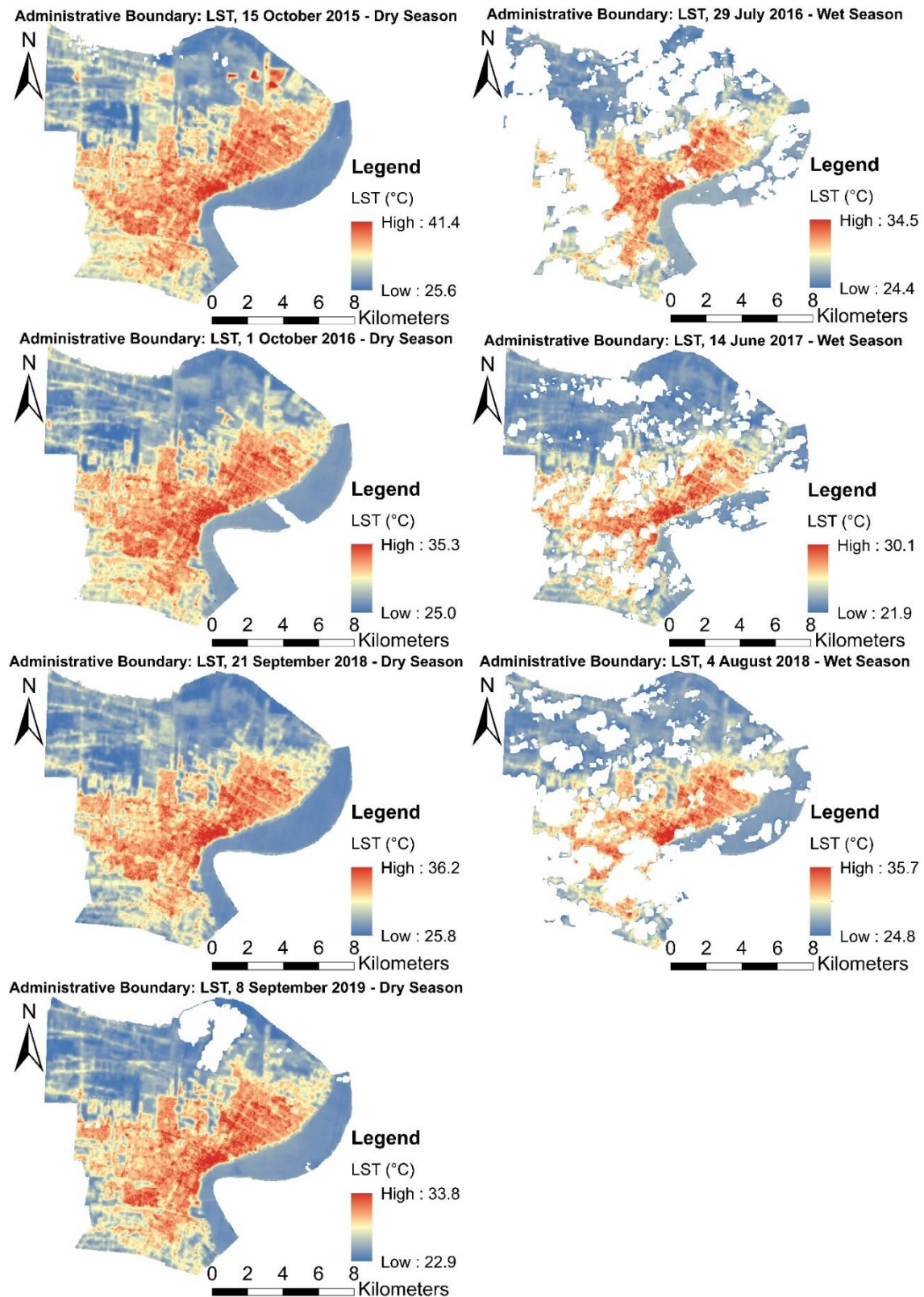


Greater Paramaribo: LST, 8 September 2019 - Dry Season

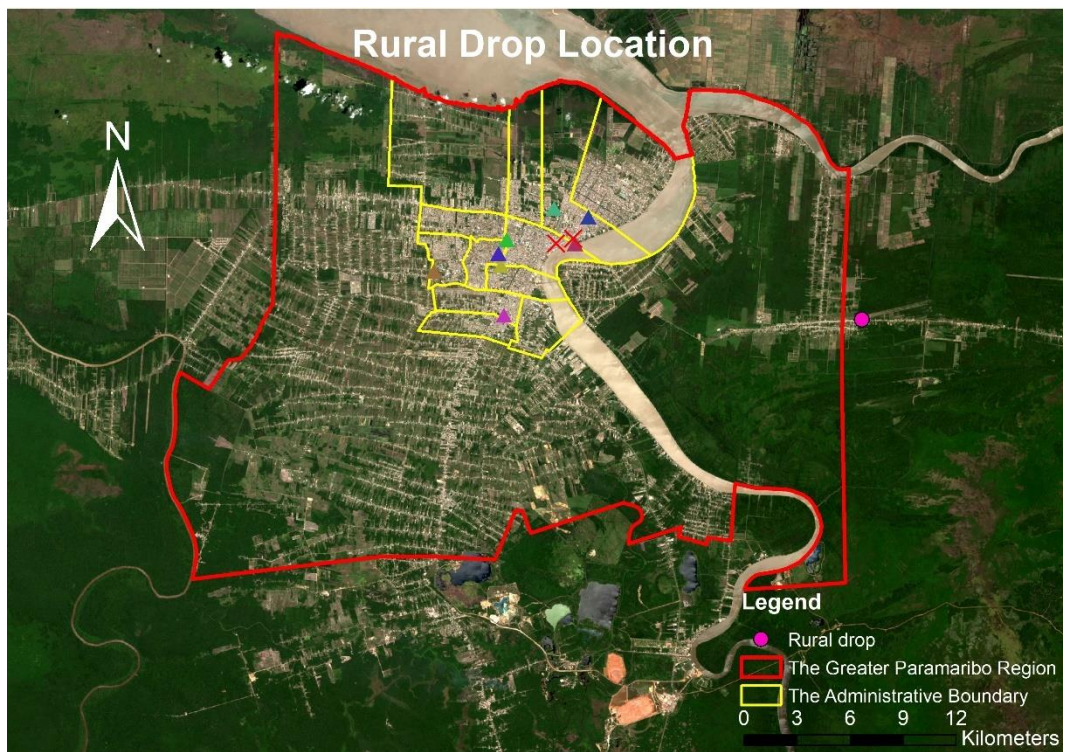


Appendix 2 – Spatial pattern of LST in the administrative boundary.

Note: White spots are areas where clouds were present in all the images used to create the seasonal composites, these clouds were removed. Therefore, the white spots in the seasonal images indicate no data.



Appendix 3 – Rural outdoor temperature logger location.



Appendix 4 – Example of the outdoor temperature logger air measuring devices used in this study.



Figure 25: Outdoor temperature logger 2 op het M.C. Ooftplein.

Appendix 5 – Summary of a descriptive seasonal analysis of $LST_{s, max}$ in the Greater Paramaribo Region.

Table 20. Mean $LST_{s, max}$ values and the standard deviation per land cover class in the Greater Paramaribo Region in the dry and wet season.

Land cover	$LST_{s, max}$ dry season (C°)		$LST_{s, max}$ wet season (C°)	
	MEAN	S.D.	MEAN	S.D.
Urban	2.2	1.0	1.9	1.2
Infrastructure	1.9	1.0	1.6	1.3
Bare soil	1.2	0.8	0.8	1.0
Grass	0.7	0.7	0.3	0.7
Mixed low vegetation	0.2	0.6	-0.2	0.5
Trees	-0.5	0.3	-0.7	0.3
Mangrove	-0.2	0.5	-0.4	0.4
Water	-0.1	0.4	-0.1	0.4

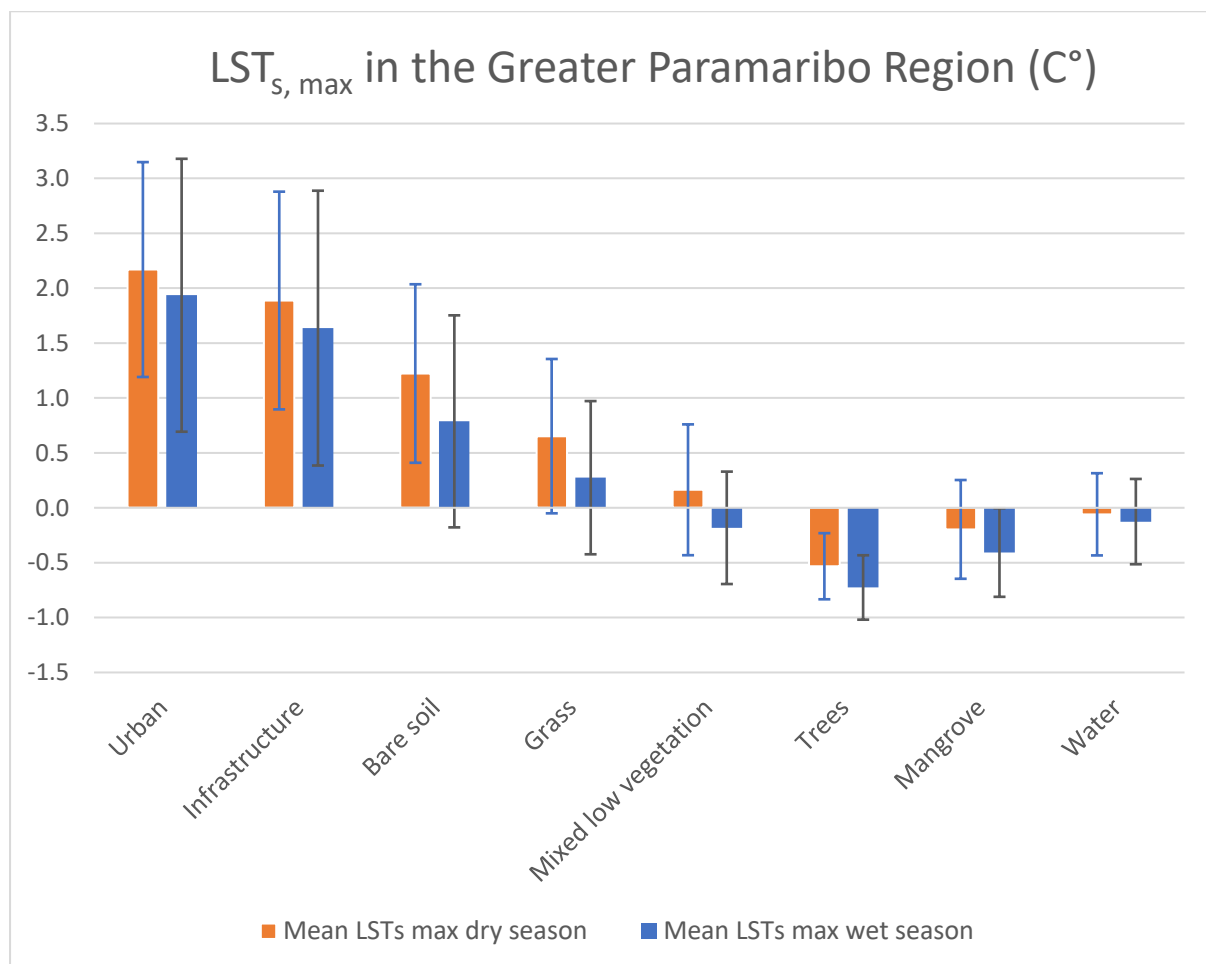


Figure 26. Mean $LST_{s, max}$ values per land cover class in the Greater Paramaribo Region in the dry and wet season.

Appendix 6 – Descriptive seasonal analysis of $LST_{s, \max}$ in the Greater Paramaribo Region.

Table 21. Full descriptive analysis of $LST_{s, \max}$ within the Greater Paramaribo Region of the different land cover types in the dry season.

The Greater Paramaribo Region								
Land cover	Coverage	$LST_{s, \max}$ dry season (C°)						LST_{\max} (C°)
	Area (km ²)	Min	Max	Range	Mean	S.D.	Sum	Mean
Urban	39.77	-0.7	4.8	5.5	2.2	1.0	95900.9	32.4
Infrastructure	47.02	-0.8	4.8	5.6	1.9	1.0	98635.6	32.0
Bare soil	66.03	-1.0	4.8	5.8	1.2	0.8	89728.3	30.7
Grass	180.27	-1.2	5.8	7.0	0.7	0.7	130736.1	29.8
Mixed low vegetation	244.90	-1.2	4.7	5.9	0.2	0.6	44621.0	28.6
Trees	220.92	-1.3	2.6	3.9	-0.5	0.3	-130668.7	26.8
Mangrove	10.86	-1.1	3.0	4.1	-0.2	0.5	-2374.8	27.6
Water	53.16	-1.0	4.7	5.7	-0.1	0.4	-3504.1	27.9

Table 22. Full descriptive analysis of $LST_{s, \max}$ within the Greater Paramaribo Region of the different land cover types in the wet season.

The Greater Paramaribo Region								
Land cover	Coverage	$LST_{s, \max}$ wet season (C°)						LST_{\max} (C°)
	Area (m ²)	Min	Max	Range	Mean	S.D.	Sum	Mean
Urban	37.02	-1.4	5.6	7.0	1.9	1.2	79633.6	29.0
Infrastructure	43.66	-1.4	5.6	7.1	1.6	1.3	79399.4	28.5
Bare soil	61.17	-1.4	5.5	6.9	0.8	1.0	53515.8	27.2
Grass	166.46	-1.4	5.3	6.8	0.3	0.7	50731.5	26.5
Mixed low vegetation	222.56	-1.4	5.2	6.7	-0.2	0.5	-45104.6	25.7
Trees	192.46	-1.4	2.7	4.2	-0.7	0.3	-155178.8	24.9
Mangrove	10.33	-1.4	3.8	5.2	-0.4	0.4	-4681.1	25.5
Water	48.74	-1.4	5.2	6.6	-0.1	0.4	-6816.7	26.1

Appendix 7 – Descriptive seasonal analysis of $LST_{s, \max}$ in the administrative boundary.

Table 23. Full descriptive analysis of $LST_{s, \max}$ within the administrative boundary of the different land cover types in the dry season.

Administrative Boundary								
Land cover	Coverage	$LST_{s, \max}$ dry season (C°)						LST_{\max} (C°)
	Area (km ²)	Min	Max	Range	Mean	S.D.	Sum	Mean
Urban	22.11	-0.8	3.0	3.9	1.4	0.6	34054.6	33.3
Infrastructure	24.72	-1.1	3.0	4.1	1.2	0.6	33269.5	33.0
Bare soil	19.34	-1.2	3.0	4.2	0.8	0.6	16426.0	31.9
Grass	29.67	-1.4	4.3	5.8	0.3	0.7	10479.1	30.9
Mixed low vegetation	39.03	-1.5	3.3	4.8	-0.3	0.6	-14287.9	29.4
Trees	8.57	-1.5	1.3	2.8	-1.0	0.4	-9107.6	27.8
Mangrove	6.50	-1.6	1.7	3.3	-1.1	0.4	-7753.0	27.5
Water	23.57	-1.3	2.9	4.3	-0.8	0.3	-21202.3	27.8

Table 24. Full descriptive analysis of $LST_{s, \max}$ within the administrative boundary of the different land cover types in the wet season.

Administrative Boundary								
Land cover	Coverage	$LST_{s, \max}$ wet season (C°)						LST_{\max} (C°)
	Area (km ²)	Min	Max	Range	Mean	S.D.	Sum	Mean
Urban	20.85	-1.6	3.6	5.1	1.3	0.8	29295.7	30.1
Infrastructure	23.09	-1.6	3.5	5.1	1.1	0.8	27890.2	29.7
Bare soil	18.08	-1.6	3.4	5.0	0.5	0.8	10223.4	28.5
Grass	27.95	-1.5	3.2	4.8	0.0	0.7	-130.4	27.4
Mixed low vegetation	36.73	-1.6	3.0	4.6	-0.6	0.5	-23510.0	26.2
Trees	8.33	-1.6	1.2	2.9	-0.9	0.3	-8293.5	25.6
Mangrove	6.36	-1.6	2.1	3.7	-0.9	0.3	-6148.5	25.7
Water	22.00	-1.6	3.3	5.0	-0.7	0.3	-15898.0	26.4

Appendix 8 – Kruskal-Wallis test: land cover types.

Table 25. Kruskal-Wallis test on the distribution of $LST_{s,max}$ across the different land cover types, including pairwise comparisons adjusted by the Bonferroni correction for multiple tests.

Pairwise Comparisons of Land Cover										
Sample 1 - Sample 2	Dry season					Wet season				
	Test Statistic	Std. Error	Std. Test Statistic	Sig.	Adj. Sig. ^a	Test Statistic	Std. Error	Std. Test Statistic	Sig.	Adj. Sig. ^a
Mangrove - Trees	161.98	124.22	1.30	.192	1.000	-0.59	119.29	-0.01	.996	1.000
Mangrove - Water	390.46	106.75	3.66	.000	.007	609.09	92.20	6.61	.000	.000
Mangrove - Mixed low vegetation	-1007.69	101.80	-9.90	.000	.000	-653.62	86.39	-7.57	.000	.000
Mangrove - Grass	-1737.87	103.86	-16.73	.000	.000	-1391.65	88.50	-15.73	.000	.000
Mangrove - Bare soil	-2292.04	108.95	-21.04	.000	.000	-1963.91	94.19	-20.85	.000	.000
Mangrove - Infrastructure	-2655.35	105.28	-25.22	.000	.000	-2356.10	90.23	-26.11	.000	.000
Mangrove - Urban	2837.70	107.99	26.28	.000	.000	2492.96	93.02	26.80	.000	.000
Trees - Water	228.49	94.70	2.41	.016	.443	608.50	102.70	5.93	.000	.000
Trees - Mixed low vegetation	-845.71	89.08	-9.49	.000	.000	-653.04	97.51	-6.70	.000	.000
Trees - Grass	-1575.89	91.44	-17.24	.000	.000	-1391.07	99.38	-14.00	.000	.000
Trees - Bare soil	-2130.06	97.18	-21.92	.000	.000	-1963.32	104.48	-18.79	.000	.000
Trees - Infrastructure	-2493.37	93.05	-26.80	.000	.000	-2355.51	100.93	-23.34	.000	.000
Trees - Urban	2675.72	96.09	27.85	.000	.000	2492.37	103.43	24.10	.000	.000
Water - Mixed low vegetation	-617.22	62.46	-9.88	.000	.000	-44.53	61.48	-0.72	.469	1.000
Water - Grass	-1347.41	65.77	-20.49	.000	.000	-782.57	64.41	-12.15	.000	.000
Water-Bare soil	-1901.57	73.54	-25.86	.000	.000	-1354.82	72.02	-18.81	.000	.000
Water - Infrastructure	-2264.88	67.99	-33.31	.000	.000	-1747.01	66.77	-26.17	.000	.000
Water - Urban	-2447.23	72.10	-33.94	.000	.000	-1883.87	70.49	-26.73	.000	.000
Mixed low vegetation - Grass	-730.18	57.39	-12.72	.000	.000	-738.03	55.77	-13.23	.000	.000
Mixed low vegetation - Bare soil	-1284.35	66.15	-19.42	.000	.000	-1310.29	64.42	-20.34	.000	.000
Mixed low vegetation - Infrastructure	-1647.66	59.92	-27.50	.000	.000	-1702.47	58.48	-29.11	.000	.000
Mixed low vegetation - Urban	1830.01	64.55	28.35	.000	.000	1839.34	62.70	29.34	.000	.000
Grass - Bare soil	-554.16	69.29	-8.00	.000	.000	-572.26	67.22	-8.51	.000	.000
Grass - Infrastructure	917.48	63.37	14.48	.000	.000	964.44	61.55	15.67	.000	.000
Grass - Urban	1099.83	67.76	16.23	.000	.000	1101.31	65.57	16.80	.000	.000
Bare soil - Infrastructure	363.31	71.40	5.09	.000	.000	392.19	69.48	5.64	.000	.000
Bare soil - Urban	545.66	75.33	7.24	.000	.000	529.05	73.07	7.24	.000	.000
Infrastructure - Urban	182.35	69.92	2.61	.009	.255	136.86	67.89	2.02	.044	1.000

Note: each row tests the null hypothesis that the Sample 1 and Sample 2 distributions are the same.

Asymptotic significances (2-sided tests) are displayed. The significance level is .05.

Adjusted significance^a values have been adjusted by the Bonferroni correction for multiple tests and are highlighted when significant.

Appendix 9 – Wilcoxon signed rank test of $LST_{s, \max}$ on different land cover, green features groups, and cold spots groups in the dry and wet season.

Table 26. Results of a non-parametric Wilcoxon signed-rank test of between $LST_{s, \max}$ values of different seasons per land cover group. N = number of pixels in sample.

Land cover	Wilcoxon Signed-Rank Test				
	Mean dry $LST_{s, \max}$ (°C)	Mean wet $LST_{s, \max}$ (°C)	N	Z	Asymp. Sig. (2-tailed)
Urban	1.4	1.3	445	-5.87	.000
Infrastructure	1.2	1.1	556	-6.06	.000
Grass	0.3	-0.2	654	-10.02	.000
Mixed low vegetation	-0.4	-0.6	831	-11.75	.000
Trees	-1.0	-0.9	187	-6.64	.000
Mangrove	-1.1	-0.9	140	-8.21	.000
Water	-0.8	-0.6	472	-15.13	.000

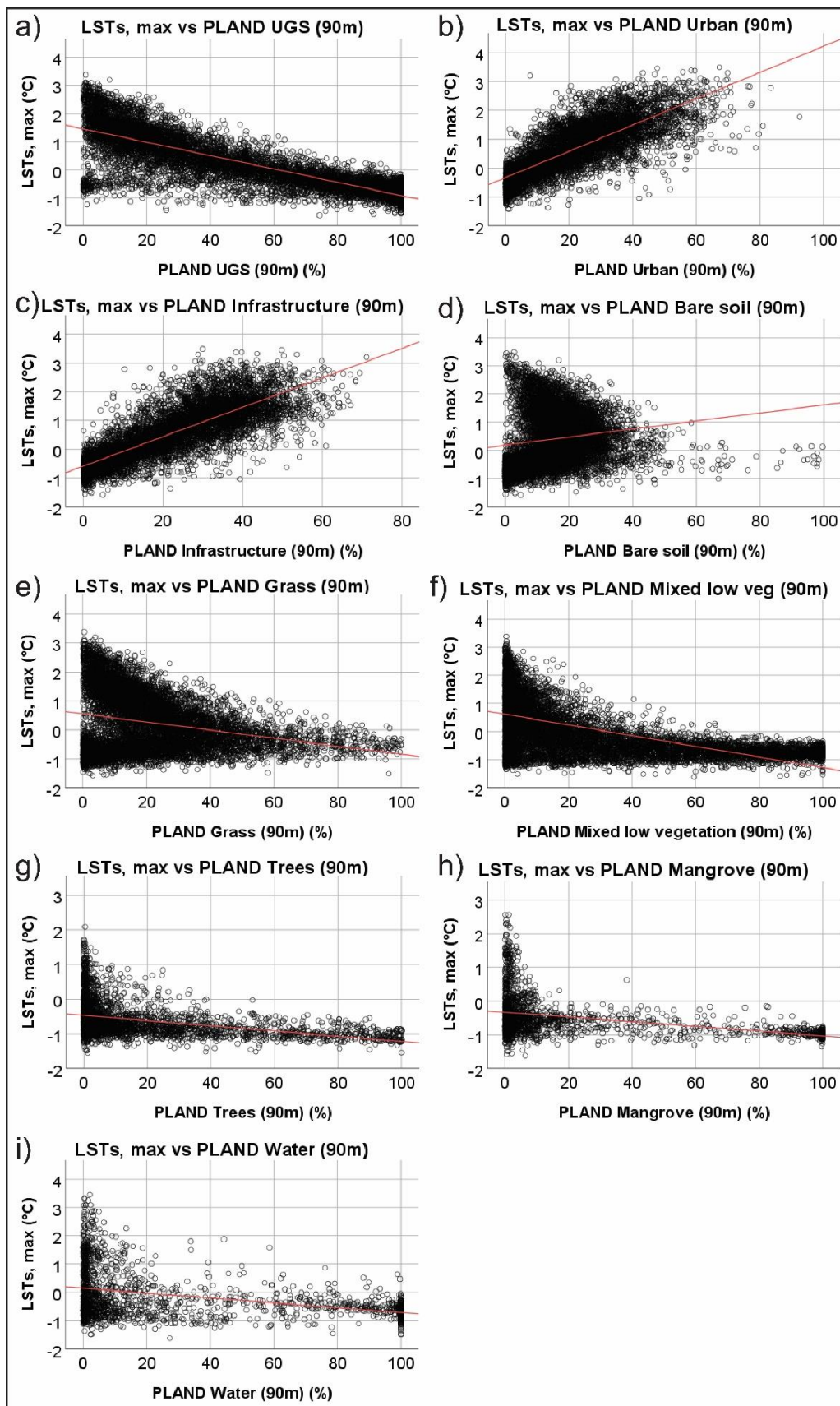
Table 27. Results of a non-parametric Wilcoxon signed-rank test of between $LST_{s, \max}$ values of different seasons per green feature group. N = number of pixels in sample.

Green Feature	Wilcoxon Signed-Rank Test				
	Mean dry $LST_{s, \max}$ (°C)	Mean wet $LST_{s, \max}$ (°C)	N	Z	Asymp. Sig. (2-tailed)
Street with trees	1.8	1.8	10	-0.76	.445
Street without trees	2.1	2.2	6	-0.73	.463
Football field	1.2	1.3	5	-0.41	.686
Large green area with trees	-0.4	-0.6	192	-8.64	.000
Large park with trees	-0.2	-0.2	169	-1.07	.284
Moderate green area, average tree cover	0.4	0.3	7	-2.03	.043
Small park with trees	0.8	0.6	7	-1.69	.091
Small patch of trees	1.3	1.3	4	-0.37	.715
Abandoned mixed vegetation field	1.4	1.6	5	-0.14	.893
Managed grass field	1.8	1.6	3	-1.60	.109
Abandoned grass field	1.8	2.1	3	-1.60	.109
Bare land	1.8	0.8	13	-3.11	.002
Moderate park with palm trees	0.5	0.2	9	-1.48	.139

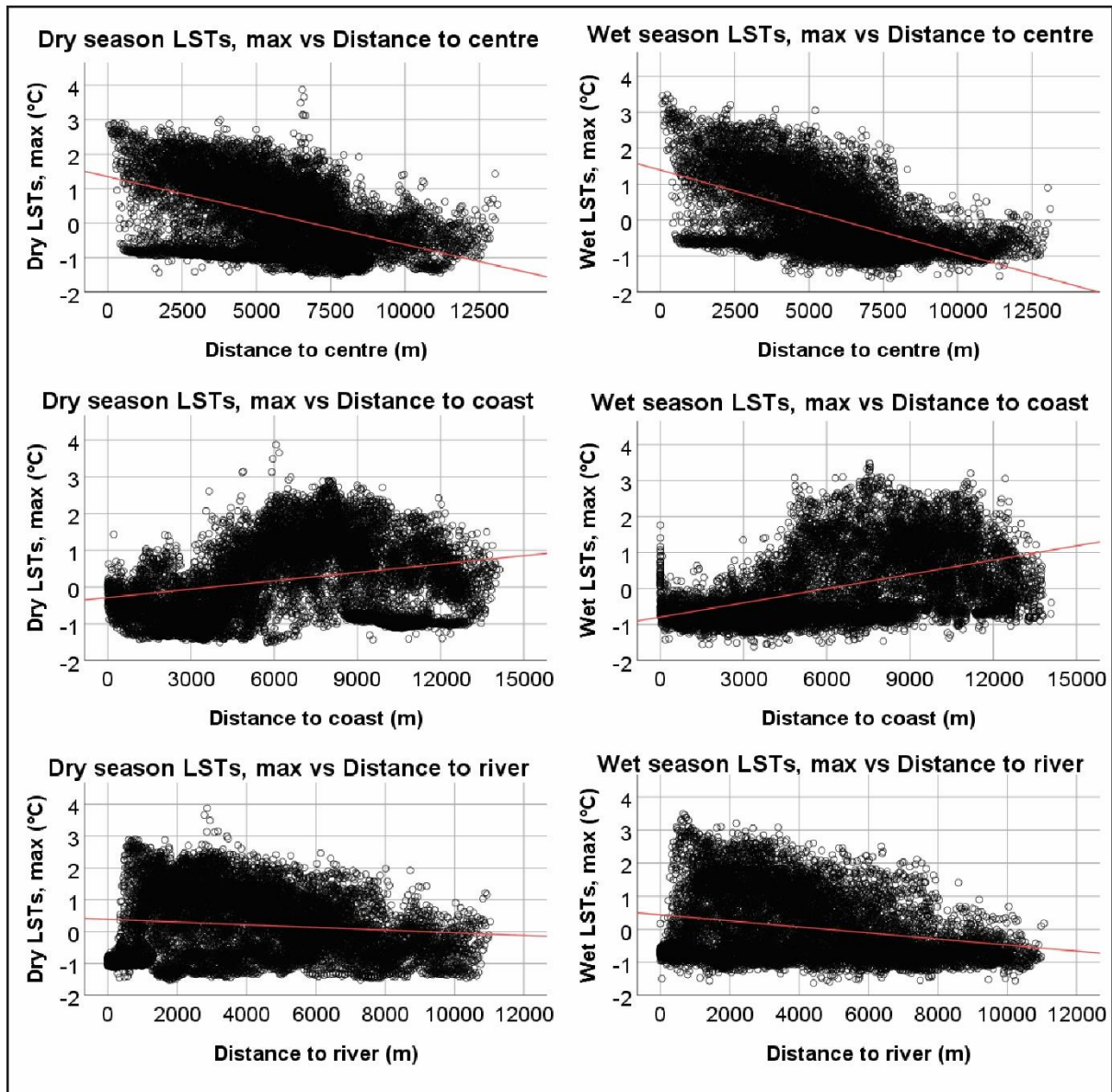
Table 28. Results of a non-parametric Wilcoxon signed-rank test of between $LST_{s, \max}$ values of different seasons per cold spot group. N = number of pixels in sample.

Cold Spot	Wilcoxon Signed-Rank Test				
	Mean dry $LST_{s, \max}$ (°C)	Mean wet $LST_{s, \max}$ (°C)	N	Z	Asymp. Sig. (2-tailed)
Mixed vegetation in large green area	-0.6	-0.6	36	-0.96	.338
Patch of high-density trees in large green area	-1.0	-1.1	38	-2.75	.006
Patch of high-density palm trees in moderate green area	-0.5	-0.6	30	-0.79	.428
Patch of high-density trees in urban	0.0	-0.1	5	-1.75	.080
Mixed vegetation in urban	0.6	-0.6	2	-1.34	.180
Patch of trees in urban	0.1	-0.1	30	-3.22	.001

Appendix 10 – Scatterplots of wet season $LST_{s, \max}$ vs UGS and individual landcover classes, after the 0% PLAND values were filtered out.



Appendix 11 – Scatterplot $LST_{s, \max}$ vs distances.



Appendix 12 – Total multiple linear regression model for the dry season containing all studied variables.

Total Model: Dry Season	Coefficients Dry Season					R ²
	Unstandardized coefficients		Standardized coefficients	t	Sig.	
	B	Std. Error	β			
(Constant)	3.291	0.389		10.087	0.000	.878
PLAND UGS (90m)	-0.019	0.001	-0.727	-13.658	0.000	
PLAND Urban (90m)	-0.015	0.004	-0.241	-3.881	0.000	
PLAND Infrastructure (90m)	-0.011	0.004	-0.181	-2.931	0.003	
PLAND Bare soil (90m)	-0.025	0.004	-0.286	-6.537	0.000	
PLAND Grass (90m)	-0.011	0.004	-0.210	-3.045	0.002	
PLAND Mixed low vegetation (90m)	-0.018	0.004	-0.515	-4.692	0.000	
PLAND Trees (90m)	-0.025	0.004	-0.386	-6.710	0.000	
PLAND Mangrove (90m)	-0.025	0.004	-0.404	-6.649	0.000	
PLAND Water (90m)	-0.045	0.004	-1.443	-11.504	0.000	
NDVI	-0.474	0.027	-0.150	-17.369	0.000	
AI (90m)	0.000	0.000	0.010	1.174	0.240	
LSI (90m)	0.013	0.015	0.012	0.860	0.390	
ED (90m)	0.000	0.000	-0.035	-3.577	0.000	
PD (90m)	-0.001	0.000	-0.072	-9.162	0.000	
Distance centre	0.000	0.000	-0.032	-5.843	0.000	
Distance coast	0.000	0.000	-0.106	-20.813	0.000	
Distance river	0.000	0.000	-0.094	-14.981	0.000	

*Dependent variable: dry season $LST_{s, max}$

Appendix 13 – Total multiple linear regression model for the wet season containing all studied variables.

Total Model: Wet Season	Coefficients Wet Season					R ²
	Unstandardized coefficients		Standardized coefficients	t	Sig.	
	B	Std. Error	β			
(Constant)	1.849	0.37		4.996	0.000	0.882
PLAND UGS (90m)	-0.014	0.001	-0.534	-15.399	0.000	
PLAND Urban (90m)	0.007	0.004	0.111	1.855	0.064	
PLAND Infrastructure (90m)	0.008	0.004	0.132	2.237	0.025	
PLAND Bare soil (90m)	-0.017	0.004	-0.195	-4.647	0.000	
PLAND Grass (90m)	-0.005	0.004	-0.097	-1.424	0.154	
PLAND Mixed low vegetation (90m)	-0.006	0.004	-0.186	-1.724	0.085	
PLAND Trees (90m)	-0.009	0.004	-0.144	-2.524	0.012	
PLAND Mangrove (90m)	-0.007	0.004	-0.112	-1.816	0.069	
PLAND Water (90m)	-0.022	0.004	-0.721	-6.013	0.000	
NDVI	-0.207	0.027	-0.066	-7.606	0.000	
AI (90m)	0.000	0.000	-0.006	-0.698	0.485	
LSI (90m)	-0.023	0.015	-0.023	-1.548	0.122	
ED (90m)	0.000	0.000	0.027	2.744	0.006	
PD (90m)	0.000	0.000	-0.038	-4.837	0.000	
Distance centre	0.000	0.000	-0.137	-23.875	0.000	
Distance coast	0.000	0.000	-0.042	-9.454	0.000	
Distance river	0.000	0.000	0.037	7.110	0.000	

*Dependent variable: wet season $LST_{s, max}$

Appendix 14 – Multiple linear regression models selected to test hypotheses in the wet season.

Table 29. Multiple linear regression model 1, used to test the hypothesis: Impervious urban surface heats the surface in the wet season.

Model 1: Urban Heats	Coefficients Wet Season					R ²
	Unstandardized coefficients		Standardized coefficients	t	Sig.	
	B	Std. Error	β			
(Constant)	0.278	0.021		13.470	0.000	.798
PLAND Urban (90m)	0.039	0.000	.622	88.285	0.000	
PLAND Water (90m)	-0.011	0.000	-.371	-41.868	0.000	
NDVI	-1.239	0.028	-.397	-44.164	0.000	

*Dependent variable: wet season $LST_{s, max}$

Table 30. Multiple linear regression model 2, used to test the hypothesis: UGS cools the surface in the wet season.

Model 2: UGS Cools	Coefficients Wet Season					R ²
	Unstandardized coefficients		Standardized coefficients	t	Sig.	
	B	Std. Error	β			
(Constant)	0.886	0.020		43.703	0.000	.842
PLAND UGS (90m)	-0.018	0.000	-.665	-75.631	0.000	
PLAND Urban (90m)	0.020	0.001	.322	39.560	0.000	
PLAND Water (90m)	-0.016	0.000	-.513	-68.699	0.000	

*Dependent variable: wet season $LST_{s, max}$

Table 31. Multiple linear regression model 3, used to test the hypothesis: Trees are the UGS type that cools the surface most effective in the wet season.

Model 3: Trees Cool Most	Coefficients Wet Season					R ²
	Unstandardized coefficients		Standardized coefficients	t	Sig.	
	B	Std. Error	β			
(Constant)	-0.065	0.018		-3.678	0.000	.795
PLAND Trees (90m)	-0.011	0.000	-.168	-33.473	0.000	
PLAND Mixed low vegetation (90m)	-0.007	0.000	-.221	-33.277	0.000	
PLAND Grass (90m)	-0.004	0.000	-.078	-13.500	0.000	
PLAND Urban (90m)	0.041	0.000	.658	90.571	0.000	
PLAND Water (90m)	-0.006	0.000	-.206	-29.145	0.000	

*Dependent variable: wet season $LST_{s, max}$

Appendix 15 – Representative images of green features groups.



2 - Street without trees



3 - Football field



6 - Moderate green area, average tree cover



8 - Small patch of trees



9 - Abandoned mix vegetation field



10 - Managed grass field



11 - Abandoned grass field

Appendix 16 – Kruskal-Wallis test: green features groups.

Table 32. Kruskal-Wallis test on the distribution of $LST_{s,max}$ across the different groups of green features, including pairwise comparisons adjusted by the Bonferroni correction for multiple tests.

Pairwise Comparisons of Green Feature Groups										
Sample 1 - Sample 2	Dry season					Wet season				
	Test Statistic	Std. Error	Std. Test Statistic	Sig.	Adj. Sig. ^a	Test Statistic	Std. Error	Std. Test Statistic	Sig.	Adj. Sig. ^a
Large green area with trees - Large park with trees	-43.07	13.42	-3.21	.001	.104	-103.68	13.20	-7.85	.000	.000
Large green area with trees - Moderate green area, average tree cover	-180.24	49.76	-3.62	.000	.023	-182.13	42.68	-4.27	.000	.002
Large green area with trees - Moderate park with palm trees	-185.98	44.09	-4.22	.000	.002	-208.27	48.15	-4.33	.000	.001
Large green area with trees - Small park with trees	-211.66	49.76	-4.25	.000	.002	-218.70	48.15	-4.54	.000	.000
Large green area with trees - Football field	232.69	58.60	3.97	.000	.006	-237.82	35.86	-6.63	.000	.000
Large green area with trees - Small patch of trees	-239.59	65.36	-3.67	.000	.019	263.53	56.69	4.65	.000	.000
Large green area with trees - Abandoned mixed vegetation field	-241.09	58.60	-4.11	.000	.003	-269.63	63.22	-4.27	.000	.002
Large green area with trees - Street with trees	252.29	41.92	6.02	.000	.000	-273.93	56.69	-4.83	.000	.000
Large green area with trees - Abandoned grass field	-253.43	75.29	-3.37	.001	.059	275.73	40.59	6.79	.000	.000
Large green area with trees - Managed grass field	-257.43	75.29	-3.42	.001	.049	-278.46	72.81	-3.82	.000	.010
Large green area with trees - Bare land	-257.86	37.02	-6.97	.000	.000	279.30	51.88	5.38	.000	.000
Large green area with trees - Street without trees	262.93	53.62	4.90	.000	.000	-284.80	72.81	-3.91	.000	.007
Large park with trees - Moderate green area, average tree cover	-137.16	49.94	-2.75	.006	.470	-78.46	42.81	-1.83	.067	1.000
Large park with trees - Moderate park with palm trees	-142.91	44.29	-3.23	.001	.098	-104.60	48.27	-2.17	.030	1.000
Large park with trees - Small park with trees	-168.59	49.94	-3.38	.001	.057	-115.03	48.27	-2.38	.017	1.000
Large park with trees - Football field	189.62	58.75	3.23	.001	.097	-134.15	36.02	-3.72	.000	.015
Large park with trees - Small patch of trees	-196.52	65.50	-3.00	.003	.210	159.86	56.79	2.82	.005	.380
Large park with trees - Abandoned mixed vegetation field	-198.02	58.75	-3.37	.001	.059	-165.96	63.31	-2.62	.009	.683
Large park with trees - Street with trees	209.22	42.14	4.97	.000	.000	-170.26	56.79	-3.00	.003	.212
Large park with trees - Abandoned grass field	-210.35	75.41	-2.79	.005	.412	172.06	40.73	4.23	.000	.002
Large park with trees - Managed grass field	-214.35	75.41	-2.84	.004	.349	-174.79	72.89	-2.40	.016	1.000
Large park with trees - Bare land	-214.79	37.26	-5.76	.000	.000	175.62	51.99	3.38	.001	.057
Large park with trees - Street without trees	219.85	53.79	4.09	.000	.003	-181.12	72.89	-2.49	.013	1.000
Moderate green area moderate tree cover - Moderate park with palm trees	-5.75	65.25	-0.09	.930	1.000	26.14	63.07	0.42	.678	1.000
Moderate green area moderate tree cover - Small park with trees	-31.43	69.21	-0.45	.650	1.000	36.57	63.07	0.58	.562	1.000
Moderate green area moderate tree cover - Football field	52.46	75.81	0.69	.489	1.000	55.69	54.27	1.03	.305	1.000
Moderate green area moderate tree cover - Small patch of trees	-59.36	81.15	-0.73	.465	1.000	81.40	69.80	1.17	.244	1.000
Moderate green area moderate tree cover - Abandoned mixed vegetation field	-60.86	75.81	-0.80	.422	1.000	87.50	75.20	1.16	.245	1.000
Moderate green area moderate tree cover - Street with trees	72.06	63.80	1.13	.259	1.000	91.80	69.80	1.32	.188	1.000
Moderate green area moderate tree cover - Abandoned grass field	-73.19	89.34	-0.82	.413	1.000	93.60	57.50	1.63	.104	1.000

Moderate green area moderate tree cover - Managed grass field	-77.19	89.34	-0.86	.388	1.000	96.33	83.43	1.16	.248	1.000
Moderate green area moderate tree cover - Bare land	-77.63	60.70	-1.28	.201	1.000	97.17	65.96	1.47	.141	1.000
Moderate green area moderate tree cover - Street without trees	82.69	72.03	1.15	.251	1.000	102.67	83.43	1.23	.218	1.000
Moderate park with palm trees - Small park with trees	25.68	65.25	0.39	.694	1.000	-10.43	66.89	-0.16	.876	1.000
Moderate park with palm trees - Football field	46.71	72.22	0.65	.518	1.000	-29.55	58.67	-0.50	.614	1.000
Moderate park with palm trees - Small patch of trees	53.61	77.80	0.69	.491	1.000	55.26	73.28	0.75	.451	1.000
Moderate park with palm trees - Abandoned mixed vegetation field	55.11	72.22	0.76	.445	1.000	-61.36	78.44	-0.78	.434	1.000
Moderate park with palm trees - Street with trees	66.31	59.49	1.12	.265	1.000	-65.66	73.28	-0.90	.370	1.000
Moderate park with palm trees - Abandoned grass field	67.44	86.31	0.78	.435	1.000	67.46	61.67	1.09	.274	1.000
Moderate park with palm trees - Managed grass field	71.44	86.31	0.83	.408	1.000	-70.19	86.36	-0.81	.416	1.000
Moderate park with palm trees - Bare land	71.88	56.14	1.28	.200	1.000	71.02	69.62	1.02	.308	1.000
Moderate park with palm trees - Street without trees	76.94	68.24	1.13	.259	1.000	-76.52	86.36	-0.89	.376	1.000
Small park with trees - Football field	21.03	75.81	0.28	.781	1.000	-19.12	58.67	-0.33	.744	1.000
Small park with trees - Small patch of trees	-27.93	81.15	-0.34	.731	1.000	44.83	73.28	0.61	.541	1.000
Small park with trees - Abandoned mixed vegetation field	-29.43	75.81	-0.39	.698	1.000	-50.93	78.44	-0.65	.516	1.000
Small park with trees - Street with trees	40.63	63.80	0.64	.524	1.000	-55.23	73.28	-0.75	.451	1.000
Small park with trees - Abandoned grass field	-41.76	89.34	-0.47	.640	1.000	57.03	61.67	0.93	.355	1.000
Small park with trees - Managed grass field	-45.76	89.34	-0.51	.609	1.000	-59.76	86.36	-0.69	.489	1.000
Small park with trees - Bare land	-46.20	60.70	-0.76	.447	1.000	60.60	69.62	0.87	.384	1.000
Small park with trees - Street without trees	51.26	72.03	0.71	.477	1.000	-66.10	86.36	-0.77	.444	1.000
Football field - Small patch of trees	-6.90	86.85	-0.08	.937	1.000	25.71	65.85	0.39	.696	1.000
Football field - Abandoned mixed vegetation field	-8.40	81.88	-0.10	.918	1.000	31.81	71.55	0.45	.657	1.000
Football field - Street with trees	19.60	70.91	0.28	.782	1.000	36.11	65.85	0.55	.583	1.000
Football field - Abandoned grass field	-20.73	94.55	-0.22	.826	1.000	37.91	52.64	0.72	.471	1.000
Football field - Managed grass field	-24.73	94.55	-0.26	.794	1.000	40.64	80.15	0.51	.612	1.000
Football field - Bare land	-25.17	68.13	-0.37	.712	1.000	41.47	61.76	0.67	.502	1.000
Football field - Street without trees	30.23	78.40	0.39	.700	1.000	46.97	80.15	0.59	.558	1.000
Small patch of trees - Abandoned mixed vegetation field	-1.50	86.85	-0.02	.986	1.000	-6.10	83.95	-0.07	.942	1.000
Small patch of trees - Street with trees	12.70	76.60	0.17	.868	1.000	-10.40	79.15	-0.13	.895	1.000
Small patch of trees - Abandoned grass field	-13.83	98.89	-0.14	.889	1.000	12.20	68.54	0.18	.859	1.000
Small patch of trees - Managed grass field	-17.83	98.89	-0.18	.857	1.000	-14.93	91.39	-0.16	.870	1.000
Small patch of trees - Bare land	-18.27	74.03	-0.25	.805	1.000	15.77	75.78	0.21	.835	1.000
Small patch of trees - Street without trees	23.33	83.57	0.28	.780	1.000	-21.27	91.39	-0.23	.816	1.000
Abandoned mixed vegetation field - Street with trees	11.20	70.91	0.16	.875	1.000	-4.30	83.95	-0.05	.959	1.000
Abandoned mixed vegetation field - Abandoned grass field	-12.33	94.55	-0.13	.896	1.000	6.10	74.03	0.08	.934	1.000
Abandoned mixed vegetation field - Managed grass field	-16.33	94.55	-0.17	.863	1.000	-8.83	95.58	-0.09	.926	1.000
Abandoned mixed vegetation field - Bare land	-16.77	68.13	-0.25	.806	1.000	9.67	80.78	0.12	.905	1.000
Abandoned mixed vegetation field - Street without trees	21.83	78.40	0.28	.781	1.000	-15.17	95.58	-0.16	.874	1.000
Street with trees - Abandoned grass field	-1.13	85.23	-0.01	.989	1.000	1.80	68.54	0.03	.979	1.000

Street with trees - Managed grass field	-5.13	85.23	-0.06	.952	1.000	-4.53	91.39	-0.05	.960	1.000
Street with trees - Bare land	-5.57	54.46	-0.10	.919	1.000	5.37	75.78	0.07	.944	1.000
Street with trees - Street without trees	-10.63	66.86	-0.16	.874	1.000	-10.87	91.39	-0.12	.905	1.000
Abandoned grass field - Managed grass field	4.00	105.71	0.04	.970	1.000	-2.73	82.38	-0.03	.974	1.000
Abandoned grass field - Bare land	-4.44	82.93	-0.05	.957	1.000	-3.57	64.62	-0.06	.956	1.000
Abandoned grass field - Street without trees	9.50	91.55	0.10	.917	1.000	-9.07	82.38	-0.11	.912	1.000
Managed grass field - Bare land	-0.44	82.93	-0.01	.996	1.000	0.83	88.49	0.01	.992	1.000
Managed grass field - Street without trees	5.50	91.55	0.06	.952	1.000	-6.33	102.18	-0.06	.951	1.000
Bare land - Street without trees	5.06	63.90	0.08	.937	1.000	-5.50	88.49	-0.06	.950	1.000

Note: each row tests the null hypothesis that the Sample 1 and Sample 2 distributions are the same.

Asymptotic significances (2-sided tests) are displayed. The significance level is .05.

Adjusted significance^a values have been adjusted by the Bonferroni correction for multiple tests and are highlighted when significant.

Appendix 17 – The selected Cold spots depicted on the seasonal $LST_{s, max}$ maps.

Cold Spots Based on Dry Season Standardized Maximum LST

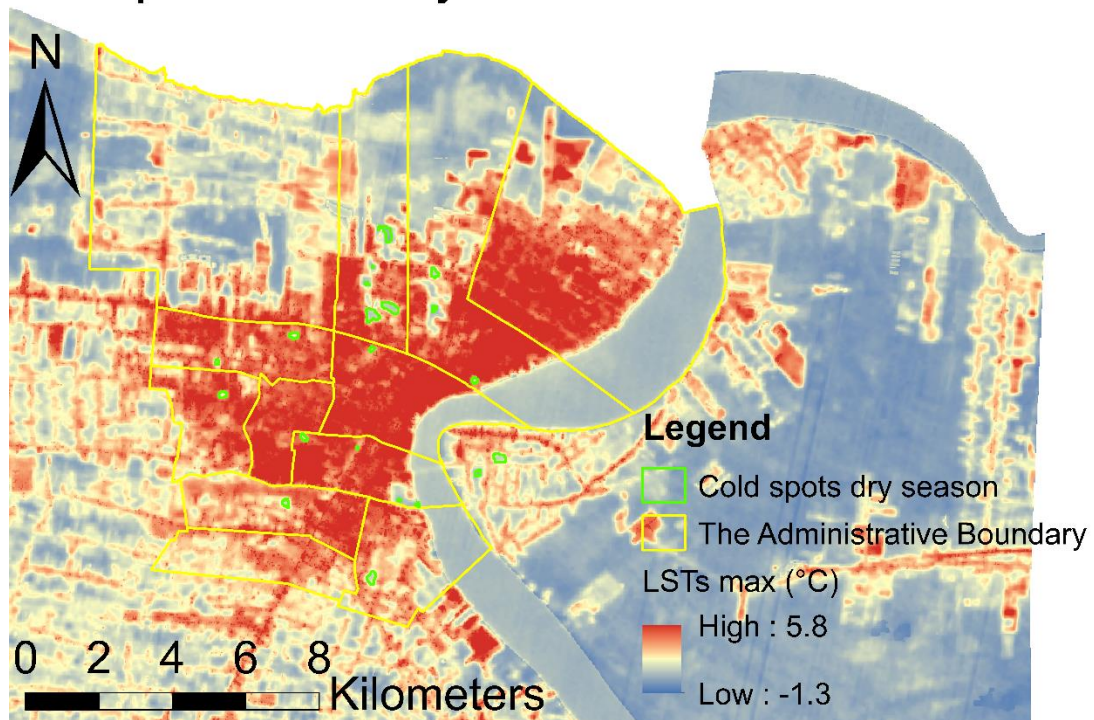


Figure 27. The pixels that were selected as cold spots in the dry season based on their low $LST_{s, max}$ values and small distance to the city centre.

Cold Spots Based on Wet Season Standardized Maximum LST

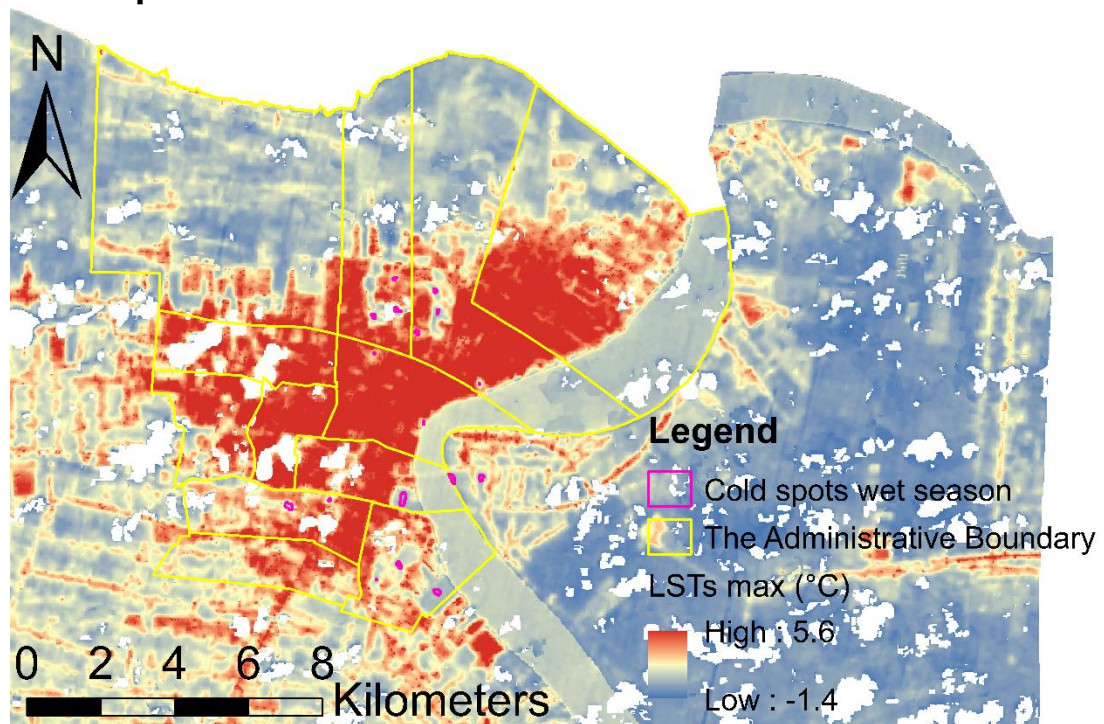


Figure 28. The pixels that were selected as cold spots in the wet season based on their low $LST_{s, max}$ values and small distance to the city centre.

Appendix 18 – Kruskal-Wallis test: cold spots groups.

Table 33. Kruskal-Wallis test on the distribution of $LST_{s,max}$ across the different cold spot groups, including pairwise comparisons adjusted by the Bonferroni correction for multiple tests.

Pairwise Comparisons of Cold Spot groups										
Sample 1 - Sample 2	Dry season					Wet season				
	Test Statistic	Std. Error	Std. Test Statistic	Sig.	Adj. Sig. ^a	Test Statistic	Std. Error	Std. Test Statistic	Sig.	Adj. Sig. ^a
Patch of high-density of trees in large green area - Patch of high-density palm trees in moderate green area	-42.51	10.11	-4.21	.000	.000	-42.75	9.98	-4.29	.000	.000
Patch of high-density of trees in large green area - Mixed vegetation in large green area	47.64	10.44	4.56	.000	.000	43.91	9.50	4.62	.000	.000
Patch of high-density of trees in large green area - Mixed vegetation in urban	-95.24	21.46	-4.44	.000	.000	-47.65	29.63	-1.61	.108	1.000
Patch of high-density of trees in large green area - Patch of high-density trees in urban	-98.08	10.69	-9.18	.000	.000	-86.95	19.43	-4.47	.000	.000
Patch of high-density of trees in large green area - Patch of trees in urban	-122.54	32.75	-3.74	.000	.003	-89.68	9.98	-8.99	.000	.000
Patch of high-density palm trees in moderate green area - Mixed vegetation in large green area	5.12	10.32	0.50	.620	1.000	1.16	10.10	0.12	.908	1.000
Patch of high-density palm trees in moderate green area - Mixed vegetation in urban	-52.72	21.40	-2.46	.014	.206	-4.90	29.83	-0.16	.870	1.000
Patch of high-density palm trees in moderate green area - Patch of high-density trees in urban	-55.57	10.57	-5.26	.000	.000	-44.20	19.73	-2.24	.025	.376
Patch of high-density palm trees in moderate green area - Patch of trees in urban	-80.02	32.72	-2.45	.014	.217	-46.93	10.55	-4.45	.000	.000
Mixed vegetation in large green area - Mixed vegetation in urban	-47.60	21.56	-2.21	.027	.409	-3.74	29.68	-0.13	.900	1.000
Mixed vegetation in large green area - Patch of high-density trees in urban	-50.45	10.89	-4.63	.000	.000	-43.04	19.50	-2.21	.027	.409
Mixed vegetation in large green area - Patch of trees in urban	-74.90	32.82	-2.28	.022	.337	-45.77	10.10	-4.53	.000	.000
Mixed vegetation in urban - Patch of high-density trees in urban	-2.85	21.68	-0.13	.896	1.000	39.30	34.18	1.15	.250	1.000
Mixed vegetation in urban - Patch of trees in urban	-27.30	37.80	-0.72	.470	1.000	-42.03	29.83	-1.41	.159	1.000
Patch of high-density trees in urban - Patch of trees in urban	24.46	32.90	0.74	.457	1.000	-2.73	19.73	-0.14	.890	1.000

Note: each row tests the null hypothesis that the Sample 1 and Sample 2 distributions are the same.

Asymptotic significances (2-sided tests) are displayed. The significance level is .05.

Adjusted significance^a values have been adjusted by the Bonferroni correction for multiple tests and are highlighted when significant.

Appendix 19 – Kruskal-Wallis test: socioeconomic status.

Table 34. Kruskal-Wallis test on the distribution of $LST_{s,max}$ across the different neighbourhoods varying in socioeconomic status based on residential class, including pairwise comparisons adjusted by the Bonferroni correction for multiple tests.

Pairwise Comparisons of Neighbourhoods Differing in Socioeconomic Status Based on Residential Class										
Sample 1 - Sample 2	Dry season					Wet season				
	Test Statistic	Std. Error	Std. Test Statistic	Sig.	Adj. Sig. ^a	Test Statistic	Std. Error	Std. Test Statistic	Sig.	Adj. Sig. ^a
Poor - Middle	2096.28	222.25	9.43	.000	.000	2341.67	212.36	11.03	.000	.000
Poor - Rich	2213.81	238.56	9.28	.000	.000	2596.96	228.10	11.39	.000	.000
Poor - Middle to low	3057.04	221.62	13.79	.000	.000	3330.75	211.74	15.73	.000	.000
Middle - Rich	117.53	112.34	1.05	.295	1.000	255.29	108.25	2.36	.018	.110
Middle - Middle to low	-960.76	69.44	-13.84	.000	.000	-989.08	67.25	-14.71	.000	.000
Rich - Middle to low	-843.23	111.08	-7.59	.000	.000	-733.80	107.03	-6.86	.000	.000

Note: each row tests the null hypothesis that the Sample 1 and Sample 2 distributions are the same.

Asymptotic significances (2-sided tests) are displayed. The significance level is .05.

Adjusted significance^a values have been adjusted by the Bonferroni correction for multiple tests and are highlighted when significant.

Appendix 20 – Comparison between LST and air temperature at the air temperature measuring stations and outdoor temperature logger locations.

Table 35. LST and air temperatures measured on 14:00 hrs, local time, at the locations of the measuring stations, Cultuurtuin and Zorg en Hoop, of the meteorological service Suriname.

Comparison LST and Air Temperature					
Station		Cultuurtuin		Zorg en Hoop	
Land cover		Middle of urban forest on grass field		On industrial site next to small river	
Season	Date	LST (°C) - 14:00	Air (°C) - 14:00	LST (°C) - 14:00	Air (°C) - 14:00
Dry	15/10/2015	29.3	33.6	32.7	32.7
	01/10/2016	28.0	34.2	30.5	34.2
	21/09/2018	28.8	34.6	32.9	34.9
	08/09/2018	27.1	30.7	31.1	32.7
	Average	28.3	33.3	31.8	33.6
Wet	29/07/2016	27.1	34.9	30.6	32.9
	14/06/2016	23.7	33.5	No data	32.4
	04/08/2018	27.9	35.3	No data	32.4
	Average	26.2	34.6	30.6	32.6
Total	Average	27.4	33.8	31.6	33.2

Table 36. Location description, LST and air temperatures on 14:00 hrs, local time, on August 8th, 2019 at the locations of outdoor temperature loggers.

LST and Air Temperature at Outdoor Temperature Logger Locations					
Outdoor temperature logger characteristics		LST (C°)		Air temperature (C°)	
Location	Landcover	Dry season 08/09/2019	Rank	Dry season 08/09/2019	Rank
D1 - Coppenamestraat 51	On the roadside of a house garden in urban area	31.0	2	33.9	3
D2 - M.C. Ooftplein	Sandy play garden half covered by large trees	29.3	3	31.0	7
D3 - Atlasstraat	House garden in urban area	32.1	1	33.9	3
D4 - Cultuurtuin	High density tropical forest in big green area	25.1	8	28.7	8
D6 - Fort Zeelandia	On balcony next to small grass park half covered by large trees	27.4	6	35.1	2
D8 - CELOS terrein	Patch of trees in green area	25.8	7	31.8	5
D9 - Boedhiastraat 5	Small house in green neighbourhood	28.8	5	31.6	6
D10 - Franklynweg (Latour)	Grass covered school play garden with some small trees	29.3	4	35.8	1
D11 - Jodenbreestraat	On balcony facing the street in urban centre	33.4	-	No data	-
D12 - Palmentuin	Public park with palm trees	27.7	-	No data	-
D13 - Samidalaan 14 (Commewijne)	On lawn in rural area	No data	-	No data	-
Total	Average	29.0	-	32.7	-
	Range	8.3	-	7.1	-